REPUBLIQUE ALGERIENNE DEMOCRATIQUE ET POPULAIRE
MINISTERE DE L'ENSEIGNEMENT SUPERIEUR
ET DE LA RECHERCHE SCIENTIFIQUE

N° d'enregistrement :

/……/……/……/……/

UNIVERSITE KASDI MERBAH -OUARGLA-
FACULTE DES SCIENCES APPLIQUEES
DEPARTEMENT DE GENIE CIVIL ET HYDRAULIQUE

THESE

Présentée en vue de l'obtention du diplôme de Doctorat LMD

Domaine : Sciences appliquées
Filière : Génie civil
Spécialité : structure en génie civil

Contribution à l'étude du l'effet de gradient de température sur le comportement des structures en zones sahariennes

Présenté par : Toaiba Afaf

Soutenue publiquement le :12/04/2025 devant le jury composé de :

BOUZIANE Mebarka	**Professeur**	**U.K.M. Ouargla**	**President**
KRIKER Abdelouahed	**Professeur**	**U.K.M. Ouargla**	**Directeur de thèse**
ABIMOULOUD Youcef	**Maître de Conférences (A)**	**U.K.M. Ouargla**	**Co-Directeur de thèse**
Allaoua Belferrag	**Maître de Conférences (A)**	**U.K.M. Ouargla**	**Examinateur**
Mohamed-Ouejdi Belarbi	**Maître de Conférences (A)**	**U.M.KH. Biskra**	**Examinateur**
TIOUA Tahar	**Maître de Conférences (A)**	**UC.A.B Mila**	**Examinateur**
Tati Abdelouahab	**Professeur**	**U.M.KH. Biskra**	**Invité**

Année universitaire: 2024/2025

PEOPLE'S DEMOCRATIC AND REPUBLIC OF ALGERIAN

Ministry of Higher Education and Scientific Research

N° d'enregistrement :

/……/……/……/……/

Kasdi Merbah University Of Ouargla

Faculty Of Applied Sciences

Departement Of Civil Engineering and Hydraulic

DOCTORAL THESIS

Sector: Civil engineering

Specialty: Structure

Contribution to the study of the effect of temperature gradient on the behavior of structures in Saharan zones.

Presented by: ***Toaiba Afaf***

In front of jury:

BOUZIANE Mebarka	**Prof**	**U.K.M. Ouargla**	**President**
KRIKER Abdelouahed	**Prof**	**U.K.M. Ouargla**	**Supervisor**
ABIMOULOUD Youcef	**MCA**	**U.K.M. Ouargla**	**Co-supervisor**
Allaoua Belferrags	**MCA**	**U.K.M. Ouargla**	**Examiner**
Mohamed-Ouejdi Belarbi	**MCA**	**U.M.KH. Biskra**	**Examiner**
TIOUA Tahar	**MCA**	**UC.A.B Mila**	**Examiner**
Tati Abdelouahab	**Prof**	**U.M.KH. Biskra**	**Invited**

University year: 2024/2025

To my dear parents, my husband, my brothers and sisters

, my little prince ''Mossaab", and to my baby girl coming soon ''Amina"

Acknowledgments

First and foremost, *Alhamdulillah,* all praise and appreciation to **Allah** Almighty for allowing me the ability and understanding to do this modest work. I am incredibly grateful to **Allah** for everything.
Above all, I am grateful to my husband, parents, brothers, and sisters for their support.

Of course, my heartfelt gratitude goes to my tutor, **Professor Abdelouahab Tati**, for his assistance, counsel, and support. I am very grateful to my supervisor, **Professor Abdelouahad Kriker**, for his assistance and support.
I would also want to thank my co-director, **Doctor ABIMOULOUD Youcef**.
I would like to express my heartfelt gratitude to the professors at the **University of Ourgla** for their assistance, which considerably aided the progress of my work.
I also like to thank all of the **PhD** students in the **LGEM** laboratory at the **University of Biskra** for their help. **Doctor M. Seyf Eddine Bougoffa's** guidance, assistance, and support have been invaluable at the academic level, and I am extremely grateful. Finally, I'd want to thank my friends, colleagues, and fellow students for their advice, support, and encouragement during this trip. Their contributions have been crucial to my work, regardless of how big or small.

Toaiba Afaf

Abstract

Desert areas are characterized by extreme temperature changes, low humidity, and intense solar radiation. Structures in these areas are exposed to thermal loads due to significant daily temperature variations, ranging from scorching daytime heat to cold nighttime temperatures. The thermal impacts t on the behavior of structural elements are of particular importance, as such conditions require a comprehensive understanding of how these thermal changes impact the performance, stability, and durability of structural elements.

The main aim objective of this work is to enhanced to the modeling of the static, vibration, and stability behaviors of structures under thermal conditions, by developing of finite element model that can precisely represent these behaviors. First, a finite element base on the Euler-Bernoulli beam theory and taking into account the temperature rise has been adapted for studying the static and vibration behavior of steel beams. Additionally, a new analytical approach has been developed to study the static behavior of elastically supported steel beams subjected to uniform temperature rise.The study revealed that temperature rise significantly influences the static behavior of structural elements, notably affecting their stiffness and strength, leading to a marked increase in deflections and bending moments. From the dynamic behavior of steel beams under heating conditions, the natural frequency decreases with increasing temperature.
Secondly, the proposed finite element model is introduced to perform the buckling analysis of functionally graded beams subjected to thermo-mechanical loading, based on the enhanced Timoshenko beam theory using a simple high-order shear deformation theory (SHSDT), with three degrees of freedom(DOFs) per node. The results show that the stability responses of functionally graded (FG) beams are accurately predicted by the developed finite element (SHSDT).

Keywords: Temperature, Static behavior, Buckling behavior, Dynamic behavior, Structures, Finite element model

ملخص

تتميز البيئات الصحراوية بتقلبات شديدة في درجات الحرارة، وانخفاض الرطوبة، والإشعاع الشمسي المكثف. تتعرض الهياكل في هذه المناطق لأحمال حرارية بسبب التغيرات اليومية الكبيرة في درجات الحرارة، والتي يمكن أن تتراوح من حرارة النهار الحارقة إلى درجات حرارة الليل الباردة. إن التأثيرات الحرارية على سلوك العناصر الإنشائية لها أهمية خاصة تتطلب مثل هذه الظروف فهمًا شاملاً لكيفية تأثير هذه التغيرات الحرارية على أداء واستقرار ومتانة العناصر الإنشائية.

الهدف الرئيسي من هذا العمل هو المساهمة في نمذجة السلوك الستاتيكي، المستقر والديناميكي للهياكل تحت الظروف الحرارية، من خلال تطوير نموذج العناصر المحدودة الذي يمكنه تمثيل هذه السلوكيات بدقة. أولاً، تم تكييف عنصر محدود يعتمد على نظرية الروافد لأويلر-برنولي، مع مراعاة ارتفاع درجة الحرارة، لدراسة السلوك الستاتيكي والديناميكي للروافد الفولاذية. كشفت الدراسة أن ارتفاع درجة الحرارة يؤثر بشكل كبير على السلوك الاستاتيكي للعناصر الإنشائية. لا سيما من خلال التأثير على صلابتها ومقاومتها، مما يؤدي إلى زيادة ملحوظة في الانحرافات وعزوم الانحناء

من خلال السلوك الديناميكي للعوارض الفولاذية تحت تأثير الحرارة، تنخفض الترددات الطبيعية مع ارتفاع درجة الحرارة

بالإضافة إلى ذلك، تم تطوير نهج تحليلي جديد لدراسة السلوك الستاتيكي للروافد الفولاذية المدعومة بشكل مرن والخاضعة لارتفاع حراري موحد. ثانياً، يتم تقديم نموذج العنصر المحدود المقترح لإجراء التحليل الستاتيكي والتحليل المستقر للروافد المصنوعة من المواد المتدرجة وظيفياً والخاضعة لأحمال حرارية ميكانيكية، وذلك بناءً على نظرية تيموشينكو المتطورة للروافد باستخدام نظرية تشوه القص المبسطة من الدرجة العالية مع ثلاث درجات (DOFs)من الحرية لكل عقدة

تظهر النتائج أن استجابات استقرار منافذ التشغيل المتدرجة (FG) يتم تقديمها بدقة من خلال طريقة العناصر النهائية المطورة (SHSDT).

الكلمات المفتاحية: الحرارة، السلوك الستاتيكي، السلوك المستقر، السلوك الديناميكي،الهياكل، نموذج العناصر المحدودة

Résumé

Les régions désertiques se caractérisent par des changements de température extrêmes, une faible humidité et un rayonnement solaire intense. Les structures de ces régions sont exposées à des charges thermiques dues à des variations de température quotidiennes importantes, allant de la chaleur torride de la journée aux températures froides de la nuit. Les effets thermiques sur le comportement des éléments structuraux sont particulièrement importants, car ces conditions exigent une compréhension globale de l'impact de ces changements thermiques sur la performance, la stabilité et la durabilité des éléments structuraux.

L'objectif principal de ce travail est de contribuer à la modélisation du comportement statique, vibratoire et de stabilité des structures sous conditions thermiques, en développant un modèle d'éléments finis capable de représenter précisément ces comportements. Tout d'abord, un élément fini basé sur la théorie des poutres d'Euler-Bernoulli, prenant en compte l'élévation de la température, a été adapté pour étudier le comportement statique et vibratoire des poutres en acier. De plus, une nouvelle approche analytique a été développée pour étudier le comportement statique des poutres en acier, supportées de manière élastique et soumises à une élévation uniforme de la température. L'étude a révélé que l'élévation de la température influence de manière significative le comportement statique des éléments structurels. notamment en affectant leur rigidité et leur résistance, ce qui entraîne une augmentation marquée des flèches et des moments de flexion. À partir du comportement dynamique des poutres en acier sous l'effet de la chaleur, la fréquence naturelle diminue avec l'augmentation de la température.Ensuite, le modèle d'élément fini proposé est introduit pour effectuer l'analyse statique et le flambement des poutres à gradients fonctionnels soumises à des charges thermo-mécaniques, en se basant sur une théorie améliorée des poutres de Timoshenko, à l'aide d'une théorie de déformation par cisaillement d'ordre élevé simplifiée (SHSDT), avec trois degrés de liberté (DDL) par nœud. Les résultats montrent que les réponses de stabilité des poutres à gradient fonctionnel (FG) sont prédites avec précision par la méthode des éléments finis développée (SHSDT).

Les mots clés : Temperature, Comportement statique, Comportement dynamique, Comportement de flambement, Structures, modele des éléments finis .

Publications and Communications

International publication:

- **A.Toaiba**, A. Tati, S.Daguiani, A.Kriker (2024) *" Numerical and analytical analysis of thermo-elastic behaviour of steel beams in a thermal environment"*. STUDIES IN ENGINEERING AND EXACT SCIENCES ·
  DOI: 10.54021/seesv5n2-208

International communications:

- **A.Toaiba**, A. Tati, A.Kriker (11-11-2021) *"Analysis behavior of steel beam under large temperature difference"*. 2nd International Symposium on Construction Management and Civil Engineering (ISCMCE- 2021) .Skikda, Algeria

- **A.Toaiba**, A. Tati, A.Kriker (04-12-2021) "*Study on the effect of high temperature on dynamic behavior of metallic beams*" . International World Energy. Turkey https://www.worldenergyconference.org/application

- **A.Toaiba**, A.Kriker, Y.Abimouloud (18-12-2021) "*Evaluation of thermal behavior of concrete beam under large temperature difference*". the ICETME 2021, the 1st Int. Conf. on Energy, Thermofluids and Mater. Eng., Online Conf .Biskra,Algeria

National communications:

- **A.Toaiba**, A.Kriker, Y.Abimouloud "*Numerical simulation of thermal behavior of concrete beam subjected to elevated temperature*" .28-06-2022. the MSE'22 at khenchela University Algeria

Contents

Acknowledgements ii

Abstract iii

Publications and communications vi

Contents vii

List of figures x

List of tables xi

Symbols and Abbreviations xiii

General Introduction 3

Literature Review 4

1 **Thermal effect in materials- Generalities** 5

1.1 Introduction……..... … …….5

1.2 Temperature fields……..

1.2.1 Uniform Temperature…… …… ……5

1.2.2 Linear Temperature…… ……....5

1.2.3 Fire …… ……..5

1.2.3.1 The course of a fire …… ……...6

1.2.3.2 Development of a fire……..……..7

1.3 Literature review on structural, deaths, and financial damages caused by fire…… ……8

1.4 Functionally Graded Materials……..10

1.4.1 Definition of FGM……..11

1.4.2 advantages of functionally graded materials…… ….11

1.4.3 Applications of FGM …… ……...11

1.5.4 Civil engineering applications…… …...12

1.6 Conclusion.....14

2 Previous Works on behavior of structural elements in a heated environment 15

2.1 Introduction.....15

2.2 Static and buckling behavior of structural elements in a heated environment.....15

2.2.1 Effect of high temperature on static behavior of steel structural elements.....15

2.2.2 Effect of high temperature on static behavior of concrete structural elements.....18

2.2.3 Effect of high temperature on static behavior of functionally graded materials in structural elements.....20

2.3 Dynamic behavior of structural elements in a heated environment.....21

2.3.1 Effect of high temperature on dynamic behavior of steel structural elements.....22

2.3.2 Effect of high temperature on dynamic behavior of concrete structural elements.....23

2.3.3 Effect of high temperature on dynamic behavior of functionally graded materials in structural elements.....24

2.4 Conclusion.....25

II Numerical and analytical study of static and vibration behavior of steel beams subjected to temperature conditions 26

3 Finite element formulation and analytical analysis 27

3.1 introduction.....27

3.2 Numerical model used finite element.....27

3.2.1 Displacement field.....27

3.2.2 The resultant force and the moment.....30

3.2.3 The total potential energy.....30

3.2.4 The displacement vector and the functions of interpolation.....30

3.2.5 The strain-displacement relationship.....31

3.2.6 The static analysis.....32

3.2.7 Buckling analysis.....33

3.2.8 The resolution procedure.....33

3.2.9 The vibration analysis.....35

3.3 analytical model.....35

3.3.1 The bending moment.....36

3.3.2 Axial force in the beam.....37

3.4 Conclusion.....38

4 Application of numerical and analytical models - Results and discussions 39

4.1 introduction.....39

4.2 Validation of finite element model.....39

4.3 Parametric Study..... ... .48

4.3.1 Effect of temperature on the natural frequency of a steel beams.....48

4.3.2 Effect of slenderness and boundary conditions on steel beams under thermal conditions.....50

4.4 conclusion.....55

III **Numerical study of mechanical and thermal buckling behavior of functionally graded beam** 58

5 formulation of beam finite element based on enhanced Timoshenko beam theory 59

5.1 introduction.....59

5.2 Numerical model based on finite element formulation.....59

5.2.1 Displacement field..... 59

5.2.2 Kenematics 60

5.2.3 constitutive equations.....60

5.2.4 Position of the physical neutral axis..... 62

5.3 The total potential energy.....62

5.4 Finite element formulation..... 63

5.4.1 Static analysis..... ... 64

5.4.2 Mechanical buckling..... 65

5.4.3 Thermal buckling..... 66

5.5 conclusion.....66

6 Application of numerical model Results and discussion 67

6.1 introduction..... 67

6.2 Numerical results and discussion 67

6.2.1 Mechanical buckling 67

6.2.2 Thermal buckling.....70

6.3 Conclusion..... 76

General Introduction 77

Bibliography 80

List of Figures

Figure 1. 1 Fire Triangle..... 6

Figure 1. 2 Fire development phases..... 7

Figure 1. 3 The temperature-time phases of a well-ventilated fire compartment (with the ideal fire curve on the left; the curve on the right represents a typical temperature history of gases within a fire compartment..... ..8

Figure 1. 1 Some of the biggest fires in recent years 9

Figure 1.5 Functionally graded beam coordinate system and geometry..... 10

Figure 1. 6The curves of hardened concrete characteristics change with a gradual increase in porosity 12

Figure 1. 7 The main application fields of FGMs.....13

Figure 3. 1 Geometry and nodal variables of the beam finite element..... 28

Figure 3. 2 Generic bending beam with elastic end supports..... ...34

Figure 3. 3 The static diagram of the beam..... 36

Figure 4. 1 Restrained beam subjected to a uniform temperature rise on the left half..... 39

Figure 4. 2 the modulus of elasticity versus temperature rise Eurocode 3..... 40

Figure 4. 3 The horizontal displacement of the middle of the beam versus temperature rise..... 41

Figure 4. 4 The steel arch under a uniformly distributed gravity load 41

Figure 4. 5 The arch structural model for finite element analysis..... 42

Figure 4. 6 The vertical deflection along the arch..... 43

Figure 4. 7 The horizontal displacement along the arch..... 43

Figure 4. 8 The rotation angle along the arch..... 44

Figure 4. 9 The generic flexural element..... 44

Figure 4. 10 The beam structural model for finite element analysis..... 45

Figure 4. 11 The vertical deflection of the beam.....46

Figure 4. 12 Fundamental frequency of beam with length 15 cm..... 47

Figure 4. 13 Fundamental frequency +of beam with length 17 cm.....47

Figure 4. 14 The effect of temperature on the natural frequency of simply supported beam with different slenderness ratio.....49

Figure 4. 15 The effect of temperature on the natural frequency of clamped beam with different slenderness ratio.....49

Figure 4. 16 Beam with pinned end.....50

Figure 4. 17 Beam with fixed end.....50

Figure 4. 18 Beam with rotational elastic supports at the ends.....51

Figure 4. 19 Beam with elastic translational and rotational supports.....51

Figure 4. 20 The deflection of a beam pinned at both ends.....53

Figure 4. 21 The bending moment at the mid-span of a beam pinned at both ends.....53

Figure 4. 22 The deflection of a beam fixed at both ends.....53

Figure 4. 23 The bending moment at the mid-span of a beam fixed at both ends.....53

Figure 4. 24 The deflection at mid-span of a beam with rotational elastic supports at both ends.....54

Figure 4. 25 The bending moment at the mid-span of a beam with rotational elastic supports at both ends.....54

Figure 4. 26 The deflection of a beam with elastic translational and rotational supports.....54

Figure 4. 27 The bending moment at mid-span of a beam with elastic translational and rotational supports.....54

Figure 5. 1 Geometry and coordinate system of functionally graded beam.....59

Figure 5. 2 Variation of Young's mo+dulus through the thickness of functionally graded beams... ..59

Figure 5. 3 Position of the neutral axis of FG beams.....60

Figure 6. 1 The effect of length-to-depth ratio L/h on critical thermal buckling temperature of Si3N4/SUS304 beams with two clamped ends.....73

Figure 6. 2 The effect of length-to-depth ratio L/h critical thermal buckling temperature of Si3N4/SUS304 beams with simply supported ends..... 73

List of Tables

Table 4. 1 The horizontal displacement u_2 (mm) of beam center as a function of temperature rise..... 40

Table 4. 2 Fundamental beam frequency (Hz) under temperature conditions 46

Table 4. 3 Natural frequency of beam (Hz) under difference of temperature.....48

Table 4. 4 The material properties of steel IPE 80..... 48

Table 6. 1 The critical buckling load P_{cr} of a C-C FG beam subjected to axial compressive loading with different power law indices and L/h.....66

Table 6. 2 The critical buckling load P_{cr} of a S-S FG beam subjected to axial compressive loading with different power law indices and L/h.....67

Table 6. 3 The critical buckling load P_{cr} of a C-F FG beam subjected to axial compressive loading with different power law indices and L/h.....68

Table 6. 4 Critical thermal buckling temperature ΔTcr comparisons of Si3N4/SUS304 beams with two clamped ends according to Timoshenko beam theory (L/h=25)….....69

Table 6. 5 Critical thermal buckling temperature ΔTcr of Si3N4/SUS304 beams with temperature independent (TID) material under various beam theory 70

Table 6. 6 Critical thermal buckling temperature ΔTcr of Si3N4/SUS304 beams with different boundary conditions 72

Symbols and Abbreviations

Symbols

$\Delta T(z)$	change in temperature
T_0	ambient temperature
u_{10}	axial displacement
u_{20}	transverse displacement
ε^0	Membrane strain vector
ε^{nl}	Nonlinear strain vector.
α_T	thermal expansion coefficient
E_T	temperature-dependent Young's modulus
N	axial force
M	moment
E_0	Young's modulus at room temperature
A	cross-section area
I	moment of inertia
N^T	axial force due to temperature rise
M^T	moment due to temperature rise
A^*	extensional rigidity of the beam
D^*	bending rigidity of the beam
U	the deformation energy
V	the work of external forces
$[B_m]$	stretching matrix

$[B_f]$	bending strain matrix
$\{\delta\}$	nodal displacement vector
$[K_e]$	stiffness matrix
$[K_m]$	extension stiffness matrix
$[K_f]$	bending stiffness matrix
$[K_g]$	geometrical matrix
$\{F^e\}$	mechanical force vector
$\{F^T\}$	thermal vector force
$[S(x_1)]$	shape functions matrix
λ	loading factor
N_0	compressive force induced by a specified thermo-mechanical load
ΔT_{cr}	critical buckling temperature
N_{cr}	critical buckling load
[M]	mass matrix
ρ	mass density
f	natural frequency
q_v	uniformly distributed load
M_A	moment at the left end of the beam
M_B	moment at the left and right end of the beam
F_a^T	axial force due to temperature rise ΔT
θ_{A0}, θ_{B0}	the rotation angles of the ends of the beam due to distributed load
E_C	columns Young modulus
A_c	columns area cross-section
h_c	columns height
L_t	length of the tie
I_c	inertia moment of the column
$f(z)$	shear function
$V_c(z)$	volume fraction of the ceramic
E_c , E_m	Young's modulus of the ceramic and metal, respectively
p	volume fraction exponent

Q coefficient of elastic stiffness

e distance from the physical neutral axis to the centroid of the FG beam

W_d , W_a work done by external axial loads, and the work of distributed loads relative to the physical neutral axis

V volume of the beam

$\nabla_d(x)$ displacement or rotation at a specific point within the element.

∇_d^i displacement component associated with node i

N_i Lagrange shape functions associated with node i

$[B_a]$ axial matrix

$[B_b]$ bending matrix

$[B_s]$ shear strains matrix

$\{q\}$ displacement vector

Abbreviations:

FEM Finite Element Method

FGM Functionally Graded Material

SHSDT Simple high-order shear deformation theory

DOFs Degree of freedom

General introduction

The thermal impacts on the behavior of structural elements are of particular significance in Saharan environments, characterized by severe temperature variations, low humidity, and intensive solar radiation. Structures in these regions are subjected to thermal loads due to substantial daily temperature changes, which can range from scorching daytime heat to cool nighttime temperatures[1][2]. Such conditions necessitate a good understanding of how these heat changes affect the performance, stability, and durability of structural elements.

The high ambient temperatures in Saharan environments can lead to significant thermal expansion of materials[3]. This expansion, combined with the possibility of rapid nighttime cooling, can induce stresses within structural components and potentially leading to cracking, warping, or other forms of structural distress. Moreover, the use of building materials that do not adequately accommodate thermal movement can exacerbate these issues, resulting in a need for careful material selection and design considerations[4][5].

The high temperatures can significantly affect the behavior of these structures. One of the key impacts of high temperatures on a structure can be categorized as follows[6]:

- Degradation of the material's mechanical properties.

- Thermal stresses resulting from temperature gradients, which may cause thermal buckling.

- Changes in the stiffness and vibration characteristics of structural elements.

It is necessary to use powerful numerical methods for studying the behavior of structures subjected to the thermal conditions. One of the most popular methods employed today is the **finite element method,** which has become an essential tool for numerical analysis of structural behavior, thanks to its versatility and broad applicability.

The motivation behind this work is the investigation of the impact of elevated temperature on the behavior of structures, which are determined through their structural elements like beams, columns, etc. in a heated environment.

Thesis objectives:

The objective of this work is to modeling the static, vibration, and stability behaviors of structures in a thermal environment by developing a finite element model able to describe precisely the behaviors of this type of structure.

Thesis organization:

This research is organized into three sections:

- The first part, titled ''*Literature Review*'' includes chapters 1 and 2.

Chapter 1:

This chapter presents general information about temperature, fire, fire damage, and some notable fire incidents that have occurred in recent years.

On the other side, this chapter presents an overview of functionally graded materials, their manufacturing method, and application fields.

In ***chapter 2***, a review of several studies from the literature on the static, buckling, and vibration behavior of structural elements in a heated environment has been carried out.

- Part two entitled ''*Numerical and analytical study of static and vibration of steel beams subjected to temperature conditions*'' contains chapter 3 and 4.

In ***chapter 3***, a novel finite element, based on the Euler-Bernoulli beam theory and accounting for temperature rise, has been developed to examine the static and vibration behavior of steel beams. This approach incorporates the second-order term in the deformation-displacement relationship by considering the nonlinear Von Karman strain. The total potential energy principal has been utilized to drive the stiffness and geometric matrices.

Furthermore, a new analytical procedure has been established to examine the static behavior of steel beams under uniformly distributed loads and uniform temperature rise.

Chapter 4 is focused on validating the formulated finite element model in the analysis of static and vibration behavior of steel beams subjected to thermos-mechanical loading. Both uniform and linear temperature distributions across the depth of the beam are taken into account. The results in terms of deflection, bending moment, and natural frequencies were compared with those found in the literature.

In addition, a parametric study was carried out to investigate the influence of various boundary conditions on the beam's thermo-elastic bending behavior, using both finite element and analytical approaches.

- Part three entitled ''*Numerical study of thermal and mechanical buckling of functionally graded beams* '' contains chapter 5 and 6.

In ***chapter 5***, a novel simple high-order shear deformation theory **(SHSDT)** has been developed using the enhanced Timoshenko beam theory. The proposed finite element model is utilized to conduct the buckling analysis of functionally graded beams under thermo-mechanical loading. This model features only three unknowns, with zero shear stress conditions at the top and bottom surfaces of the beam. The beam's material properties are assumed to vary across its thickness according to a power law distribution based on the volume fractions of the constituent materials. The stiffness, geometric, and mass matrices are derived using the total potential energy and the Hamilton principles. No shear correction factor for the calculation of shear deformation is required.

Chapter 6:

Presents the results of thermal and mechanical buckling analysis of FG beams obtained with the finite element model **(SHSDT)** introduced in Chapter 5. A comparison of the results with existing literature demonstrates the effectiveness and accuracy of the suggested formulation.

The influence of various parameters, notably length/thickness ratio, power law index and boundary conditions, on the critical thermal buckling temperature and critical buckling load of functionally graded beams (FG) has been also studied.

At the final, the study concludes with a brief summary of the problem, describing the objectives and highlighting the main results. It also offers some perspectives for further research or development.

Part I
Literature Review

Chapter 1: Thermal effects in materials – Generalities

1.1 introduction

Structures in Saharan regions often operate under very harsh environmental conditions, such as high temperature, which can significantly influence the behavior of these structures. Consequently, the thermal effect of the materials presented in this study has been meticulously investigated to provide a solid foundation for understanding key aspects of nonlinear analysis. This approach aims to equip engineering students with the knowledge needed to tackle the complex nonlinear challenges they will face now and in the future.

It is therefore essential to understand the mechanical behavior of structures and their components under thermal loads.

This chapter presents the generalities of temperature, fire, damages caused by fire, and some notable fire incidents from recent years.

This chapter also deals with functionally graded materials (FGMs), a new class of advanced composites that are increasingly used in various fields of engineering, particularly in high-temperature applications such as thermomechanical load-bearing structures.

1.2 Temperature fields

1.2.1 Uniform Temperature

A uniform temperature indicates that the temperature is the same throughout a given space or medium. There are no temperature variations; every point in the defined area has the same temperature value. This condition often simplifies analysis in thermal studies, as it implies steady-state conditions.

$$T(z) = T_0 + \Delta T(z) \tag{1.1}$$

Where

$\Delta T(z)$ represents the change in temperature, while T_0 denotes the ambient temperature.

1.2.2 Linear Temperature

Linear temperature refers to a temperature distribution that varies uniformly in a straight line. This means that as one moves along a certain direction in a medium.

The relationship can be represented mathematically as a linear function, often depicted graphically as a straight line.

$$T(z) = T_0 + \Delta T\left(\frac{z}{h} + \frac{1}{2}\right) \quad (1.2)$$

1.2.3 Fire

A fire is a form of combustion. It occurs in controlled environments like furnaces and boilers. However, in the context of fire incidents, it can turn into uncontrolled combustion, leading to a fire outbreak

1.2.3.1 The course of a fire

For a fire (combustion) to start, three conditions must be simultaneously present, as illustrated in Figure 1.1:

Fuel: This includes flammable materials such as solids (wood, coal, paper), liquids (gasoline, alcohol), or gases (butane, propane).

Oxidizer: A chemical substance that supports the combustion process, such as oxygen, air, or peroxide.

Heat Source: An energy source needed to initiate combustion, which can be a flame, spark, or electrical discharge.

The presence of these three elements together forms what is known as the fire triangle, as shown in Figure 1.1. If any one of these elements is missing, combustion cannot occur

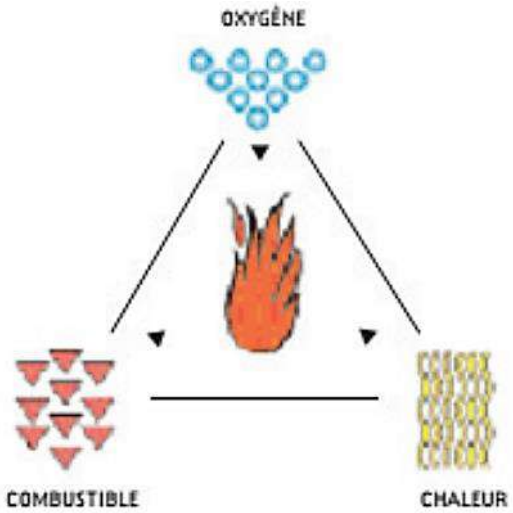

Figure 1. 1 Fire Triangle [7]

1.2.3.2 Development of a fire

Generally, the duration of a fire consists of the following stages: the development phase (ranging from ignition to flashover), the fully developed phase, and the decay phase. These stages are depicted in Figure 1.2, illustrating how temperature evolves in a compartment over time.

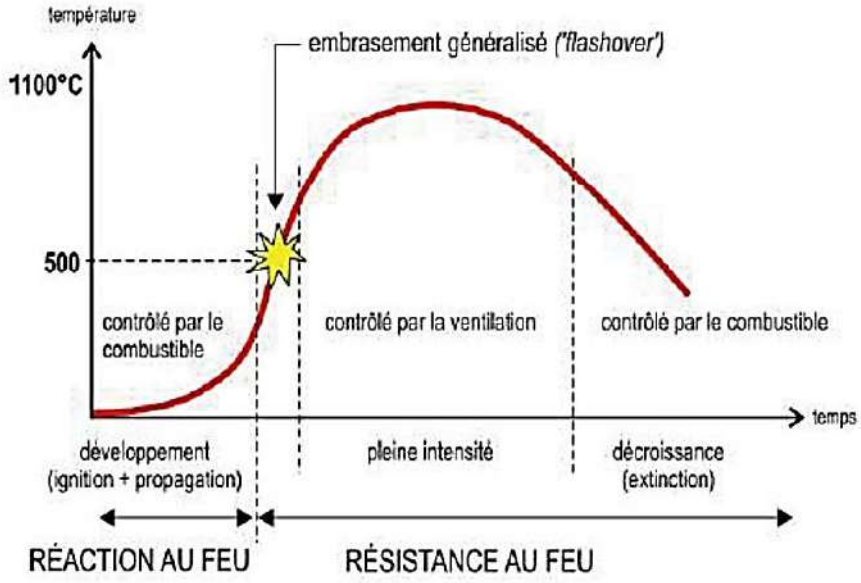

Figure 1. 2 Fire development phases [8]

During the evolution of a fire, a rapid transition between the first two stages, known as flashover, can occur. This typically happens at temperatures between 500 °C and 600 °C, depending on factors such as the availability of fuel, ventilation, and the fire's ability to spread. If these conditions are not met, the fire in the compartment may not generate enough heat for the flashover to take place, and it will remain weak near the ignition point (see Figure 3, left side, below the curve).

- *First phase "Fire development"*

A smoldering phase occurs, where the temperature remains localized at the ignition point. During this phase, the first signs of gas and smoke appear, and the fire smolders at a very low temperature, making its duration difficult to predict.

Next is the ignition phase, where the fire becomes more active but is still confined to a localized area. The heat radiation or direct contact from the flames starts affecting nearby materials, releasing hot gases that gradually fill the space.

Flashover:

As the hot gases accumulate, they heat nearby combustibles to the point of ignition. This results in a sudden and rapid spread of fire within a short period.

- *Second phase "Fully Developed"*

The temperature reaches its peak and then gradually decreases, as noted in[9] , until it drops to 80% of the maximum value (Figure 1.3, right).

➢ *Third phase "Decay"*

The fire's intensity diminishes as the available fuel is progressively exhausted.
The intensity of the fire and the duration of each phase are influenced by several factors:

- the amount and distribution of combustible materials (fuel load);
- the combustion rate of these materials
- ventilation conditions (openings);
- compartment geometry;
- thermal properties of the compartment walls;
- active fire suppression measures.

Among these factors, fuel load and ventilation are the most critical. A fire is fuel-controlled when sufficient oxygen is available for combustion, while it becomes ventilation-controlled when oxygen is limited.

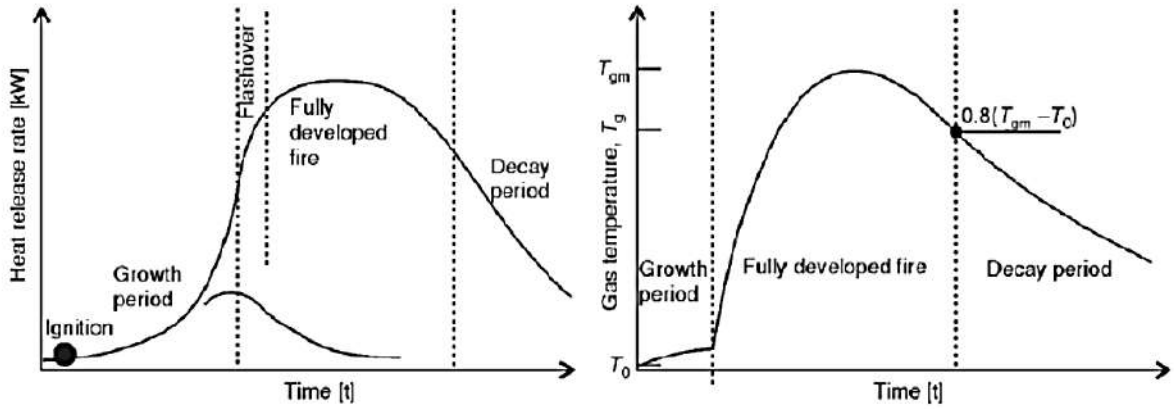

Figure 1. 3 The temperature-time phases of a well-ventilated fire compartment (with the ideal fire curve on the left; the curve on the right represents a typical temperature history of gases within a fire compartment.

1.3 Literature review on structural, deaths, and financial damages caused by fire :

Fire risk re- remains the main challenge, every year around 3.8 million fires are recorded worldwide, causing the death of some 44,300 people. Between 1993 and 2015, over 86.4 million fire incidents were recorded, resulting in more than one million deaths related to fires and causing an estimated financial loss of approximately USD 858 billion. Developed countries report an average of 5,000 fire-related deaths annually, while developing countries experience around 15,000 fire fatalities each year [9]. In Spain, 77% of fatal fires are reported to occur in residential buildings.[10].

Between 2005 and 2015, Canada recorded approximately 460,000 fire incidents, resulting in 15,327 deaths and causing financial losses estimated at CAD 7.3 billion.[11]. Approximately 1.2 million Canadians were directly impacted by fires [12].

In 2017, the United States experienced over 1.3 million fires, which led to 3,400 deaths, 14,670 injuries, and an estimated $23 billion in property damage. The fire and burn death rates were 0.38 per 100,000 individuals in Spain, 1.16 in the USA, and 0.88 in Canada. British Columbia,

Canada, reported approximately 24,000 fires across eight major cities, with 67% of these incidents linked to residential buildings. Additionally, 55% of the fires were associated with multi-unit residential buildings (MURBs), resulting in significant consequences [9].

In the United Kingdom, approximately 450 individuals lose their lives to fires, while Sweden sees around 100 fatalities each year, and the United States experiences over 3,000 fire-related deaths. In many Western countries, the annual fire death rate ranges from 0.5 to 1.5 per 100,000 people[13]. The probability of fire incidents occurring in certain social environments such as facilities handling hazardous chemicals, historic buildings, and educational campuses can be illustrated in Figure 1.4[14].

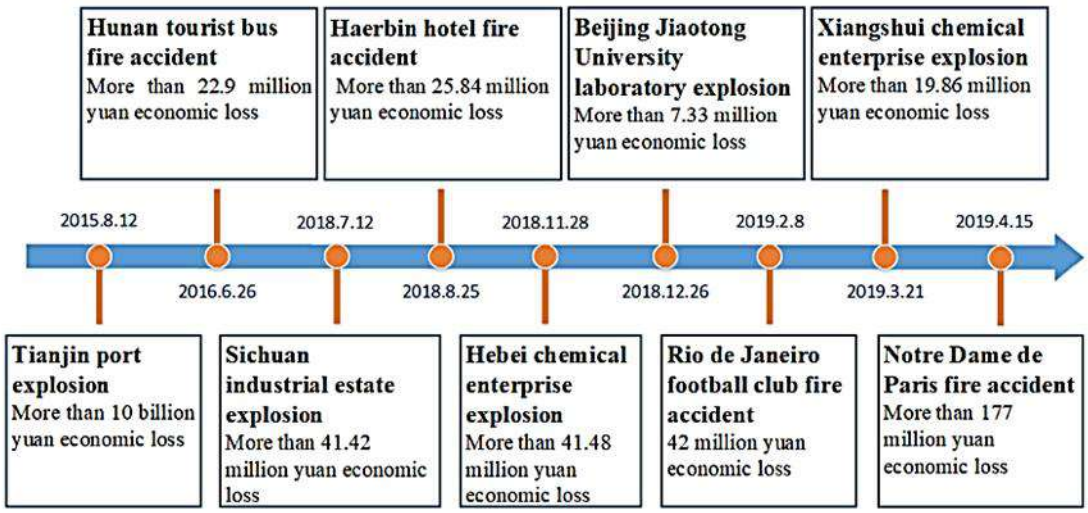

Figure 1. 4 Some of the biggest fires in recent years[8]

Here are some notable fire incidents from recent years that had significant impacts:

- **Notre Dame Cathedral Fire (2019, Paris, France)**: A catastrophic fire broke out on April 15, causing extensive damage to the historic structure, particularly its roof and spire. Approximately 400 firefighters worked for two days to contain the blaze, successfully saving much of the cathedral's structure. Thankfully, no lives were lost during this incident.
- **Camp Fire (2018, Paradise, California, USA)**: This devastating wildfire, ignited by a damaged electrical transmission line, burned over 153,000 acres and destroyed nearly 14,000 structures. It resulted in 85 fatalities, marking it as the deadliest fire in California's history.
- **Grenfell Tower Fire (2017, London, England)**: A small refrigerator fire escalated into a major incident, claiming 71 lives and making it one of the deadliest fires in British history. The fire highlighted serious safety issues in high-rise residential buildings.
- **Ghost Ship Warehouse Fire (2016, Oakland, California, USA)**: A fire in a converted warehouse during a party led to the deaths of 36 people. The building lacked proper safety measures and was considered an illegal residence, prompting discussions about fire safety regulations.

- **Yarnell Hill Fire (2013, Yarnell, Arizona, USA)**: Triggered by a lightning strike, this fire tragically claimed the lives of 19 firefighters, marking it as one of the deadliest days for U.S. firefighters in recent history.

Various researchers have explored fire risk factors in specific types of buildings, including residential structures [15], hotels[16], high-rise buildings [17], older buildings[18], and wooden constructions[19].

1.4 Functionally Graded Materials:

The rise of industries and the growing need for advanced structural expertise in multiple engineering disciplines have led to the development of new composite materials called Functionally Graded Materials (FGMs) Chen and Goto [20]

1.4.1 Definition of FGM:

The concept of FGMs was first introduced in Japan in 1984, during a space plane project, where they were utilized for thermal barrier applications[21]. The idea behind FGMs was developed to address thermal stress issues in conventional laminated composite materials used in reusable rocket engines[22]. In summary, the FGM concept consists of replacing the abrupt composition change at the interface between various materials with a gradual composition change transition with a graduated composition. This approach helps reduce stress concentrations within the structure.

In general, an FG porous material is composed of a mixture of isotropic components like ceramic and metal, Thermo-mechanical properties vary continuously from one surface to another. Metal-ceramic FGMs are generally used in high-temperature applications, when the ceramic component gives superior thermal resistance. While the metal component enhances mechanical strength and lowers the risk of catastrophic fracture.

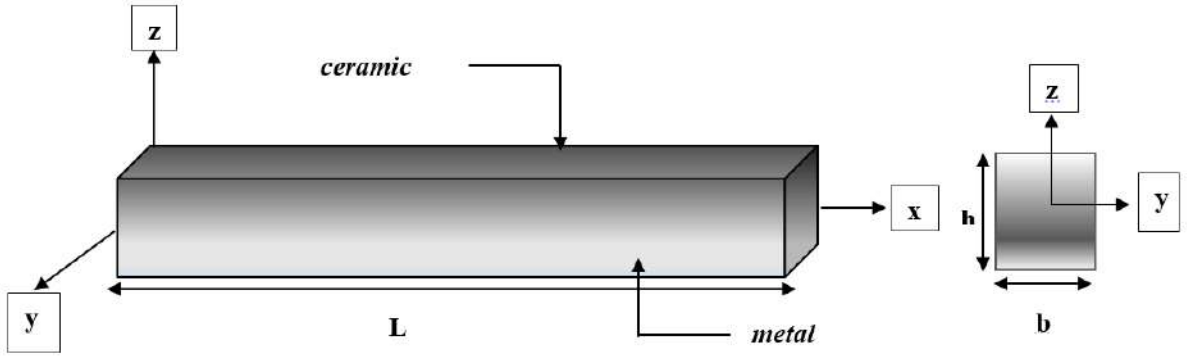

Figure 1.5 Coordinate system and geometry of functionally graded beam

1.4.1 advantages of functionally graded materials

A number of advantages of functionally graded materials may be identified , which we would like to briefly highlight [23]

- Thanks to their gradient interfaces, FGMs can effectively reduce thermal and mechanical stress concentrations, which helps prevent relamination in crack-prone areas and enhances the durability of load-bearing structures.
- Metal-ceramic FGMs smooth out the transition between differing thermal expansion rates, offer protection against thermal and corrosion damage, and enhance load-bearing performance.
- - FGMs can be used as an interface layer between two different incompatible materials. improving bond strength and reducing crack-driving forces within the material. They offer multifunctionality, such as controlling deformation, wear, corrosion, and vibration. Additionally, FGM coatings help reduce internal residual stresses.
- - FGMs with calibrated porosity effectively absorb shocks from side to the other, provide thermal insulation, improve the catalytic efficiency, and help reduce electrical and thermal stress.

1.4.2 Applications of FGM

Figure 1.8 illustrates the different applications of functionally graded materials (FGMs). They were originally designed for aerospace structures and fusion reactors because of their ability to endure extreme thermal stresses. Over time, their application has broadened to numerous fields, thanks to their impressive performance under very harsh conditions. Due to its resistance to thermal fatigue and long lifespan, ceramics are commonly utilized as thermal barriers in engines, gas turbines, optical applications, probes, triggers, metal/ceramic armor, photoelectric detectors, and dental implants. Nowadays, the materials produced are lighter and more efficient, exhibiting exceptional strength and durability. Their applications have broadened to include numerous fields such as civil engineering, public works, nuclear energy, electronics, and optics[24].

1.4.3 Civil engineering applications

Functionally graded materials have received a great deal of attention and found applications in a wide range of fields. which includes mechanical and civil engineering, aerospace, and electronics, among others[25][26].

The functional gradation of concrete elements makes it possible to adapt the internal composition of structural components to meet specific structural and thermal performance requirements. This alignment is achieved by continuously varying the material's properties, like porosity, strength or rigidity, up to three spatial dimensions. This approach can be employed to reduce the mass of the element while introducing multifunctional properties. Reducing porosity improves concrete's structural strength, while increasing porosity enhances its thermal insulation properties. Figure 1.9 shows the relationship between the properties of hardened concrete and a progressive increase in porosity[27].

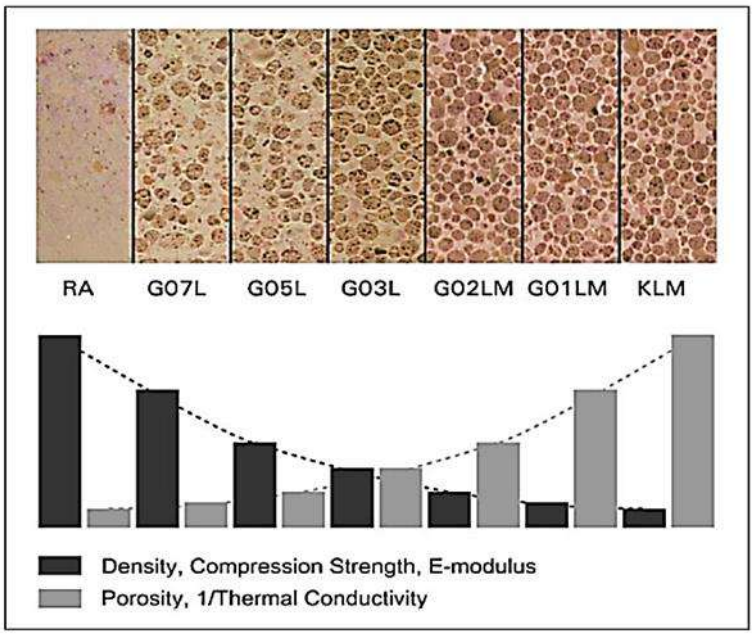

Figure 1.6 curve of the characteristics of hardened concrete change with a progressive increase in porosity [27]

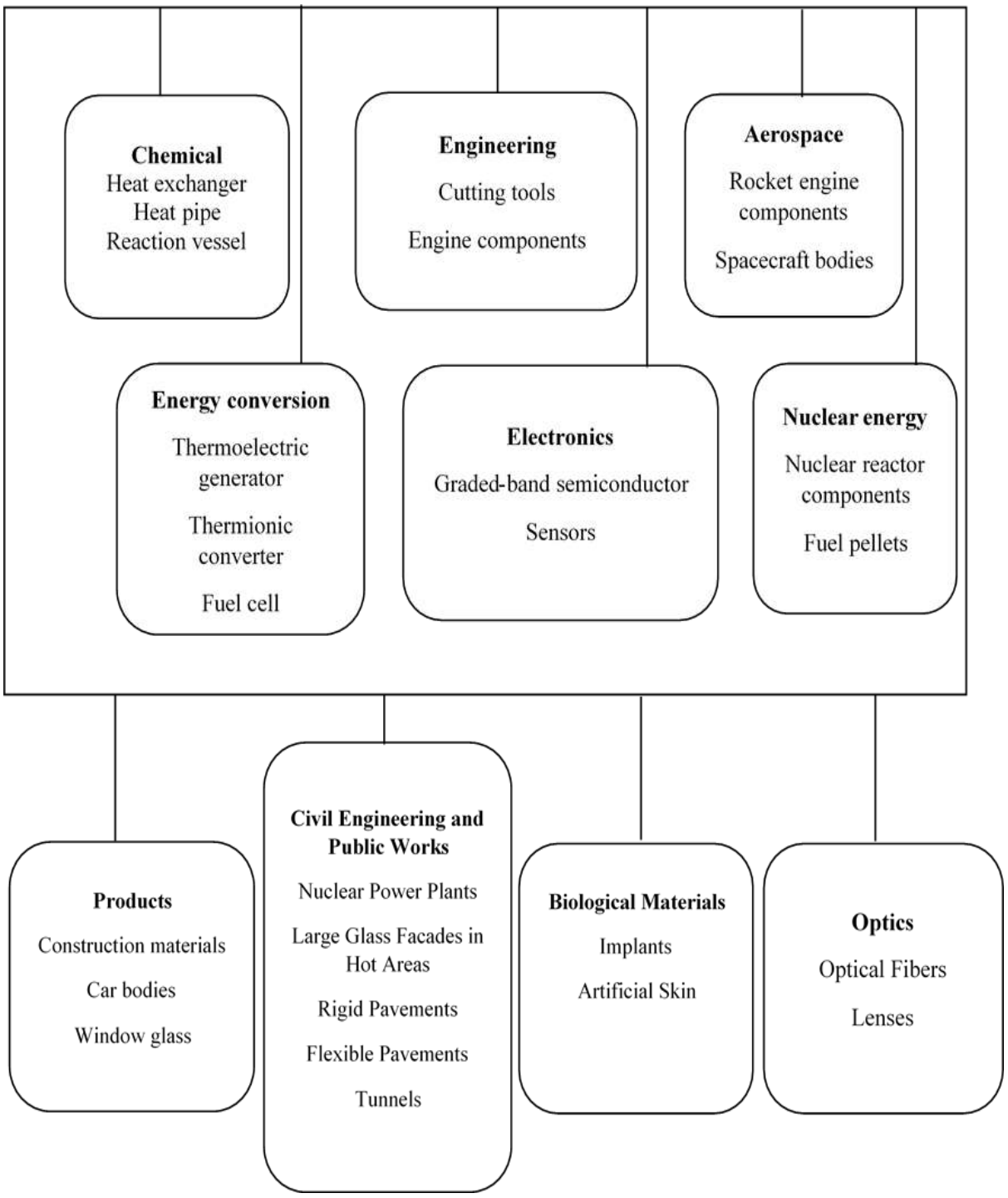

Figure 1.7 The main application fields of FGMs

1.5 conclusion

The generalities of temperature, fire, damages caused by fire, and some notable fire incidents from recent years are given in this chapter.

Other hand, this chapter includes the generalities of Functionally Graded Materials, advantages of functionally graded materials, and Applications. In view of the wide applicability of FGMs, it is essential to study their behavior. Precise prediction of the behavior of FG structures. Numerous theoretical, analytical, and numerical approaches have been documented in the literature.

The next chapter reviews the differing theories used to analyze the thermal effect on structural behavior and gives an overview of investigations into the static, buckling, and vibration behavior of certain material structures such as steel, concrete and FGM.

Chapter 2 : Previous works on the behavior of structural elements in a heated environment

2.1 Introduction

In this section, we aim to review the work carried out to date to study the behavior of structural elements in a heating environment. The review is focused primarily on statics, buckling, and dynamic analysis of structural elements. The objective here is to highlight the breadth of research in the field of the behavior of structural elements in a heated environment while emphasizing that there remains significant work to be done in this area.

The analysis of static, buckling, or dynamic behavior of structures subjected to high temperatures represents a major challenge due to the nonlinearity of the phenomenon. A number of studies have been carried out over the last few decades to assess this phenomenon using numerical, analytical, or experimental methods.

2.2 Static and buckling behavior of structural elements in a heated environment :

2.2.1 Effect of high temperature on static behavior of steel structural elements

The study of steel structures exposed to different extreme loads, like fire and impact, has received particular attention[3][28]. The effect of high temperatures is one of the most important factors in efficient structural design. Therefore, it is important to understand the mechanical behavior of structural steel components when subjected to thermal loads. It is well known that a significant increase in temperature can have an impact on the steel's mechanical properties, such as modulus of elasticity and elastic limit, causing them to decline rapidly[4][5].

One of the first experimental studies on this subject was carried out by Rubert and Schaumann (1986)[29]. A series of mechanical tests were carried out on steel beams and frames exposed to the fire.

Saab and Nethercot (1991) [30] proposed a finite element formulation to examine the non-linear behavior of two-dimensional steel frames under fire conditions.

Najjar and Burgess (1996)[31] developed an analytical method to study the non-linear behavior of 3D steel frames in fire conditions. Pchelintsev et al(1997)[32] introduces experimental heat transfer and temperature correlations to examine the behavior of steel beams under localized fires. Additionally, the authors developed a finite volume code, CV-FEM, and utilized the finite element software ANSYS for numerical simulations.

The impact of connected heated steel beams on column behavior when subjected to fire in a multi-story braced steel frame was examined by Bailey et al (1999) [33].

In 2000, the authors presented an analytical study of the structural behavior of columns in different structural and fire scenarios[34]. Also, Rodrigues [35]carried out an experimental study of the critical temperature of compressed restrained steel elements. In addition, a simple numerical method was suggested by Song et al[36] to integrate adaptive nonlinear analysis of the static behavior of steel structures under the effect of fire and explosion.

Theoretical models suggested by Usmani et al (2001) [37] for studying the behavior of framed structures under the effects of temperature. Liu et al (2002)[38] studied the effect of connections and axial stress in a steel beam tested under fire conditions. Test results indicated that the catenary action was more pronounced at lower load levels and greater axial stress, but only became apparent at high deflections. Tan et al (2002)[39] introduced a new finite element model for analyzing steel frames at elevated temperatures. Z Huang et al (2004)[40] created a three-dimensional nonlinear finite element model to investigate steel-reinforced concrete and composite structures exposed to fire conditions. The element is modelled on Bathe's general formulations and is suitable for a variety of cross-sections. Ali et al. (2004)[41] presented a non-linear finite element model for studying the fire performance of steel structures. An analytical study to assess the impact of support conditions on the performance of steel beams and steel-concrete composite beams in the fire was presented by Moss et al (2004)[42]. The analysis was conducted under conditions of temperatures that increased linearly over time. Yin and Wang (2004)[43] also carried out a numerical study of the behavior of axially restrained steel beams subjected to fire conditions. The authors have taken into account the influence of non-uniform temperature distribution. Wald et al (2006)[44] implemented an experimental program within a collaborative research project to study the behavior of structures exposed to natural fire.

In 2007, The behavior of axially restrained steel beams subjected to fire conditions was studied by Li et al[45] with a numerical approach. Gardner [46] employed the finite element software ABAQUS for analyzing the buckling behavior of stainless steel structural elements. The author discovered that the interaction between strength and stiffness at elevated temperatures has a major influence on the buckling performance of stainless steel columns and beams.

Li and Guo (2007)[47] studied the behavior of constrained steel beams exposed to natural fire and uniform fire. Bradford et al(2008)[48] conducted a generic nonlinear analysis of a steel beam with restrained ends in the elastic domain of structural response, utilizing the principle virtual work principle. Qian et al (2009)[49] carried out a series of numerical and analytical studies to analyze the behavior of steel-beam-column joints exposed to high temperatures. In the same year, Heidarpour and Bradford [50]conducted a generic nonlinear study of an insulated steel beam whose ends are restrained at elevated temperatures. Heidarpour et al (2010)[51] introduced a non-linear thermoelastic investigation of steel arches exposed to uniformly distributed loading at elevated temperatures, using a formulation that takes into account the degradation of steel arc stiffness before failure at elevated temperatures. The steel bow is retained at two ends by translational springs in the horizontal and vertical directions and by the corresponding rotational springs. The impact of transverse thermal gradients on the behavior of steel beam-columns under fire conditions was examined by[52]et al (2010). These

studies used different heating techniques and tested specimens using and not using fireproof materials, resulting in significant transverse temperature gradients in some cases. Lien et al (2010) [53]examined the nonlinear behavior of steel structures in fire conditions by applying the vector-form intrinsic finite element method. A new numerical approach was developed by Dwaikat and Kodur(2011)[54] assess fire-affected forces and deflections in the retained steel beams. Lopes et al (2012) [55] created of innovative design proposals for stainless steel structural elements exposed to axial compression and bending in the case of fire. A novel method was proposed by Xu and Zhoo (2012)[56] for analyzing simply supported beams with varying thicknesses under thermo-mechanical load. Jeffers and Sotelino (2012)[57] used a computationally efficient fiber element model to represent the thermo-mechanical behavior of a simple-supported steel beam subject to localized fire.

Jiang and Usmani (2013)[58] introduced a numerical model applying Opensees software to analyze the fire behavior of beams, frames and plates. An experimental approach and numerical simulation of a steel beam to investigate a localized fire scenario under real and controlled fire loading conditions conducted by Zhang et al (2013)[59].

Sharma and Kaur (2015)[60] applied a meshless method using Euler-Bernoulli theory to study the bending vibration behavior of homogeneous, simply supported structures. The numerical analysis of the flexural and compressive strength of numerous steel sections at elevated temperatures was carried out using SAFIR finite element analysis software. was carried out by Couto et al.(2015)[61]. Prachar et al (2015)[62] performed a number of tests to investigate the local and lateral-torsional buckling of Class 4 beam sections under fire conditions in steady-state conditions. The large deflections of retained corrugated steel beams under non-uniform temperature distribution across the section exposed to fire conditions are calculated using a finite element model (Wang et al. 2016)[63].

A study was carried out to analyze the behavior of a steel I-beam under constant and variable temperature conditions. Based on the results, a formula was proposed to calculate the capacity of the beam, taking into account the temperature gradient, the shape of the section and the type of steel used. However, the expertise is limited to the study of local failure under uniform bending load conditions Ragheb (2017) [64]. Li and Zhang (2017)[65]explored the integrated fire-structure simulation approach for performance-based fire safety design. Varol and Cashell (2017)[66]examined the lateral-torsional buckling performance of beams that are not laterally restrained. A finite element model was built to analyze this behavior at ambient and high temperatures.

Zhang et al(2018)[67] studied the thermal response of the elements of a steel structure using finite element software. A numerical investigation was studied by Pournaghshband et al. (2019) [68]for analyzing the behavior of axially restrained steel beams under fire conditions.

In 2020. Ramesh et al [69]carried out an experimental study of the behavior of steel columns and simply supported steel beams exposed to fire. A novel multidimensional material model was developed by Zhou et al [70]to investigate combined isotropic and kinematic plasticity in the thermomechanical study of stainless steel structures at high temperatures. In the same year, the analysis of lateral-torsional buckling of steel beams at elevated temperatures with a finite element model was investigated by Kucukler[71]. Zhong Zhang et al[5] also examined the thermo-elastic behavior of steel beams subjected to thermomechanical loads, utilizing the exact

2D thermoelasticity theory. The beams are simply supported and the material is temperature dependent. Tests to evaluate the fire resistance and loading capacity of box columns was carried out by Yang et al (2020)[72]. Laim et al (2020)[73]examined the behavior of cold-formed, intermediate and edge-stiffened steel exposed to fire.

A numerical method for studying the behavior of stainless steel frames at high temperatures was used by Segura et al.(2021)[74]. A numerical study on steel H-beams under pure bending was presented by Nguyen and Park (2021)[75]. They found that the lateral-torsional buckling (LTB) resistance of a beam exposed to a localized fire decreases more slowly than when exposed to an ISO-834 compliant fire. It was shown that the position of the fire source and the beam's length-to-height ratio significantly affect its resistance to lateral-torsional buckling (LTB).

Suman and Samanta [76][77][78]studied the response of monosymmetrical beams to fire and different load conditions, and found that beams presenting a greater degree of monosymmetry performed better than beams presenting a lesser degree of monosymmetry.

Kucukler (2022)[79]examined a finite element model to investigate the response and design of steel I-beam columns under fire conditions. Suman et al. (2022)[80] carried out tests in an open environment to investigate the localized propagation of fire on hot-rolled and cold-formed steel beams, in both longitudinal and transverse directions, using a gas burner as the source of fire. Gurupatham et al (2022)[81] investigated both open and closed channels columns through experimental and numerical studies to assess the applicability and the accuracy of the Direct Strength Method (DSM) in predicting axial capacity and post-buckling behavior. A parametrical analysis of cold-formed, back-to-back steel sections subjected to axial compressive loads at high temperatures, with the temperature varying between 20 and 700 ◦C. was carried out by Fang et al (2022).[82]

Suman and Samanta (2023)[83] examined experimentally the behavior of laterally unrestrained beams in the event of localized fire, using a series of ten full-scale tests on simply supported beams of short to medium length. The tests involved applying a single point load at mid-span of the I-beam. X. Guo et al (2023)[84] studied the failure modes and impact resistance of three common joint types in restrained beams exposed to impact after a localized fire, using experiments and numerical simulations.

Recently,in 2024, Suman et al[85] examined the behavior of monosymmetrical steel I-beams under uniform fire conditions and gradually increasing loads . Habashneh et al[86]proposed a topology optimization for steel beams exposed to elevated temperatures, taking into account the geometrically nonlinear analysis of imperfect structures.

2.2.2Effect of high temperature on static behavior of concrete structural elements

Concrete is a versatile construction material valued for its strength, durability, and fire resistance. However, when subjected to elevated temperatures, its properties can change significantly, potentially leading to structural failure[87].

In 1988,Schneider [88]conducted study on the mechanical properties of concrete at elevated temperature.This includes changes in flexural strength, compressive strength, and stress-strain

behavior.Terro(1998)[89]developed finite element thermal and structural computer models for predict the behavior of three-dimensional reinforced concrete structures exposed to fire.

The failure temperature of a system consisting of a restrained column subjected to fire conditions was investigated by Franssen (2000)[90].Lim et al (2002)[91] performed the fire tests on three reinforced concrete slabs. The test results indicate that corner restraints significantly affect the deformation of concrete slabs.In 2004,Lim et al[92] also utilized the Von Mises plasticity theory to simulate the biaxial behavior of concrete under high-temperature conditions. The model results aligned with the fire tests and indicated that the associated plasticity model for concrete under biaxial compression could provide a suitable approximation. Bailey and Toh (2007)[93] examined the concrete slabs under both ambient and elevated temperatures. Two failure modes were observed at ambient temperature: reinforcement fracture and concrete crushing at the corners of the slab. At elevated temperatures, all tests resulted in failure due to reinforcement fracture. The behavior of concrete in fire is not well understood and further research is needed in nearly every aspect of this field. The response of concrete materials to heating is fundamentally complex and its properties can change dramatically when exposed to high temperatures (Fletcher et al) 2007[94]. A numerical model to simulate the behavior of reinforced concrete (RC) beams subjected to fire was introduced by Kodur and Dwaikat(2008)[95]. An efficient nonlinear 3-D finite element model was presented by Young and Ellobody(2011)[96] for analyzing axially restrained, pin-ended concrete-encased steel composite columns at elevated temperatures. The behavior of self-compacting reinforced concrete slabs when exposed to fire was investigated by Ammar et al (2012)[97]. The study revealed that the slabs' ultimate load-carrying capacity decreased and their deflections increased when subjected to fire. Wang et al(2013)[98] introduced a transient strain model for concrete that includes a transient modulus under biaxial stress conditions. Along with a failure criterion to evaluate the fire resistance of two-way reinforced concrete slabs. Bikhiet et al (2014)[99] examined an experimental investigation of reinforced concrete short columns exposed to fire under axial load to evaluate the reduction in column compressive capacity after the fire. Liao & Huang (2015)[100]developed a model with advanced numerical techniques to evaluate both the structural stability (global behavior) and integrity (localized fractures) of reinforced concrete members under fire conditions. Experimental studies have been carried out on the fire behavior of composite columns made up of hollow sections filled with concrete under various structural conditions Rodrigues and Laim(2017)[101]. A numerical analysis of the mechanism of tensile membrane action in reinforced concrete slabs subjected to large displacements and high temperatures was presented by Jiang and Li(2018)[102]. Waleed et al (2019)[103] examined the impact of fire on reinforced-concrete slabs. They observed that the load capacity of the slabs diminishes with longer exposure times and higher temperatures. Additionally, they found that spalling reduced as the thickness of the concrete cover increased. A design method for structural fire safety of square and rectangular textile-reinforced concrete (TRC) columns was developed by Yang et al (2021)[104], using fire resistance tests and numerical studies.

Balamurali et al (2023)[105] presented the behavior of self-compacting concrete (SCC) with the incorporation of fly ash (FA), silica fume (SF), and metakaolin (MK) following exposure to high temperatures. The results indicated that specimens with metakaolin (MK) exhibited lower strength compared to those with silica fume (SF) and fly ash (FA) mixes. The structural

performance of reinforced truss concrete composite slabs during and after the fire through an experimental study was discussed by Bing Li et al (2023)[106]. Salihu et al (2023)[107]presented a fire resistance behavior of two-way reinforced concrete (RC) slabs. The study examines how specific parameters such as concrete cover thickness, span, and support conditions affect the fire resistance of the slabs.

Aldarf et al (2024)[87] studied the impact of increased temperatures and larger flame areas on the resistance of reinforced concrete slabs. The results revealed that higher temperatures and larger flame areas significantly decrease the resistance of the slabs.

2.2.3Effect of high temperature on static behavior of functionally graded materials in structural elements

Numerous authors have applied different theories to analyze the thermomechanical behavior of functionally graded beams.

In 1998, Praveen and Reddy[108]investigated the nonlinear transient thermoelastic deformations of an FGM plate. Khdeir (2001)[109]examined the buckling of cross-ply laminated composite beams using various beam theories and different edge conditions. He found that the results from the third-order and first-order beam theories showed good agreement. Mossavarali and Eslami (2002)[110] utilized the higher-order displacement formulation for shear-deformable plates to determine the critical buckling temperature of imperfect orthotropic plates. The buckling of functionally graded material curved beams under linear thermal loading, examining both in-plane and out-of-plane buckling was explored by Rastgo et al. (2005)[111]. A numerical thermal post-buckling of clamped FGM TBs was studied by Liet al(2006) [112]with the shooting method using the non-linear first-order shear deformation beam theory(FSDT).

Song and Li [113] and Li and Batra (2007)[114] presented an analysis of thermal buckling and post-buckling deformations of Euler-Bernoulli beams (EBBs) resting on two-parameter non-linear elastic foundations under various boundary conditions. The static behavior of FGM beams under a uniformly distributed load and ambient temperature using the Higher-Order Shear Deformation Theory (HSDT) was studied by Kadoli et al (2007)[115]Vaz et al(2007)[116] employed the perturbation analysis to derive an analytical method for the initial post-buckling behavior of a slender rod supported by a linear elastic foundation and exposed to a uniform temperature gradient.

The uniaxial and uniform temperature rise buckling of functionally graded plates with circular or square holes, using the first-order shear deformation plate theory. The study considered fully clamped and fully simply supported edge conditions and employed the Element-free Kp-Ritz formulation was examined by Zhao et al. (2009)[117].Kiani and Eslami(2010)[118] presented the thermal buckling analysis of FGM beams using the Euler-Bernoulli beam theory. A numerical study on the non-linear first-order shear deformation beam theory(FSDT), utilizing the shooting method of S-SFGM beams exposed to uniform in-plane thermal loads was introduced by Ma and Lee (2011)[119].

Esfahani et al(2013)[120]examined the thermal buckling and post-buckling deformations of FGM Timoshenko beams (TBs) based on three-parameter nonlinear elastic foundations under

five possible boundary conditions, considering two types of thermal loads. Shen et al(2014)[121]discussed the thermal post-buckling of FGM beams with simply supported ends resting on an elastic foundation, using Reddy's higher-order shear deformation beam theory. The nonlinear thermal buckling and post-buckling behavior of functionally graded beams resting on a nonlinear elastic foundation, using the first-order shear deformation beam theory was studied by Sun et al (2016)[122]. She et al (2017)[123] introduced research on the thermal buckling and post-buckling behavior of FGM beams with or without piezoelectric layers under clamped end conditions.

In 2018, The nonlinear thermal behavior of geometrically imperfect functionally graded material (FGM) beams under heat conduction was investigated by Dehrouyeh-Semnani [124]. Mojahedin et al[125] developed an analytical method for FG porous beams thermoelastic behavior analysis.

In the following year, Babaei et al[126][127]conducted a study on the buckling and post-buckling behavior of geometrically imperfect functionally graded material (FGM) tubes with immovable clamped and pinned boundary conditions, subjected to both mechanical and thermal loads.

A study on the buckling and post-buckling behavior of beams on an elastic foundation subjected to thermal loading was introduced by Wen et al (2020)[128]. The virtual work principle is used to derive the governing equation for buckling and the differential equilibrium equation for post-buckling.

Penna (2021)[129] utilized the elasticity theory to examine the impact of moisture, temperature, and mechanical loading on the bending behavior of porous functionally graded (FG) nano-beams. The buckling behavior of functionally graded rectangular plates subjected to mechanical and thermal loads was analyzed by Tati (2021)[130], utilizing a four-node finite element approach for simple high-order shear deformation theory. The bending sensitivity of functionally graded plates on two-parameter elastic foundations under hygro-thermomechanical loading was investigated by Rachedi et al (2023)[131]. This analysis using a quasi-3D high-shear deformation theory, which involves only five unknowns.

2.3 Dynamic behavior of structural elements in a heated environment:

In general, temperature has an impact on the vibratory properties of a structure: by modifying the modulus of elasticity, by altering structural damping, and affecting the size of the structure.

A small change in temperature can lead to a significant variation in beam vibration behavior[132].

In this context, various analytical, numerical, and experimental methods have been employed to obtain exact solutions.

2.3.1 Effect of high temperature on the dynamic behavior of Steel structural elements

Numerous studies was focused on the dynamic behavior of steel exposed to elevated temperatures, both during and after exposure to high temperatures.

Rodrigo and Daniel (2002)[133] presented an analytical study on the vibration behavior of a clamped beam under the effect of a uniform temperature, using an analytical model, based on Euler-Bernoulli's beam theory incorporating the appropriate boundary conditions.

The mathematical model was developed by Avsec and Oblak(2007)[132] for analyzing the thermal impact on the dynamical behavior of clamped and simply supported beams.

Nayeri et al(2008)[134] developed a novel approach for monitoring A 17-story steel frame building, revealing a strong correlation between structural frequencies and air temperature. However, changes in frequency lagged a few hours behind temperature variations. Sun et al(2012)[135]developed a new model for studying the dynamic and static behavior of steel buildings during the local and global progressive collapse of the structures subjected to fire conditions, using the Vulcan software.

The thermal impact on the steel beam was examined by Zhang et al (2014)[136] utilizing the energy flow method. This study highlighted that thermal vibrations intensify as temperature rises, primarily due to thermal loads and alterations in material properties. In the same way, Cui and Hu (2014)[137] studied the thermal buckling and vibration of a simply supported steel beam, It was noted that temperature-dependent material properties have minimal impact on the natural frequency at low temperatures. However, a significant impact was observed as the temperature increased.

Lai and Zhang (2018)[138]analyzed the thermal effects of vibration and buckling behavior of cracked thin plates. Their findings showed that thermal effects have a substantial impact on the dynamic behavior of structural elements. A modal analysis of a heated rectangular plate with a non-uniform temperature distribution was conducted by Silva et al(2019)[139] using digital image correlation. They discovered that the resonant frequencies of the plate were higher with transverse heating compared to longitudinal heating. Hossain and Lellep (2020)[140] investigated the impact of temperature on the dynamic behavior of cracked metallic and composite beams was investigated utilizing the Euler-Bernoulli beam model.

The effects of heating rates on the vibrational behavior of a cantilever beam, both with and without cracks was presented by Kamei et al (2021)[141]. The results indicated that the modal parameters of the cantilever beam are influenced by changes in temperature and heating rate. The buckling and vibration characteristics of cold-formed steel sections subjected to a temperature field was examined by Wu et al(2022) [142] utilizing the finite strip method.

Recently, Theoretical analysis and experimental validation of vibration in interconnected composite steel beams with fixed ends operating under thermal conditions was carried out by Zang et al(2024)[143].

2.3.2 Effect of high temperature on the dynamic behavior of concrete structural elements

Mainly research has concentrated on the dynamic behavior of concrete at room temperature and its degradation under fire conditions. However, studies combining the effects of strain rate and strain-rate hardening remain relatively limited.

For nearly two years, Xia et al(2006)[144] introduced experiments that were carried out on a continuous concrete slab. It was obtained that the frequencies exhibited a strong negative correlation with both temperature and humidity, while the damping ratios showed a positive correlation, but no distinct correlation was observed between mode shapes and variations in temperature or humidity. A long-term vibration test on two reinforced concrete buildings was performed by Clinton et al(2006)[145], one with three stories and the other with nine stories. Liu and DeWolf(2007) [146] also presented the study of the thermal vibration on a curved post-tensioned concrete bridge.

Tao and Li (2009)[147] conducted an experimental investigation on the dynamic behavior of concrete at elevated temperatures, reaching up to 600°C, using a split-Hopkinson pressure bar (SHPB) test apparatus. The test results revealed a significant reduction in dynamic strength with increasing temperature, while the ductility of the concrete showed a noticeable improvement.

Yuen and Kuok (2010)[148] studied the modal frequencies of a 22-story reinforced concrete building extracted over a one-year period. They observed that the first three frequencies increased as ambient temperature rose, which contradicted their analytical predictions. Huo and Xiao (2011) [149]conducted preliminary impact tests to examine the dynamic behavior of concrete at elevated temperatures. The test results indicated that concrete at elevated temperatures generally became more strain-rate sensitive as the temperature increased. in the same year, the non-uniform temperature distribution across an RC slab was measured, and Young's modulus of each component was determined by Xia et al[150] based on the relationship between temperature and Young's modulus. The natural frequencies of the structure were then calculated and demonstrated good agreement with the measured values. It was observed that the natural frequencies of structures decrease as the temperature increases.

Xu, and Bai (2012)[151]performed a series of SHPB tests on concrete during and after high-temperature exposure. The results demonstrate that high temperatures have a substantial impact on the mechanical properties under impact conditions. Huo and Xiao (2013)[152] carried out an experimental analysis on the dynamic behavior of concrete after exposure to elevated temperatures up to 700 °C. It was observed that fire-damaged concrete still exhibited a significant strain rate effect. Wang et al(2014)[153] conducted a series of tests on concrete. It was shown that high temperatures resulted in a more pronounced strengthening effect of strain rate on the dynamic behavior of concrete. Li(2016)[154] carried out laboratory experiments to analyze the impact of ambient temperature on the natural vibration characteristics of concrete beams. Zhai et al (2017)[155] examined an experimental investigation into the effects of strain rate on normal-weight concrete exposed to high temperatures up to 1000°C, utilizing a microwave oven and a split-Hopkinson pressure bar (SHPB).

Research on the relationship between temperature, humidity, and bridge modal frequency using a concrete continuous beam bridge model in the laboratory was performed by Sun Limin et

al(2018)[156]. Liu et al (2020)[157]studied the dynamic behavior of concrete following exposure to height temperatures, utilizing a split-Hopkinson pressure bar (SHPB) test setup. Cai et al (2021)[158]investigated the natural vibration characteristics of the simply supported reinforced concrete beam under the impact of temperature.

Concrete beams reinforced with glass fiber-reinforced polymer (GFRP) bars have been experimentally investigated by Zima and Krajewski (2022)[159] under elevated temperature conditions. Liu et al(2022)[160] evaluated the static and dynamic performance of T-beams under fire exposure, three T-beams were designed and cast in this study. Static and dynamic tests were conducted both before and after fire exposure.

2.3.3Effect of high temperature on dynamic behavior of functionally graded materials in structural elements

Sundararajan et al(2005)[161] analyzed the nonlinear dynamic behavior of functionally graded (FG) rectangular and skew plates in a thermal environment using von Karman nonlinearity. Wattanasakulpong et al (2011)[162] studied the buckling and vibration issues in functionally graded (FG) beams subjected to uniform, linear, and nonlinear temperature rises employing the Ritz method

of the nonlinear eigenfrequency and dynamic analysis of simply supported FGM plates in the thermal environment was examined by Alijani et al(2011)[163] based on first-order shear deformation theory (FSDT) and von-Karman nonlinearity. Zhang (2014)[164]investigated the nonlinear thermal buckling and vibration responses of functionally graded (FG) beams subjected to a nonlinear temperature rise, using the Ritz method.

In 2015, The nonlinear dynamic analysis of functionally graded (FG) thick plates exposed to thermal and mechanical loads was studied in[165],[166] utilizing the First-Order Shear Deformation Theory (FSDT). Akbaş[167] also presented free vibration analysis and wave propagation of FG beams under temperature-dependent. Zahedinejad [168]examined the thermal vibration of functionally graded (FG) beams resting on an elastic foundation under thermal conditions utilizing third-order shear deformation beam theory. Wattanasakulpong and Ungbhakorn[169] conducted a linear and nonlinear vibration analysis of porous functionally graded (FG) beams resting on different types of elastic supports. They found that increasing the power-law exponent decreases the frequencies in the linear vibration problem. On the other hand, for nonlinear vibration analysis, a higher power-law exponent leads to an increase in nonlinear frequency ratios.

Trinh et al (2016)[170]addressed buckling and vibration behavior on functionally graded (FG) beams under uniform, linear, and nonlinear temperature rises, using the state-space approach. Dinh Duc et al (2017)[171] presented the nonlinear responses of FG shells in a thermal environment utilizing Airy stress functions and classical shell theory.

Chen et al (2018)[172]applied the Rayleigh-Ritz method combined with an improved Fourier series to study the thermal vibration of functionally graded (FG) beams, incorporating various higher-order shear deformation theories thermo-elastic vibration behavior of a functionally graded (FG) curved beam with porosity was presented by Amir and Talha(2018)[173] utilizing the finite element method (FEM) based on Higher-Order Shear Deformation Theory (HSDT).

The authors in 2019 also studied the nonlinear dynamic responses of a functionally graded (FG) panel under temperature effects [174]. Singh and Harsha(2019)[175] reported an analysis of the nonlinear dynamic behavior of a functionally graded (FG) sandwich flat panel under a thermal environment using a Hamiltonian formulation and Galerkin's method.

Li et al(2020)[176]developed a unified dynamic model to predict the free and forced thermal vibration characteristics of stepped functionally graded porous composite structures (FGPCS), using characteristic orthogonal polynomials and the First-Order Shear Deformation Theory (FSDT). The study on the nonlinear dynamic behavior and free vibration characteristics of piezoelectric functionally graded material (FGP) truncated conical panels under thermal environmental conditions was explored by Thanh et al(2020)[177]. Liu et al (2021)[178] presented the dynamic responses of piezoelectric functionally graded (FG) plates under temperature effects using is a geometric analysis based on First-Order Shear Deformation Theory (FSDT). Binh et al(2021)[179]studied the nonlinear vibration of functionally graded material (FGP) toroidal shells with variable thickness in a thermal environment, employing the Galerkin method and an improved Double Superposition Technique (DST).

The numerical study of the nonlinear frequency prediction of porous functionally graded shell panels in a thermal environment was examined by Ramteke et al (2022)[180], based on the finite element method (FEM). Eiadtrong (2023) [181]investigated the modified Fourier method for studying the vibration responses of functionally graded porous beams in thermal environments using the third-order shear deformation theory. Mamen et al (2023)[182] developed a novel three-dimensional approach to examine the impact of various thermal loadings on the free vibrational behavior of porous functionally graded (FG) beams.

2.4 Conclusion

In this chapter, a number of studies from the present literature on the static and buckling vibration analysis of structural elements in a thermal environment has been reviewed.

Various theories, as well as numerical, analytical and experimental methods, have been used to define the behavior of structural elements made of steel, concrete and functionally graded materials under temperature conditions.

Following this review, it can be observed that the behavior of structures is determined by the behavior of their elements like beams, columns, and so on. The motivation of this work is to first study the static and vibratory behavior of steel beams in a heated environment, using analytical and numerical methods developed by the finite element method. In addition, the buckling behavior of functionally graded beams is based on the finite element method.

Part II

Numerical and analytical study of static and vibration of steel beams subjected to temperature conditions

Chapter 3: Finite element formulation and analytical analysis

3.1 introduction

In this chapter, A novel finite element frame model based on Euler-Bernoulli beam theory and considering temperature rise has been developed to evaluate the static and vibration behavior of steel beams. The second-order term in the strain -displacement relationship is included by considering the nonlinear von Karman strain. The total potential energy principle was employed to determine the stiffness and geometry matrices.

A novel analytical procedure has also been formulated for analyzing the static behavior of a steel beam subjected to a uniformly distributed load and a uniform temperature rise.

3.2 Numerical model used finite element:

3.2.1 Displacement field

A novel finite element model for beams is created from Bernoulli's beam theory. This element combines a Lagrange-type bar element with a Hermite-type beam element, featuring two nodes and three degrees of freedom per node. To account for high-temperature effects, the Von Karman nonlinear strain formulation is applied. Figure 1 illustrates the geometry and nominal variables. The displacement components at any point along the beam are expressed as follows:

$$u_1(x_1,x_2)=u_{10}(x_1)-x_2\frac{du_2(x_1)}{dx_1} \qquad (3.1)$$

$$u_2(x_1,x_2)=u_{20}(x_1)$$

where:

u_{10} and u_{20} represent the axial and the transverse displacement components, respectively. at points $M(x_1,0)$ located on the neutral axis in the beam.

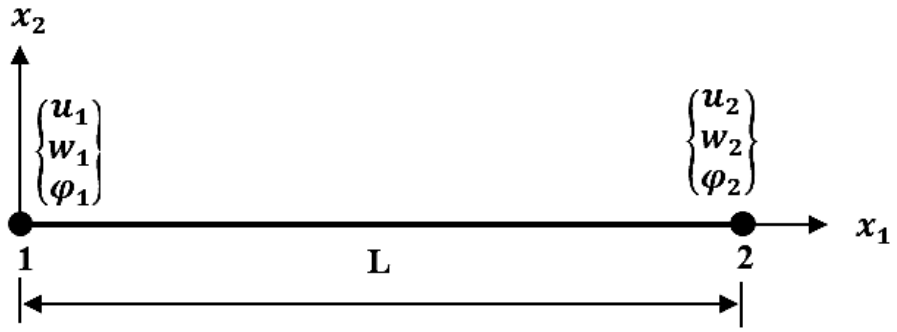

Figure 3. 1 Geometry and nodal variables of the beam finite element

Using Von Karman's theory, the deformation is described by the following expressions:

$$\varepsilon_1 = \frac{du_1(x_1,x_2)}{dx_1} + \frac{1}{2}\left(\frac{du_2(x_1)}{dx_1}\right)^2 = \frac{du_1(x_1)}{dx_1} - x_2\frac{d^2u_2(x_1)}{dx_1^2} + \frac{1}{2}\left(\frac{du_2(x_1)}{dx_1}\right)^2 \quad (3.2)$$

The eq.2 can be reformulated as follows:

$$\varepsilon_1 = \varepsilon_1^0 + \varepsilon^{nl} + yk_1 \quad (3.3)$$

where:

$$\varepsilon_1^0 = \frac{du_{10}(x_1)}{dx_1};\quad \varepsilon^{nl} = \frac{1}{2}\left(\frac{du_2(x_1)}{dx_1}\right)^2;\quad k_1 = -\frac{d^2u_2(x_1)}{dx_1^2} \quad (3.4)$$

Hooke's law, considering the effect of temperature rise, is expressed as follows:

$$\sigma_1 = E_T\left(\varepsilon_1^0 + \varepsilon^{nl} - \alpha_T T(x_2)\right) + E_T x_2 k_1 \quad (3.5)$$

where:

α_T is the of thermal expansion coefficient

E_T is the temperature-dependent Young's modulus according to Eurocode 3 Figure 7 [183].

The temperature rise $T(x_2)$ varies linearly with the beam thickness and is expressed as follows:

$$T(x_2) = \Delta T\left(\frac{1}{2} + \frac{x_2}{h}\right) + \Delta T_b \quad (3.6)$$

where

ΔT Represents the temperature difference between the upper surface temperatureΔT_{T} and the lower surface temperature $\Delta T_b$of the beam and h is the depth of the beam cross-section.

3.2.2 the resultant force and the moment:

The axial force and bending moment in the beam are described by the following expressions:

For $0 \leq T \leq 100°C$

$$N = \int_A \sigma_1 dA = A^* \varepsilon_1^0 - N^T \tag{3.7}$$

The moment M is given by:

$$M = \int_A \sigma_1 x_2 dA = D^* k_1 - M^T \tag{3.8}$$

where $A^*$and D^* represent the extensional and bending rigidities of the beam cross-section, respectively, and are defined as follows:

$$A^* = E_0 A; \quad \mathrm{D}^* = E_0 I \tag{3.9}$$

E_0 is Young's modulus at room temperature.

A and I are the beam's cross-section and moment of inertia, respectively.

N^T and M^T represent the axial force and moment due to temperature rise. They are defined as:

$$N^T = b \int_{-\frac{h}{2}}^{\frac{h}{2}} E_0 \alpha_T T(x_2) dx_2$$
$$M^T = b \int_{-\frac{h}{2}}^{\frac{h}{2}} E_0 \alpha_T T(x_2) x_2 dx_2 \tag{3.10}$$

For $T \geq 100°C$

$$N = b \int_{-\frac{h}{2}}^{\frac{h}{2}} E_T \varepsilon_1^0 dx_2 - N^T = A^* \varepsilon_1^0 - N^T$$
$$M = b \int_{-\frac{h}{2}}^{\frac{h}{2}} E_T k_1 x_2^2 dx_2 - M^T = D^* k_1 - N^T \tag{3.11}$$

where $A^*$and D^* are the extensional and bending rigidities of the beam cross-section respectively. They are defined as follows:

$$A^* = b\int_{-\frac{h}{2}}^{\frac{h}{2}} E_T dx_2; \qquad \mathrm{D}^* = \int_{-\frac{h}{2}}^{\frac{h}{2}} E_T x_2^2 dx_2 \tag{3.12}$$

$$\begin{aligned} N^T &= b\int_{-\frac{h}{2}}^{\frac{h}{2}} E_T \alpha_T T(x_2) dx_2 \\ M^T &= b\int_{-\frac{h}{2}}^{\frac{h}{2}} E_T \alpha_T T(x_2) x_2 dx_2 \end{aligned} \tag{3.13}$$

3.2.3 The total potential energy:

The governing equations are derived from the total potential energy, which is represented as follows:

$$\Pi = U - V \tag{3.14}$$

Where:

U and V represent the deformation energy and work of external forces respectively, given by :

$$\begin{aligned} U &= \frac{1}{2}\int_v \sigma_1 \varepsilon dv = \frac{1}{2}\int_0^L \left(\left\{\varepsilon_1^0\right\}^T A^* \left\{\varepsilon_1^0\right\} + \left\{k_1\right\} D^* \left\{k_1\right\} \right) dx_1 \\ &- \int_0^L \left(\left\{\varepsilon_1^0\right\}^T N^T + \left\{k_1\right\}^T M^T \right) dx_1 + \int_0^L \left\{\varepsilon^{nl}\right\} N\, dx_1 \end{aligned} \tag{3.15}$$

The external forces work of a distributed force q_v is defined as:

$$V = \int_0^L q_v u_2(x_1) dx_1 \tag{3.16}$$

3.2.4 The displacement vector and the functions of interpolation

The displacement components at any point within the element are expressed as follows:

$$\begin{aligned} u_{10}(x_1) &= S_1(x_1)u_1 + S_2(x_1)u_2 \\ u_2(x_1) &= S_3(x_1)w_1 + S_4(x_1)\varphi_1 + S_5(\mathrm{x}_1)\,\mathrm{w}_2 + S_6(x_1)\varphi_2 \end{aligned} \tag{3.17}$$

where:

$S_i(x_1)$ $(i = 1.2)$ represent the interpolation functions of Lagrange. They are given by:

$$S_1(x_1) = 1 - \frac{x_1}{L}; \qquad S_2(x_1) = \frac{x_1}{L} \tag{3.18}$$

and

$S_i(x_1)$ $(i = 3.4.5.6)$ are the Hermite shape functions, which are given by:

$$S_3(x_1) = 1 - \frac{3x_1^2}{L^2} + \frac{2x_1^3}{L^3}$$
$$S_4(x) = x_1 - \frac{2x_1^2}{L} + \frac{x_1^3}{L^2}$$
$$S_5(x) = \frac{3x_1^2}{L^2} - \frac{2x_1^3}{L^3} \quad (3.19)$$
$$S_6(6) = -\frac{x_1^2}{L} + \frac{2x_1^3}{L^2}$$

3.2.5 The strain displacement relationship

The strain displacement relationship is given by:

$$\varepsilon_1^0 = [B_m]\{\delta\}$$
$$k_1 = [B_f]\{\delta\} \quad (3.20)$$
$$\frac{du_2}{dx_1} = [G]\{\delta\}$$

where:

$[B_m]\ is\ (1 \times 6)$ stretching matrix given by:

$$[B_m] = \begin{bmatrix} \frac{dS_1(x_1)}{dx_1} & 0 & 0 & \frac{dS_2(x_1)}{dx_1} & 0 & 0 \end{bmatrix} \quad (3.21)$$

$[B_f]\ is\ (1 \times 6)$ bending strain smatrix defined as follows:

$$[B_f] = \begin{bmatrix} 0 & \frac{d^2S_3(x_1)}{dx_1^2} & \frac{d^2S_4(x_1)}{dx_1^2} & 0 & \frac{d^2S_5(x_1)}{dx_1^2} & \frac{d^2S_6(x_1)}{dx_1^2} \end{bmatrix} \quad (3.22)$$

$[G]$is a (1×6) matrix that relates the first derivative of the transverse displacement component to the displacement vector. It is defined as follows:

$$[G] = \begin{bmatrix} 0 & \frac{dS_3(x_1)}{dx_1} & \frac{dS_4(x_1)}{dx_1} & 0 & \frac{dS_5(x_1)}{dx_1} & \frac{dS_6(x_1)}{dx_1} \end{bmatrix} \quad (3.23)$$

and

$\{\delta\}$ is the nodal displacement vector given by:

$$\{q\}^T = \{u_1 \quad w_1 \quad \varphi_1 \quad u_2 \quad w_2 \quad \varphi_2\} \quad (3.24)$$

3.2.6 The static analysis

Substituting Eqs (20).(21).(22) and (23) into Eq(14). The total potential energy can be defined as:

$$\Pi = \frac{1}{2}\int_0^L \{q\}^T \left([B_m]^T A^* [B_m] + [B_f]^T D^* [B_f] \right) \{q\} dx_1 -$$
$$\int_0^L \{q\}^T \left([B_m]^T N^T + [B_f]^T M^T \right) dx_1 + \frac{1}{2}\int_0^L \{q\}^T [G]^T N [G] \{q\} dx_1 -$$
$$\int_0^L \{q\}^T [S(x_1)]^T q_v dx_1 \qquad (3.25)$$

Eq (25) can be reformulated as follows:

$$\Pi = \frac{1}{2}\{q\}^T \left([K_m] + [K_f] + [K_g] \right) \{q\} - \{q\}^T \left(\{F^e\} + \{F^T\} \right) \qquad (3.26)$$

Utilizing the total potential energy principle $\partial\Pi = 0$. we can arrive at the following equilibrium equation:

$$\left([K_e] + [K_g] \right) \{q\} = \{F^e\} + \{F^T\} \qquad (3.27)$$

where $[K_e]$ represent the stiffness matrix expressed as:

$$[K_e] = [K_m] + [K_f] \qquad (3.28)$$

with:

$[K_m]$ represent the extension stiffness matrix given by:

$$[K_m] = \int_0^L [B_m]^T A^* [B_m] dx_1 \qquad (3.29)$$

$[K_f]$ is the bending stiffness matrix expressed as:

$$[K_f] = \int_0^L [B_f]^T D^* [B_f] dx_1 \qquad (3.30)$$

and

$[K_g]$ is the geometrical matrix expressed as:

$$[K_g] = \int_0^L [G]^T N [G] dx_1 \qquad (3.31)$$

$\{F^e\}$ and $\{F^T\}$ represent the mechanical force vector and the thermal vector force, respectively. They are expressed as follows:

$$\left\{F^e\right\} = \int_0^L \left[S(x_1)\right]^T q_v dx_1 \tag{3.32}$$

$$\left\{F^T\right\} = \int_0^L \left(\left[B_m\right]^T N^T + \left[B_f\right] M^T\right) dx_1 \tag{3.33}$$

$[S(x_1)]$is the shape functions matrix given by:

$$\left[S(x_1)\right] = \left[S_1(x_1) \quad S_3(x_1) \quad S_4(x_1) \quad S_2(x_1) \quad S_5(x_1) \quad S_6(x_1)\right] \tag{3.34}$$

3.2.7 Buckling analysis

It is widely recognized that a compressive force in a beam reduces its flexural rigidity. When this force reaches the critical buckling value, the stiffness approaches zero. Consequently, the bending moments and deflections increase dramatically, theoretically approaching infinity. Thus, determining the critical buckling load or the critical buckling temperature is crucial in a thermo-elastic analysis.

The stability of a beam under thermo-mechanical loading is governed by thr flowing eigenvalue problem:

$$\left(\left[K_e\right] + \left[K_g\right]\right)\{\delta\} = 0 \tag{3.35}$$

by setting

$$\left[K_g\right] = \lambda\left[K_g^0\right]$$

The Eq. (35) can be rewritten as follows:

$$\left(\left[K_e\right] + \lambda\left[K_g^0\right]\right)\{\delta\} = 0 \tag{3.36}$$

Where:

λ is the loading factor

$$\left[K_g^0\right] = \int_0^L \left[G\right]^T N_0 \left[G\right] dx \tag{3.37}$$

N_0 represents the compressive force induced by a specified thermo-mechanical load.

The critical buckling temperature ΔT_{cr} or the critical buckling load N_{cr} can be expressed as:

$$\Delta T_{cr} = \lambda_{cr} \Delta T_0; \qquad \mathrm{N}_{cr} = \lambda_{cr} N_0 \tag{3.38}$$

ΔT_0 is the given temperature rise.

3.2.8 The resolution procedure:

A Fortran code was developed, following the flowchart in Figure 2, to solve the equations and calculate the displacements and bending moments of the beams**.**

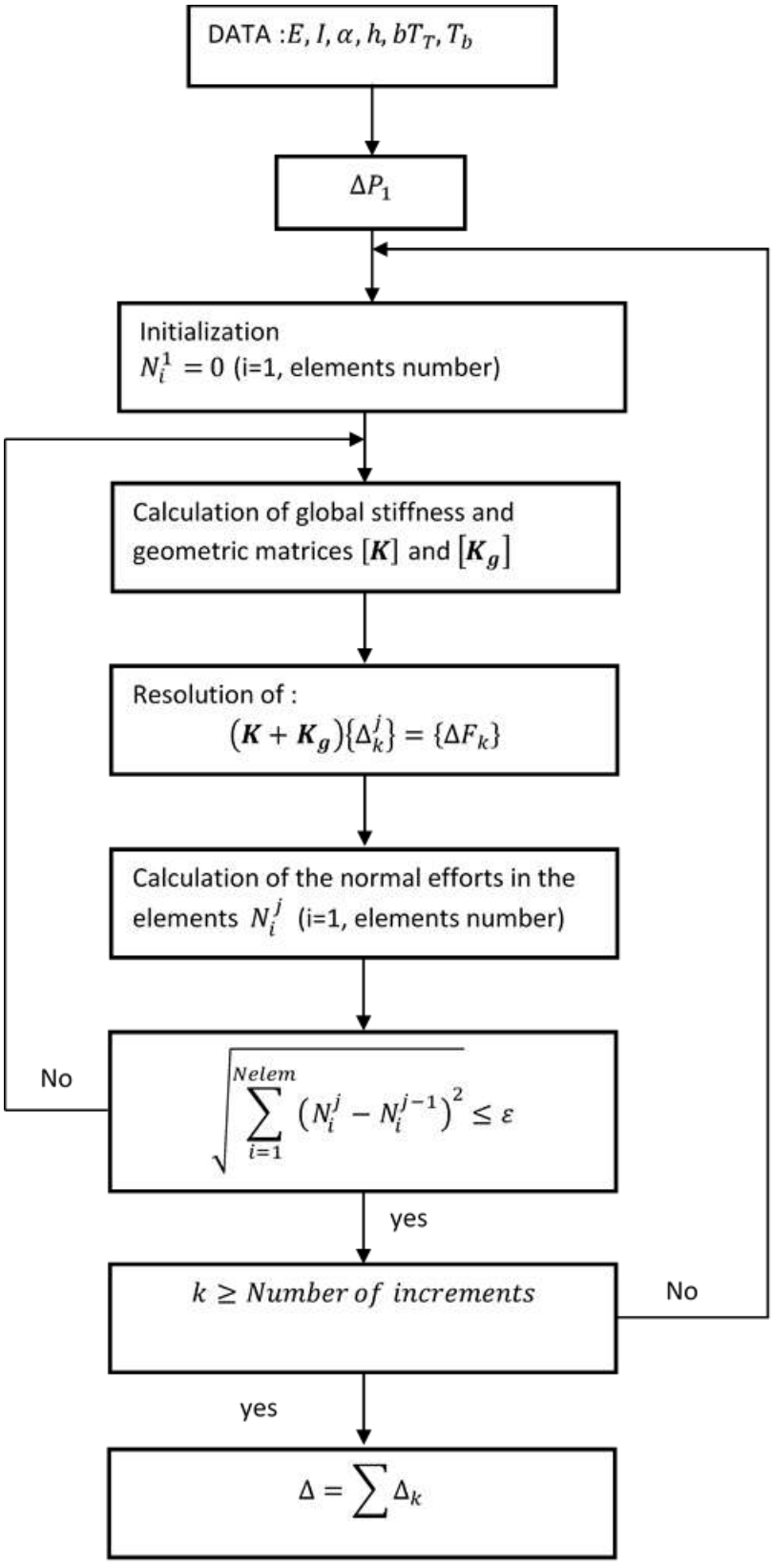

Figure 3.2 The flow chart for the iterative solution method

3.2.9 the vibration analysis:

The system equations of motion are obtained by writing the Lagrangian, L=T-U and first-order stationary conditions in the form of Hamilton's equation

$$\frac{d}{dx}\left(\frac{\partial L}{\partial qi}\right) - \left(\frac{\partial L}{\partial qi}\right) = Fi \tag{3.39}$$

The general equation of motion to find the vibrational characteristics of any structure is:

$$[M]\{\ddot{U}\} + [K]\{U\} = 0 \tag{3.40}$$

$$U(x) = U_0 \cos(\omega t + \theta) \tag{3.41}$$

The generalized eigenvalue problem for the vibration analysis including thermal effects can be written as:

$$\{[K] + [Kg]\}\{\Delta\} - \omega^2 \{[M]\}\{\Delta\} = 0 \tag{3.42}$$

It is noted that [K] and [K_g] are stiffness and geometrical matrices respectively and the vector Δ is the eigenvector.

and The mass matrix is defined by the following relation:

$$[M] = \int_v [N]^T \rho [N] dv \tag{3.43}$$

When

ρ : is a mass density

The natural frequency is related with the circular natural frequency as:

$$f = \frac{\omega}{2\pi} \tag{3.44}$$

3.3 Analytical model:

This section outlines an analytical procedure for the thermo-elastic analysis of the bending of a steel beam subjected to high temperatures. The material properties of the beam are assumed to vary with temperature. The beam is considered to be part of a braced frame structure. Figure 3.3 and Figure 3.4 illustrate a beam with length L under bending subjected to a uniformly distributed load q_v and to a uniform temperature rise Δ_T. The transverse displacements of the ends of the beam are equal to 0 ($w(x = 0) = w(x = L) = 0$). The beam's left and right ends are supported by elastic rotational springs with stiffnesses R_L and R_r respectively. The

translation supports at the left and right ends are elastic and are represented by springs of stiffness K_L and K_r respectively.

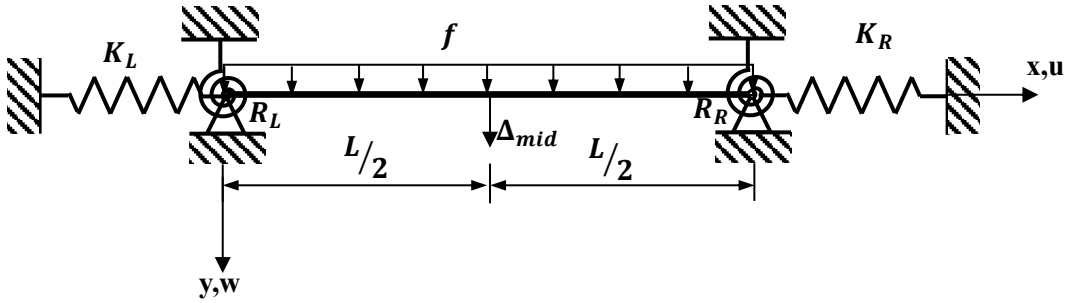

Figure 3. 3 Generic bending beam with elastic end supports

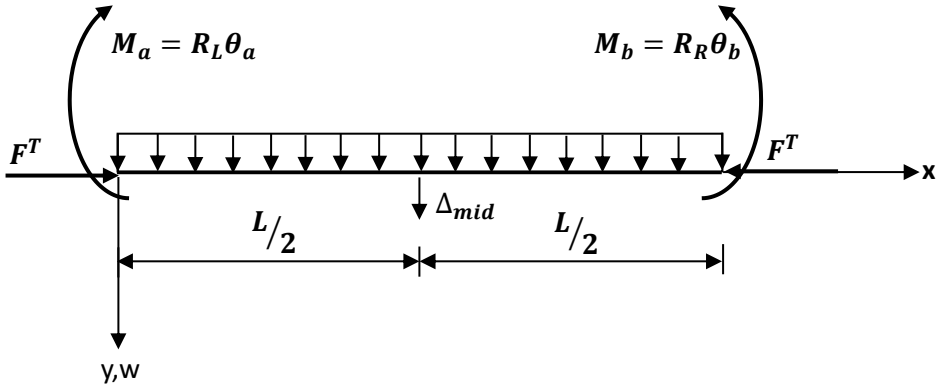

Figure 3. 4 The static diagram of the beam

3.3.1 the bending moment

The bending moment at any cross-section of the beam considering large displacements, is expressed as:

$$M(x) = -\frac{q_v x^2}{2} + M_A + F_a^T w(x) + \left(\frac{q_v L}{2} + \frac{M_B - M_A}{L}\right)x \tag{3.45}$$

where

q_v is the uniformly distributed load

M_A and M_B represents the moment at the left and right ends of the beam respectively.

F_a^T is the axial force due to temperature rise ΔT

3.3.2 The axial force in the beam

The total elongation of the beam, resulting from temperature changes and the effects of translational springs, is given by:

$$u_L + u_r = L\alpha_T \Delta T - \frac{F_a^T L}{E_T A} \tag{3.46}$$

Where u_L and u_r represents the left and right springs elongations respectively and are expressed as follows:

$$u_L = \frac{F_a^T}{K_L}; \quad \mathrm{u}_r = \frac{F_a^T}{K_R} \tag{3.47}$$

Substituting Eqs (3.47) into Eq(3.47). we can derive the expression for the axial force, which is given by:

$$F_a^T = \frac{K_L K_R}{\frac{E_T A}{L}\left(K_L + K_R\right) + K_L K_R} E_T A \alpha_T \Delta T \tag{3.48}$$

According to Bernoulli beam theory, the differential equation governing the deformation of a beam can be given as follows:

$$\frac{d^2 w(x)}{dx^2} + \frac{F_a^T}{E_T I} w(x) = \frac{q_v x^2}{2E_T I} - \frac{M_A}{E_T I} - \frac{x}{E_T I}\left(\frac{q_v L}{2} + \frac{M_B - M_A}{L}\right) \tag{3.49}$$

by Setting $\mathrm{K}^2 = \frac{F_a^T}{E_T I}$. and integrating Eq. (3.49) according to x the transversal displacement at any cross-section of the beam can be described as follows :

$$w(x) = C_1 \cos \mathrm{K}x + C_2 \sin \mathrm{K}x + \frac{q_v x^2}{2E_T I \mathrm{K}^2} - \frac{M_A}{E_T I \mathrm{K}^2} - \frac{x}{E_T I \mathrm{K}^2}\left(\frac{q_v L}{2} + \frac{M_B - M_A}{L}\right) \tag{3.50}$$

C_1 and C_2 are integration constants determined utilizing the mentioned boundary conditions. we can then have:

$$C_1 = \frac{M_A}{E_T I \mathrm{K}^2} \quad \text{and } C_2 = \frac{C_1}{\tan \mathrm{K}L} + \frac{M_B}{E_T I \mathrm{K}^2 \sin KL}$$

by setting $\frac{Kl}{2} = v$. The deflection at the midpoint of a beam (x=L/2) can be formulated as (3.51)

$$w_{mid} = \frac{M_A L^2}{8E_T I v^2}\left(\frac{\sin^2 v}{\cos v} - 1\right) + \frac{M_B L^2}{8E_T I v^2}\left(\frac{1-\cos v}{\cos v}\right) + \frac{5q_v L^4}{384E_T I}\frac{12\left(2\sec v - 2 - v^2\right)}{5v^4} \tag{3.51}$$

$$\begin{aligned} M_A &= \theta_{A0}\frac{\beta - \alpha_1}{\beta^2 - \alpha_1\alpha_2} \\ M_B &= \theta_{B0}\frac{-\beta + \alpha_2}{\beta^2 - \alpha_1\alpha_2} \end{aligned} \tag{3.52}$$

where θ_{A0} and θ_{B0} represents the rotation angles of the ends of the beam due to distributed load and are defined by:

$$\begin{aligned} \theta_{A0} &= \frac{q_v L^3}{8E_T I v^2}(\tan v - v) \\ \theta_{B0} &= \frac{q_v L^3}{8E_T I v^2}(-\tan v - v) \end{aligned} \tag{3.53}$$

where the moments of the ends M_A and M_B are given by[3.52]:

$$\begin{aligned} \alpha_1 &= \frac{3}{2v}\left(\frac{1}{2v} - \frac{1}{\tan v}\right)\frac{L}{3E_T I} + \frac{1}{R_L} \\ \alpha_2 &= \frac{3}{2v}\left(\frac{1}{2v} - \frac{1}{\tan v}\right)\frac{L}{3E_T I} + \frac{1}{R_R} \\ \beta &= \frac{3}{v}\left(\frac{1}{\sin v} - \frac{1}{2v}\right)\frac{L}{6E_T I} \end{aligned} \tag{3.54}$$

The bending moment at mid-span ($x = \frac{L}{2}$) is expressed as:

$$M_{mid} = \frac{q_v L^2}{8} + \frac{3}{2}M_A + \frac{4E_T I v^2}{L^2}w_{mid} \tag{3.55}$$

3.4 Conclusion

To analyze the static and vibration behavior of steel beams in temperature conditions. A novel finite element model using Bernoulli beam theory and nonlinear von Karman deformation has been developed in this chapter. The total potential energy principle is used to derive elemental stiffness and geometric matrices. In addition, an analytical approach has been introduced to study the static behavior of elastically supported steel beams exposed to a uniform temperature rise. The supports are modeled by translational and rotational springs, representing the influence of the columns in finite element simulations.

Chapter 4: Application of numerical and analytical models - Results and discussions

4.1 introduction

This work focuses on the analysis of the static and vibration behavior of steel beams exposed to thermomechanical loads. Uniform and linear temperature distributions over the depth of the beam are taken into account. The performance and accuracy of the finite element developed were confirmed by comparing the results with those reported in the literature.

In addition, a parametric study was carried out to examine the impact of various boundary conditions on the thermo-elastic bending behavior of the beam, using both finite element and analytical methods.

4.2 the validation of the finite element model:

Validation of the finite element model proposed to study the static and dynamic behavior of beams in steel structures under heated conditions.

Example 4.1

The first example, analyzed previously by Jiang and Usmani [58] involves a clamped steel beam where the left half, as shown in Figure 4.1, is submitted to a uniform temperature increase from 0°C to 800°C. The right half remains unheated, acting as an elastic support, restricting the displacement of the left half.

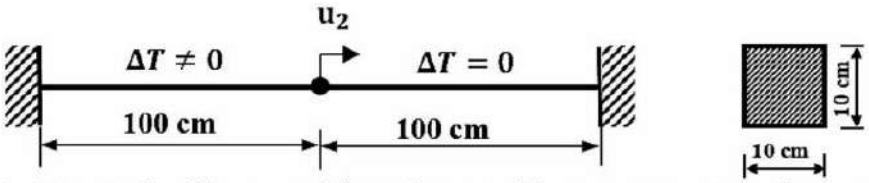

Figure 4. 1 Restrained beam subjected to a uniform temperature rise on the left half.

The beam is constructed from Steel 37, with temperature-dependent mechanical properties as specified by Eurocode 3 [183] Figure 4.2. The coefficient of thermal expansion is set at $\alpha_T = 12 \times 10^{-6}/°C$. A mesh consisting of 8 elements was used for the analysis.

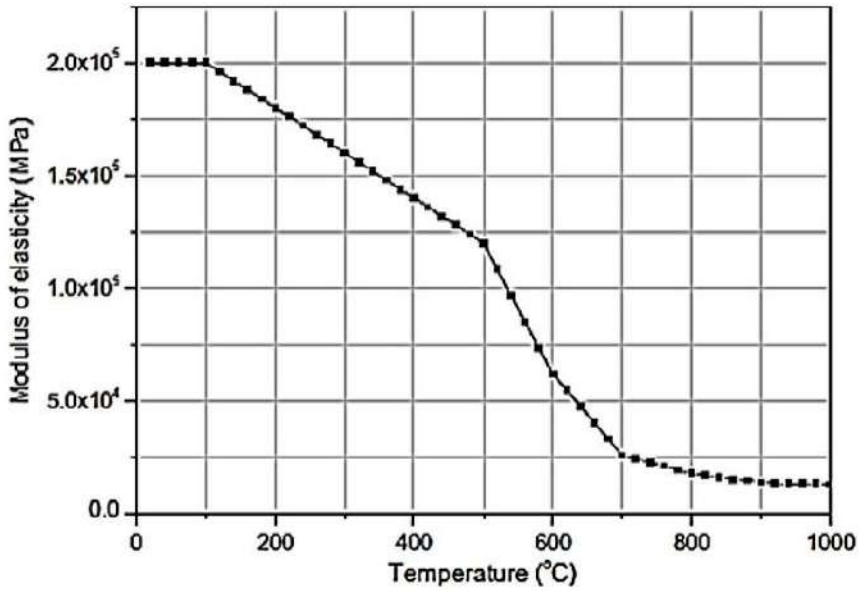

Figure 4. 1 The modulus of elasticity versus temperature rise Eurocode 3 [183].

Table 4.1 shows the axial displacement at the beam's midpoint as a function of temperature increase. The results show good agreement with the results reported by Jiang and Usmani[58] The curve in Fig. 4.3 shows that displacement increases with temperature up to 500°C. After 500°C, displacement begins to decrease progressively. After 500°C, the displacement begins to decrease progressively. This reduction is due to the fact that the right-hand part retains its extensional stiffness, while the extensional stiffness of the left-hand part decreases due to the drop in Young's modulus.

Table 4.1 Horizontal displacement u_2 (mm) of beam center as a function of temperature rise

Temperature (°C)	*Jiang and Usmani* [58]	*Present finite element*
0	0.000	0.000
20	0.100	0.120
50	0.305	0.300
100	0.603	0.600
150	0.866	0.874
200	1.130	1.136
250	1.367	1.378
300	1.597	1.600
350	1.784	1.800
400	1.970	1.976
450	2.110	2.127
500	2.240	2.250
550	2.064	2.094
600	1.707	1.703
700	0.960	0.990
750	0.883	0.891
800	0.773	0.796

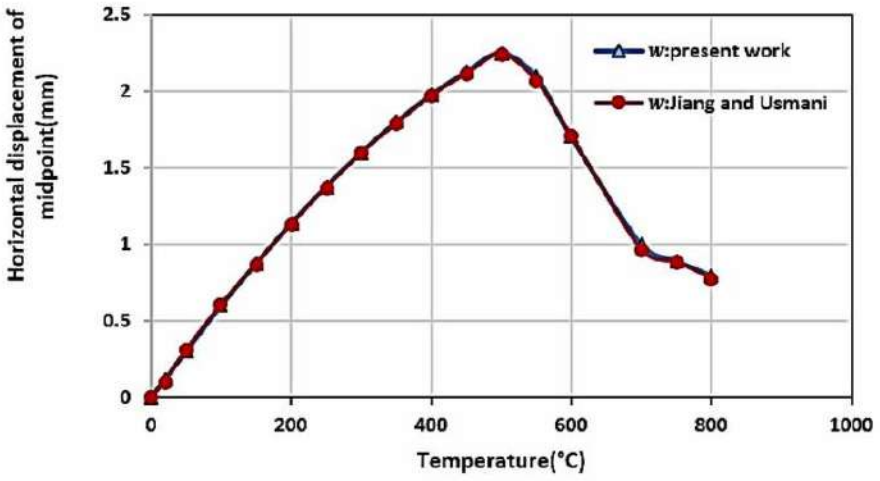

Figure 4. 3 The horizontal displacement of the middle of the beam versus temperature rise.

Example 4.2

Examine the bending behavior of a steel circular arch with elastic restraints at both ends when exposed to high temperatures (as shown in Figures 4.4 and 4.5. The arch with a length of $L = 10\ m$ and a subtended angle of θ=60° is exposed to a uniformly distributed load of

$q_v = 30\ kN/m$ and a linearly varying temperature rise across the depth of its 610UB125 cross-section. At ambient temperature, the Young's modulus and the coefficient of thermal expansion for the steel are $E_0 = 200\ GPa$ and $\alpha_T = 11 \times 10^{-6}/°C$. Respectively. The reference temperature at the centroid of the cross-section is $T_{ref} = 150°C$.

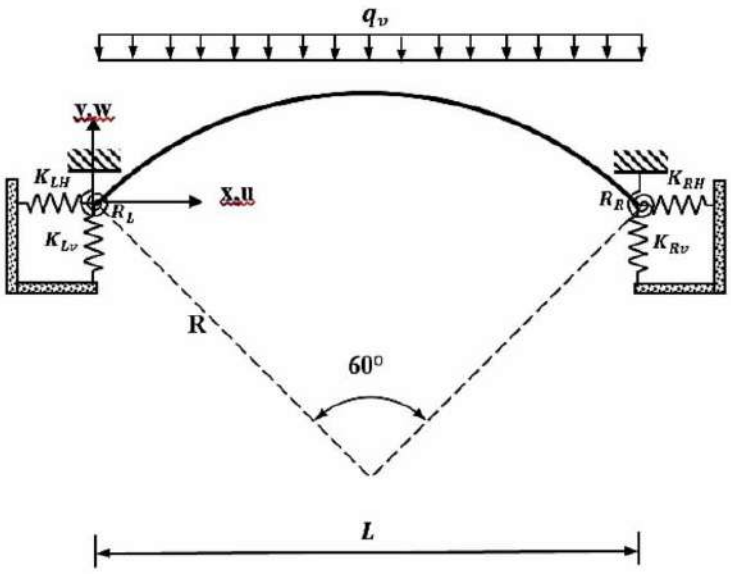

Figure 4. 4 The steel arch under a uniformly distributed gravity load [48]

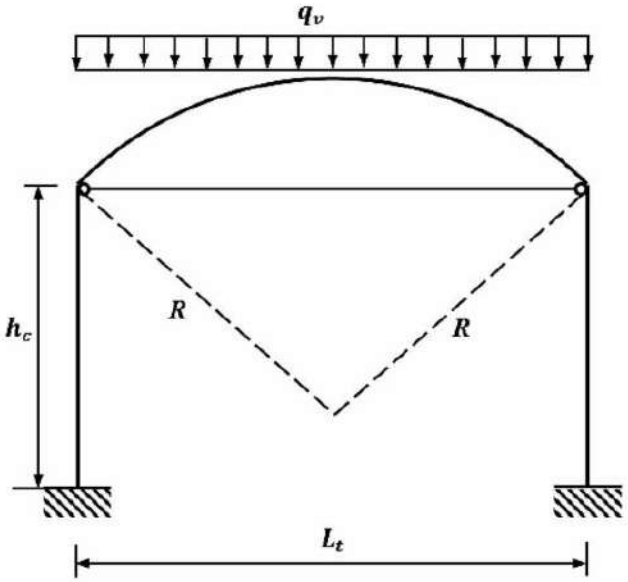

Figure 4. 5 The arch structural model for finite element analysis

Multiple meshes were utilized in the finite element analysis to model the arch shown in Figure 4.5, until convergence was reached.

The elastic supports of the arch are modeled using translational and rotational springs (Figure 4.4), with their rigidities are calculated as follows:

- The stiffness of the translational springs in Figure 4.4 is determined based on the axial rigidities of the columns and the tie rod shown in Figure 4.5 using the following equations:

$$K_{Rv} = K_{Lv} = \frac{E_C A_C}{h_C}$$
$$K_{RH} = K_{LH} = \frac{E_t A_t}{L_t} \quad (4.1)$$

Where:

E_C, A_c and h_c represent the column's Young modulus, area cross-section, and height, respectively.

and E_t, A_t, and L_t represent Young modulus, the cross-sectional area, and the length of the tie rod, respectively

The rotation spring rigidities in Figure. 4.4 are calculated using the bending rigidities of the columns at the column-arch connections in Figures. 4.5, based on the following equation:

$$R_R = R_L = \frac{4E_C I_C}{h_C} \quad (4.2)$$

Where I_c is the inertia moment of the columns, respectively.

Figures 4.6, 4.7 and 4.8 illustrate the deflection, the horizontal displacement and the angle of rotation along the steel arch. The results obtained with the developed finite element method closely match those derived from the analytical method of Heidarpour et al[51]. The comparison validates the current finite element method's accuracy. The figures also show that maximum deflection occurs at mid-span, while maximum horizontal displacement and rotation are observed a quarter of the length of the arc from each end. These findings have been corroborated by Heidarpour et al[51].

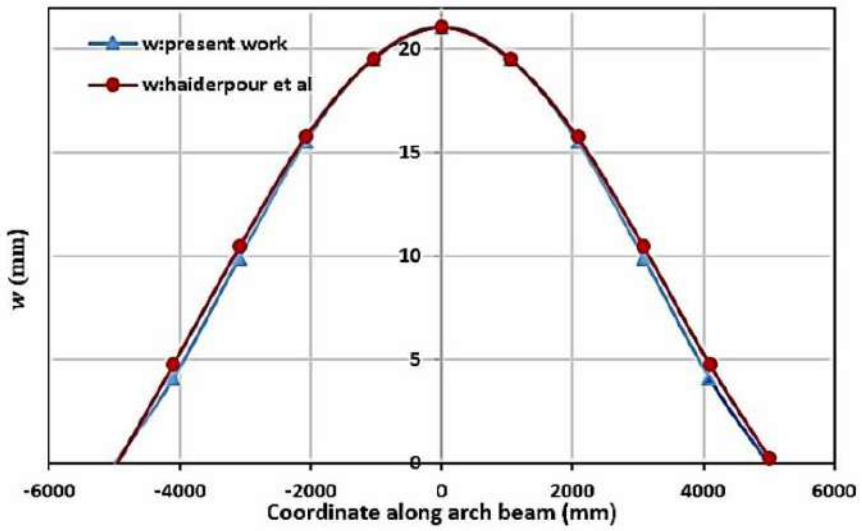

Figure 4. 6 The vertical deflection along the arch

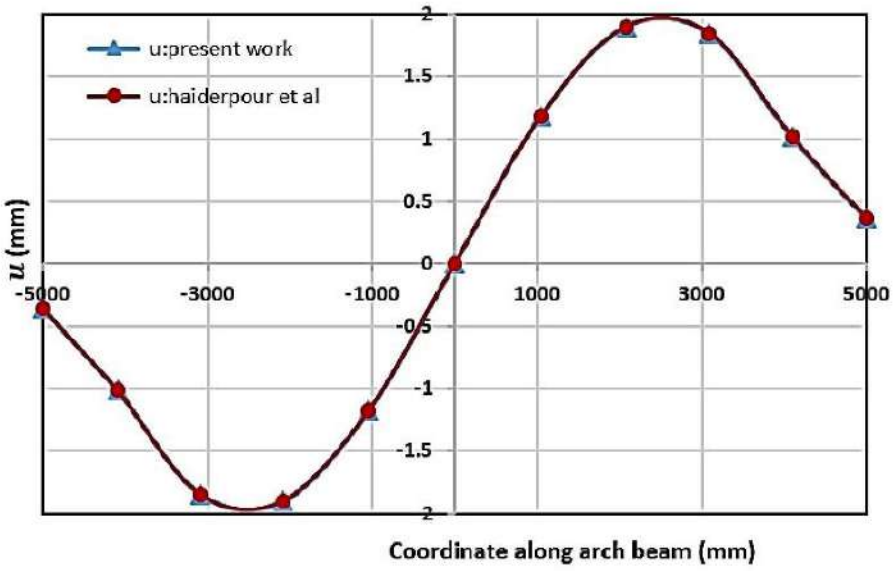

Figure 4. 7 The horizontal displacement along the arch

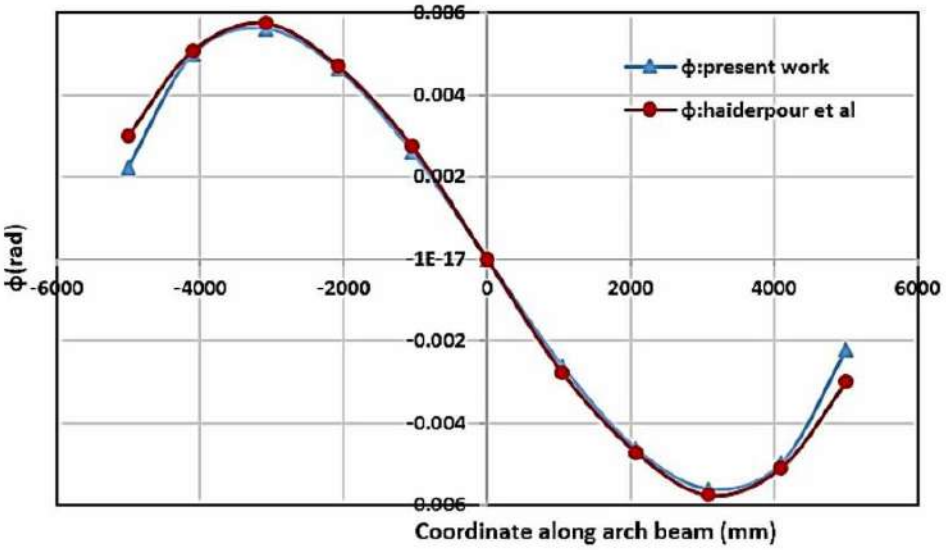

Figure 4. 8 The rotation angle along the arch

Example 4.3

For this example, the beam previously analyzed by Bradford et al [184]. Using the analytical method (Figures. 4.9 and 4.10) is re-evaluated using the current finite element approach.

The beam is elastically supported at the ends by both translational and rotational springs and is exposed to a uniformly distributed load of q_v=10 N/mm, it experiences a linear temperature gradient, with temperatures rising between 50°C at the top and 100°C at the bottom. The ambient temperature is considered to be 20°C.

The young's modulus varies with temperature and is taken as $E_0 = 200 \times 10^3 N/mm^2$ at ambient temperature. The steel beam has a rectangular cross-section with dimensions of $d = 400\ mm$ and $b = 200\ mm$. Its length is $2L = 4000\ mm$.

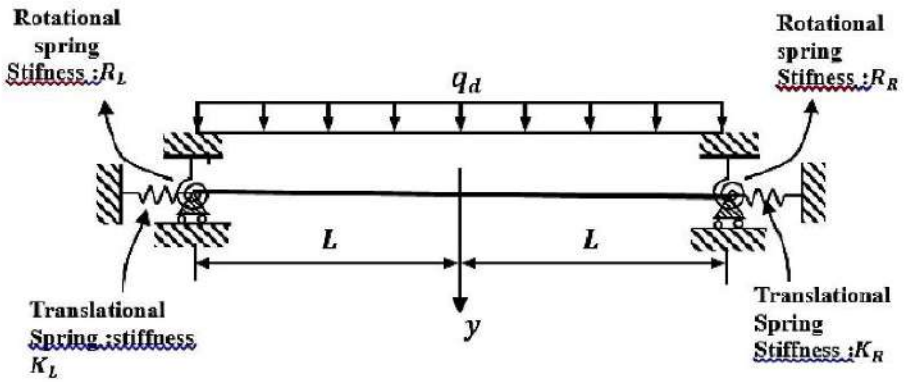

Figure 4. 9 The generic flexural element [45].

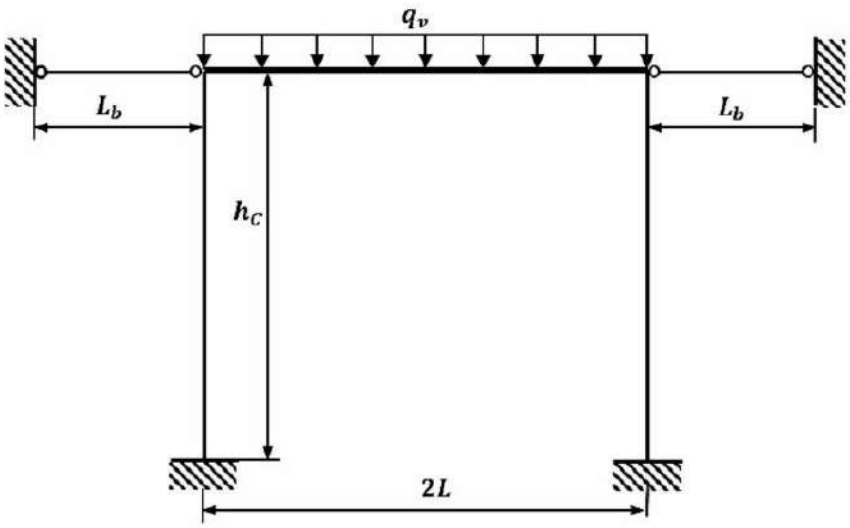

Figure 4. 10 The beam structural model for finite element analysis

The translation spring stiffness of Figure 4.9 is determined utilizing the bar axial stiffness in Figure 4.10 it is expressed as:

$$K_L = K_R = \frac{E_b A_b}{L_b} \tag{4.3}$$

E_b, A_b,and L_b represent the bar's elastic modulus, cross-sectional area, and length, respectively

The rotation spring rigidities in Figure. 4.9 are derived from the bending rigidity of the columns at the beam-column connections of the frame shown in Figure. 4.10. They are calculated as follows:

$$R_L = R_R = \frac{4E_C I_C}{h_C} \tag{4.4}$$

The steel beam is divided into several mesh segments until convergence is reached, for finite element analysis.

The vertical displacements at mid-span, under a linearly distributed temperature rise and a uniformly distributed load q_v , are illustrated in Figure 4.11. It can be seen that the present results are in good agreement with those obtained by Bradford et al [184]. However, it is clear to see that the deflections obtained using the present finite element method are slightly lower than those reported by Bradford et al. This discrepancy is probably due to the shortening of the column shown in figure (4.10). Overall, the results demonstrate the effectiveness of the finite element approach formulated.

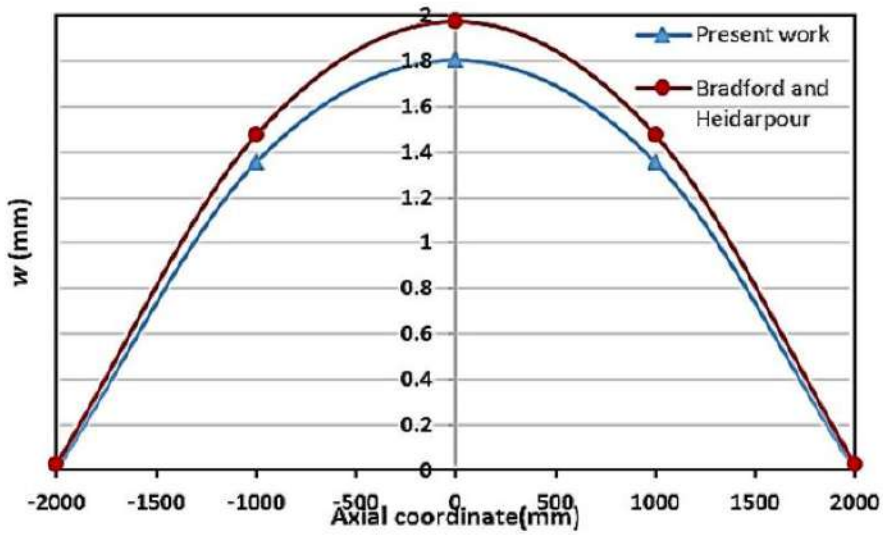

Figure 4. 11 The vertical deflection of the beam

Example 4.4

In this example, cantilever beams with a uniform thickness of 0.5 mm were used in two different lengths: 15 cm and 17 cm. Each beam of the same length was studied at four different temperatures: non-heating, 100, 200, and 300 °C. Table 4.2 presents the fundamental frequency values of the beam at various lengths and different temperatures. It can be observed that the current results are in excellent agreement with the references mentioned.

Table 4.2 Fundamental beam frequency (Hz) under temperature conditions:

Temperature (°C)	Young's modulus (Pa)	Length of beam (Cm)	Present finite element	Analytical[185]	Experimental[185]
0	6.9×10^{10}	15	20.88	21	22
		17	16.25	16.3	16.8
100	6.62×10^{10}	15	20.45	20.6	21.5
		17	15.91	16.1	16.2
200	6.09×10^{10}	15	19.61	19.7	21
		17	15.27	15.3	16.5
300	5.69×10^{10}	15	18.95	18.5	21
		17	14.76	14.4	15.8

To provide a clearer illustration, the data from Table 4.2 are represented in Figures 4.12 and 4.13, respectively. Figure 4.12 and 4.13 depicts the effect various lengths with different temperatures in natural frequency of the beam. It can be seen from the figures that natural frequency decreases with increase of temperature. Also, as the length decreases while keeping the thickness constant, the natural frequency increases.

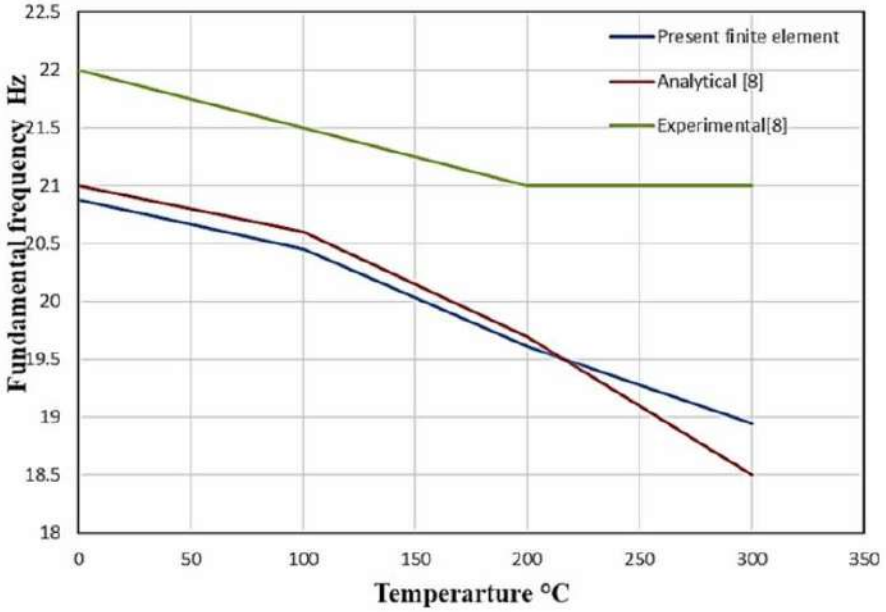

Figure 4.12 Fundamental frequency of beam with length 15 cm

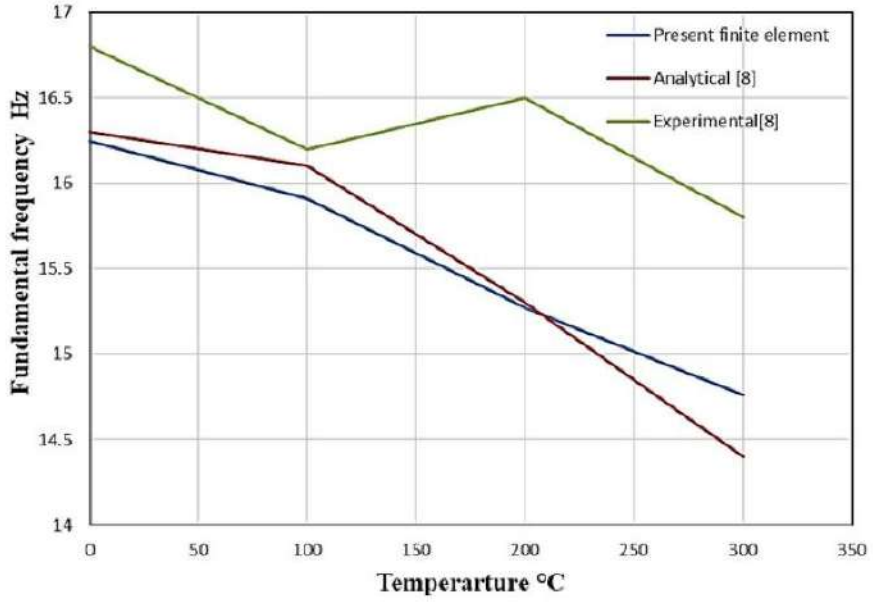

Figure 4. 12 Fundamental frequency of beam with length 17 cm.

Example 4.5

In order to valid the development of finite element in the evaluation of natural frequency of beams under difference of temperature, an isotropic cantilever beam exposed to a large temperature difference by Kamei et al [141]. The results for natural frequencies are presented in Table 4.3. A comparison between the analytical results from Kamei et al and the present study is provided, focusing on the natural frequencies of beams under various temperature.

Table 4. 3 Natural frequency of beam (Hz) under difference of temperature

Temperature (°C)	Young's modulus (Gpa)	Thermal Expansion (α) µm/◦C	Analytical[141]	Present work
25	73,4	0.1066	58,19	57,2
50	72,7	0.1078	57,96	56,93
100	69,3	0.1091	57,37	55,58
150	68,5	0.1266	57,02	55,26
200	65,2	0.1359	56,77	53,91

It may be noted that the present results are in excellent agreement with those obtained by Kamei et al. The natural frequency decreases with increasing temperature.

4.3 Parametric Study

In the last section,The reliability of the proposed finite element model has been confirmed by comparison with the available literature. In this part, a parametric study has been carried out using both the present finite element model and the proposed new analytical model.

4.3.1 The effect of temperature on the natural frequency of a steel beam

Example 4.6

In this example, a steel beam (IPE 80) with various boundary conditions (a simply supported and clamped beam) subjected to a high difference of temperature, with width b =0.046 m and thickness h = 0.08 m, respectively. Table 4.4 presents the material properties of steel IPE 80.

Table 4. 4 The material properties of steel IPE 80.

Parameters	Values
Young modulus (GPa)	200
Thermal expansion coefficient (1/°C)	$1.17^{*}10^{-5}$
Density (kg/m3)	7850

In this study, we aim to investigate the natural frequencies of a steel beam in extreme thermal conditions, using a finite element program based on the theory of Bernoulli. The stiffness and geometric matrices are obtained using the principle of total potential energy.

Figures 4.14 and 4.15 depicts the effect of temperature, slenderness ratio and boundary conditions on the natural frequency of a beam.

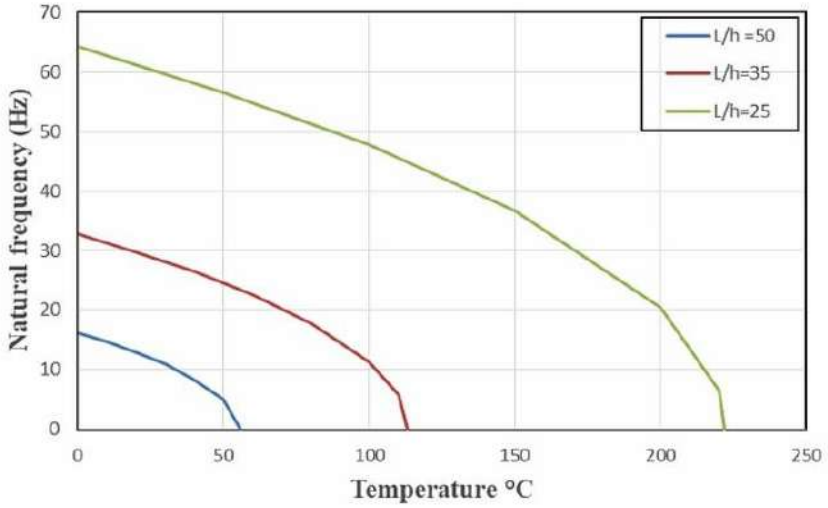

Figure 4. 14 The effect of temperature on the natural frequency of simply supported beam with different slenderness ratio

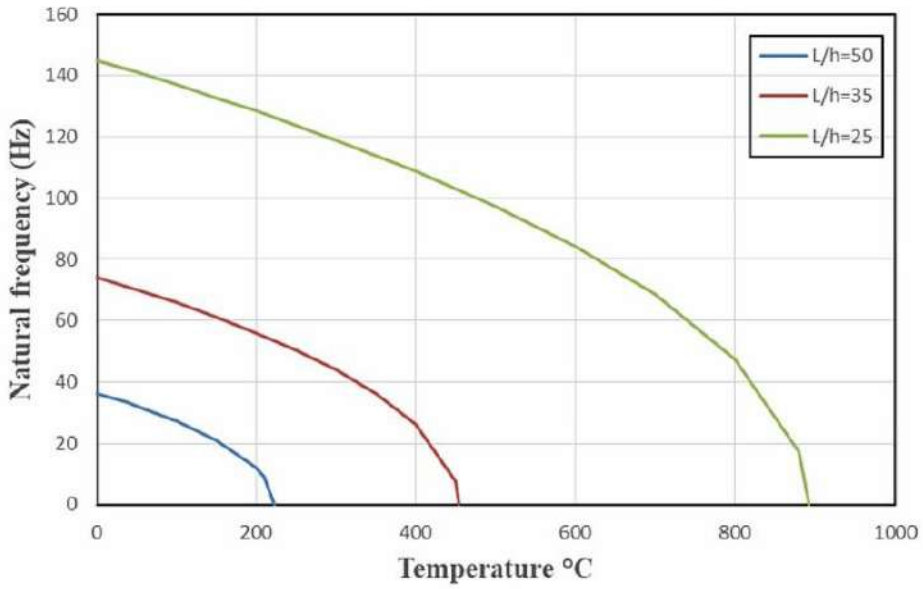

Figure 4. 15 The effect of temperature on the natural frequency of clamped beam with different slenderness ratio

The figures show that the increase in critical buckling temperature in all cases for the clamped beam is greater than for the simply supported beam. In addition, the natural frequency decreases as the slenderness ratio increases.

This figure also shows that the natural frequency decreases as the temperature increases.

For simply supported beam case: It can be observed that for a length-to-height ratio (L/h) of 50, the critical temperature is 55.6°C; for L/h = 35, the critical temperature is 113°C; and for L/h = 25, it is 221°C. Moreover, for clamped beam case it can be noted that if length to height ratio L/h =50 the critical temperature 223 ° C, if that L/h= 35 the critical temperature 454 ° C and if that L/h =25 the critical temperature 892 ° C.

4.3.2 Effect of slenderness and boundary conditions on steel beams under thermal conditions

Example 4.7

The study aims to examine the effects of parameters such as slenderness and boundary conditions on the static behavior of steel beams under thermal conditions.

Figures 4.16 - 4.19 present four case studies of steel beams with varying elastic support conditions at their ends. In each case, the beams are exposed to a uniformly distributed load q_v = 10 N/mm and a uniform temperature rise. The beams have a length of L=8000 mm and have a rectangular cross-section with dimensions (d=400 mm and b=200 mm). The elastic modulus, which is temperature-dependent is $E_0 = 2 \times 10^5 N/mm^2$ at 20°C. The thermal expansion coefficient is $\alpha_T = 1 \times 10^{-5}/°C$.

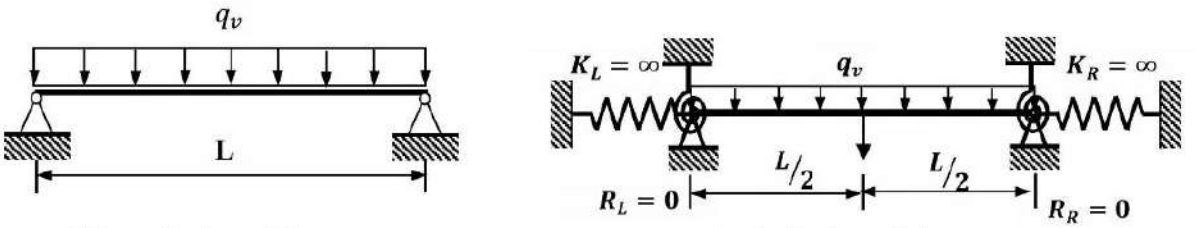

Figure 4. 16 Beam with pinned end.

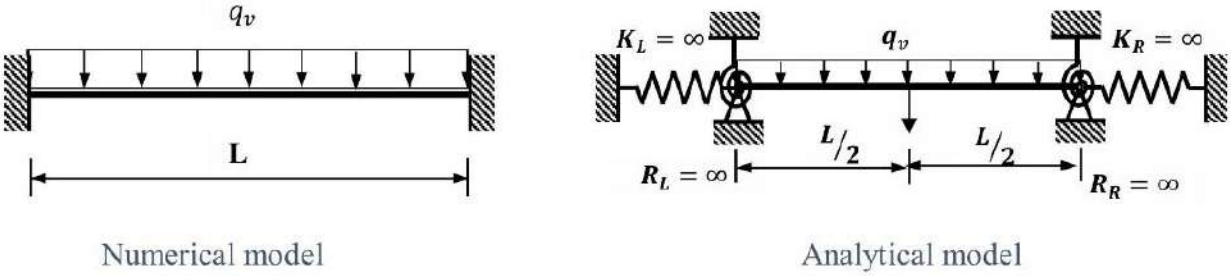

Figure 4. 17 Beam with fixed end.

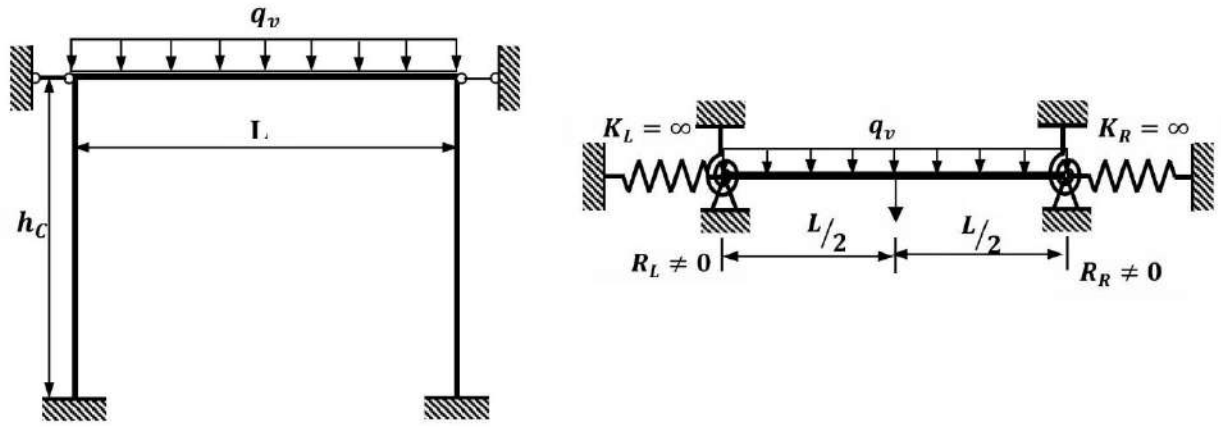

Numerical model Analytical model

Figure 4.18 Beam with rotational elastic supports at the ends.

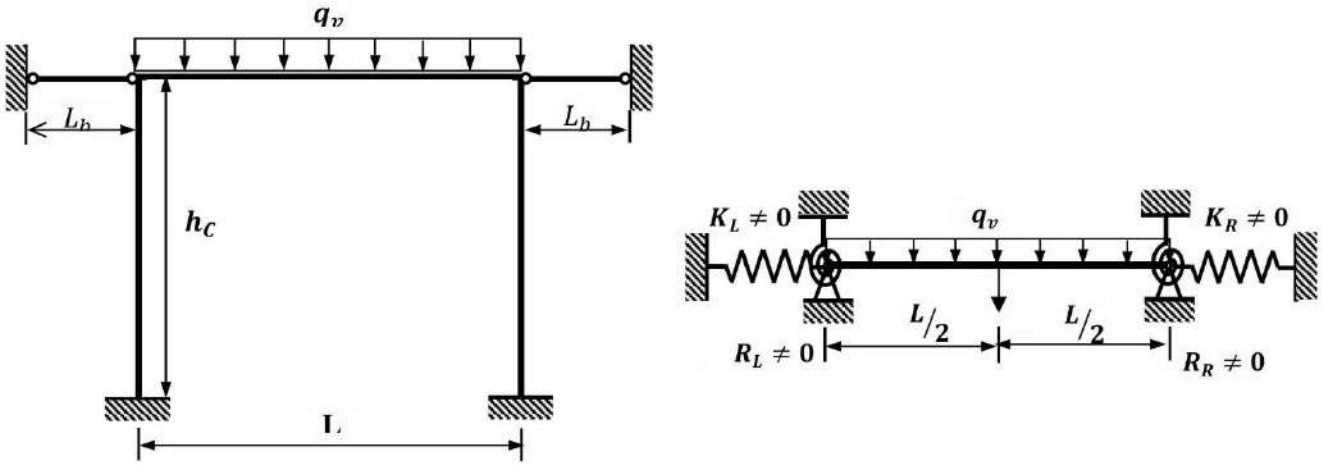

Numerical model Analytical model

Figure 4.19 Beam with elastic translational and rotational supports.

The stiffness factors R_L and R_R of rotational springs at the beam ends correspond to the bending stiffness of the columns at the beam-column connections in the associated frame, are given by: $R_L = R_R = 5.333 \times 10^9$ (N.mm)

The stiffness factors K_L and K_R of the translational springs correspond to the extensional stiffnesses of the bars, are given by: $K_L = K_R = 8 \times 10^6$ (N.mm).

For the finite element computation, multiple meshes were employed to model the beams until the desired convergence was achieved.

For comparison purposes, the impact of temperature variation on the vertical displacement and bending moment at the mid-span of the beams was calculated using both the new analytical model and the current finite element model.

Figures 4.20 to 4.27 illustrate the mid-span deflection and bending moment of beams subjected to a uniform distributed load and a uniform temperature rise. In all cases, the results from the analytical procedure are in good agreement with those obtained from the finite element analysis.

It can be seen that in all cases. As the temperature rises and approaches the critical buckling temperature, the mid-span deflection and bending moment of beams tend to increase significantly approaching infinite values. This occurs because the thermal loads induce compressive stresses within the beam, leading to a reduction in its overall bending stiffness.

It is observed that the critical buckling temperature is lowest for pinned beams and highest for fixed beams. Moreover, the critical buckling temperature is higher for beams with elastic rotational supports compared to those with elastic translational and rotational supports.

In the case of pinned beams. The critical buckling temperature is around 206°C. While a temperature rise of 100°C leads to a deflection of about 4.87 mm. However, for beams with fixed ends, the critical buckling temperature exceeds the elastic limit. At 100°C. The deflection is approximately 0.56 mm.

The impact of elastic supports, represented by translational and rotational springs, is illustrated in Figures 4.24 and 4.26. It can be observed that the critical buckling temperature is approximately 223°C in case 3 and 283°C in case 4. While it is about 206°C in the case of the beam with pinned ends. In addition. The deflections are 4.25 mm and 3.44 mm for a temperature rise of 100°C in cases 3 and 4, respectively.

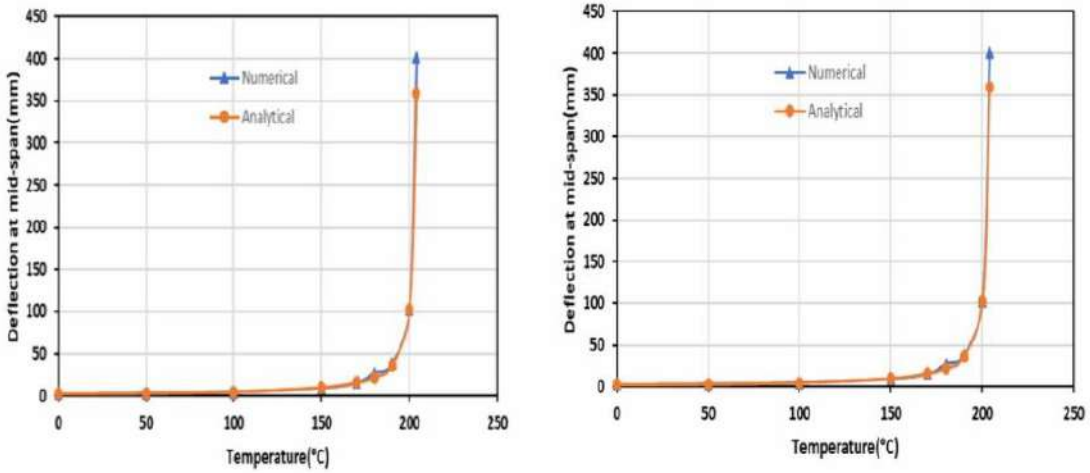

Figure 4. 20 The deflection of a beam pinned at both ends

Figure 4. 21 The bending moment at the mid-span of a beam pinned at both ends

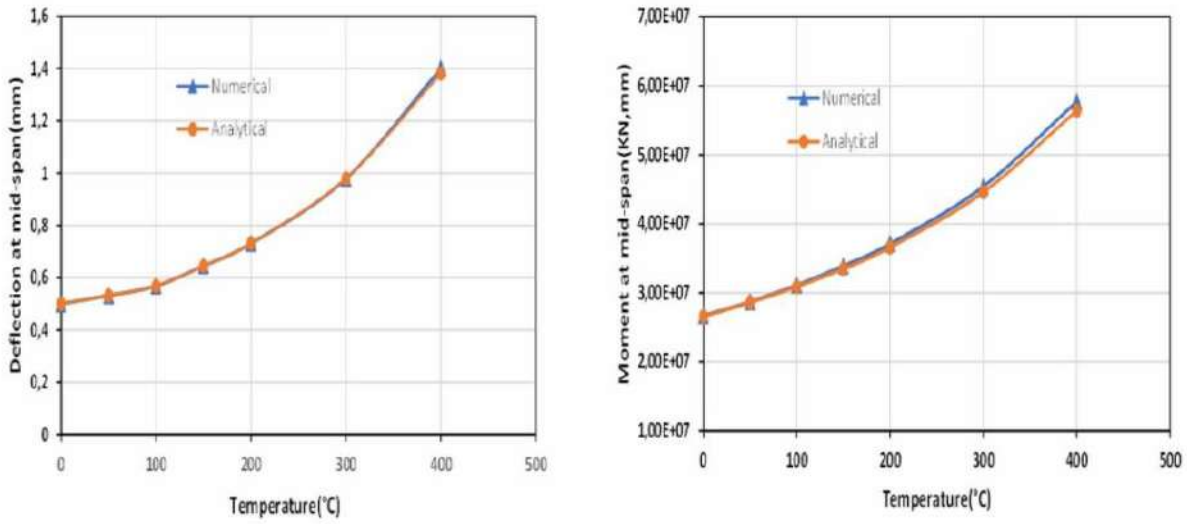

Figure 4. 22 The deflection of a beam fixed at both ends

Figure 4. 23 The bending moment at the mid-span of a beam fixed at both ends

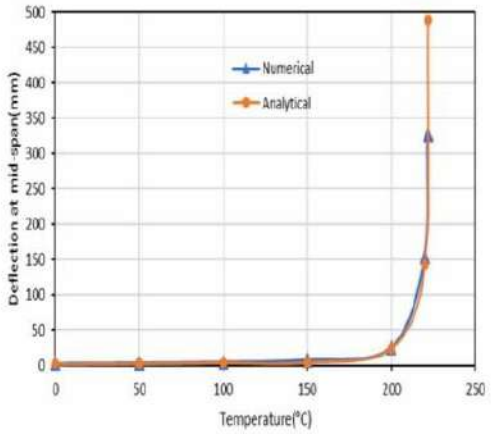

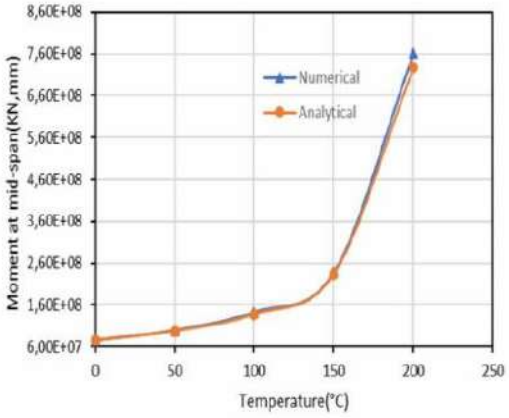

Figure 4. 24 The deflection at mid-span of a beam with rotational elastic supports at both ends

Figure 4. 25 The bending moment at the mid-span of a beam with rotational elastic supports at both ends

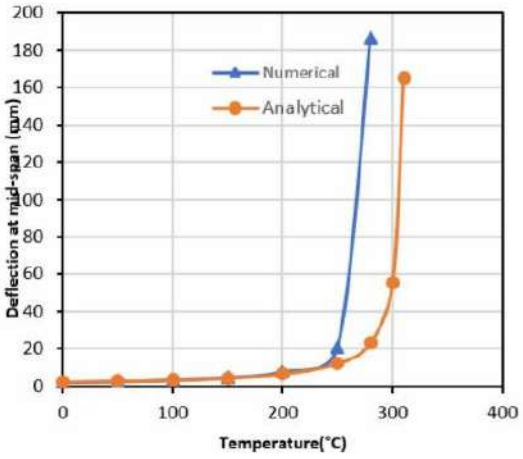

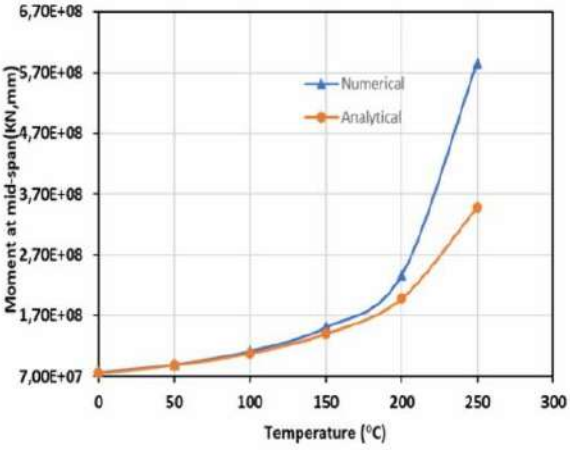

Figure 4. 26 The deflection of a beam with elastic translational and rotational supports

Figure 4. 27 The bending moment at mid-span of a beam with elastic translational and rotational supports

4.4 conclusion

In this chapter, the validation of the performance of the finite element developed by comparing its results against those available in the literature. All comparisons show that results obtained with the proposed element agree perfectly with those of the references, confirming the performance and precision of the formulation.

- From *dynamic behavior* of steel beams under heating conditions:
  The natural frequency decreases with increasing temperature.

As the length of the steel beam is reduced, while the thickness remains constant, the natural frequency increases.

The critical temperature rise for a clamped beam is greater than for a simply supported beam

The natural frequency decreases as the slenderness ratio increases.

When the slenderness ratio decreases so the critical temperature increases.

- From *static* behavior of steel beams under temperature conditions: In all cases , it is observed that as the temperature increases and nears the critical buckling point, the deflection and bending moment at the beam's mid-span increase significantly, approaching infinity.

Additionally, a parametric study was conducted using both the analytical and finite element models to examine the impact of various support conditions on the thermoelastic behavior of the steel beams. The study revealed that temperature rise significantly influences the static behavior of structural elements, notably affecting their stiffness and strength, leading to a marked increase in deflections and bending moments.

Part III

Numerical analysis of mechanical and thermal buckling of functionally graded beams

Chapter 5: Formulation of a finite beam element based on enhanced Timoshenko beam theory:

5.1 introduction

In this chapter, a novel simple high-order shear deformation theory (SHSDT), using the enhanced Timoshenko beam theory, has been introduced. The suggested model previously used to study static, dynamic, and buckling behavior of FGM plates by Sadgui and Tati[186] has been adapted here and used to conduct static and buckling analyses of functionally graded beams submitted to thermomechanical loads. The present model has only three unknowns taking into account the zero-shear stress condition at the top and bottom surfaces of the beam.

The material properties of the beam are supposed to vary across its thickness according to a power law distribution based on the volume fractions of the component materials. The geometric and stiffness matrices are derived using total potential energy principles. In addition, the utilization of a shear correction factor is not necessary.

5.2 Numerical model based on finite element:

5.2.1 The displacement field

The component of the displacement field of a point on the beam is proposed as follows: [186]

$$\begin{aligned} u(x,z)&=u_0(x)+z\varphi_x(x) \\ w(x,z)&=f(z)w_0(x)+(f(z)-1)G(x) \end{aligned} \tag{5.1}$$

The function $f(z)$ represents the shear function, which governs the distribution of transverse shear strains and stresses in the beam's thickness. This is chosen so that the transverse shear stress is zero on the top and bottom surfaces of the beam.

The sinusoidal shear function employed is given by:

$$f(z) = \frac{2\sqrt{5}}{3}\left(1-\left(sin\frac{\pi z}{h}\right)^2\right) \tag{5.2}$$

The function $G(x)$ is defined as:

$$\varphi_x(x) = \frac{\partial G(x)}{\partial x} \tag{5.3}$$

5.2.2 Kinematics

The components of the von Karman strain associated with the displacement field in equation (1) are as follows:

$$\begin{aligned}\varepsilon_x &= \varepsilon_x^0 + \varepsilon_x^{nl} + zk_x \\ \gamma_{xz} &= f(z)\gamma_{xz}^0\end{aligned} \tag{5.4}$$

Where:

$$\varepsilon_x^0 = \frac{\partial u_0}{\partial x} \tag{5.5}$$

$$\varepsilon_x^{nl} = \frac{1}{2}\left(\frac{\partial w}{\partial x}\right)^2 \tag{5.6}$$

$$k_x = \frac{\partial \varphi_x}{\partial x} \tag{5.7}$$

$$\gamma_{xz}^0 = \varphi_x + \frac{\partial w_0}{\partial x} \tag{5.8}$$

5.2.3 Constitutive equations

Consider a functionally graded beam (FG) with a cross-section S, length L, depth h and width b, as shown in figure 5.1. Material properties are considered to change progressively through the thickness of the beam following a power law. Specifically, the relationship for Young modulus and thermal expansion coefficient is expressed as follows:

$$E(z) = E_m + (E_c - E_m)V_c(z) \tag{5.9}$$

$$\alpha(z) = \alpha_m + (\alpha_c - \alpha_m)V_c(z) \tag{5.10}$$

The subscripts c and m denote the ceramic and metal components of the FG beam, respectively. $V_c(z)$represents the volume fraction of the ceramic, defined by:

$$V_c(z) = \left(\frac{z}{h} + \frac{1}{2}\right)^p \tag{5.10}$$

For $-h/2 \le z \le h/2$ and $0 \le p \le \infty$

E_c and $E_m$represent Young's modulus of the ceramic and the metal, respectively.

α_c and α_m represent the thermal expansion coefficient of the ceramic and the metal, respectively.

p is the volume fraction exponent which determines the gradation of the volume fraction Figure 5.2

When p is zero, the beam is entirely ceramic, while when p approaches infinity, the beam becomes entirely metallic.

Figure 5.1 Functionally graded beam coordinate system and geometry.

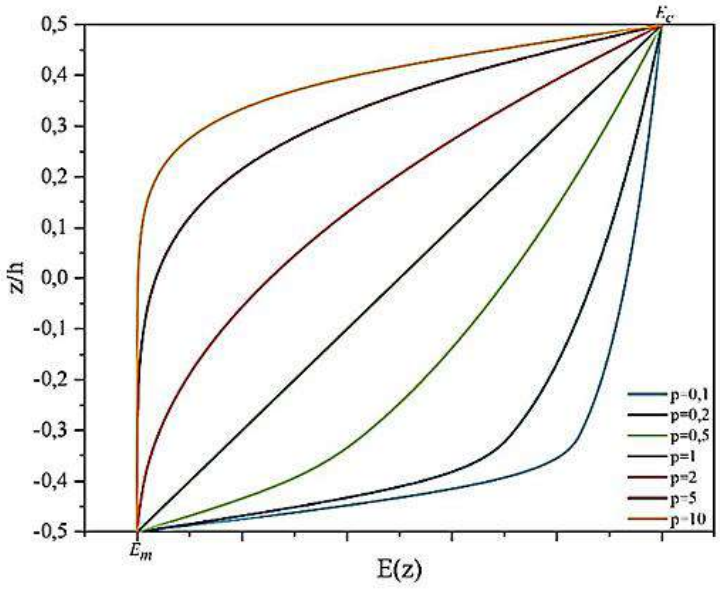

Figure 5. 2 Variation of Young's modulus through the thickness of functionally graded beams[16].

The strain-stress relationships for a functionally graded elastic beam are expressed as follows:

$$\begin{matrix}\sigma_{x=E(z)\varepsilon_x-\sigma_T} \\ \tau_{xz=Q\gamma_{xz}}\end{matrix} \quad (5.11)$$

Where

$$\sigma_T = E(z)\alpha(z)\Delta T \quad (5.12)$$

ΔT is the temperature rise

For the case of shear deformation that varies with respect to depth, the shear stress can be expressed as:

$$\tau_{xz} = Qf(z)\gamma_{xz}^0 \quad (5.13)$$

Where

$$Q = \frac{E(z)}{2(1+v)} \quad (5.14)$$

Q represents the elastic coefficient.

5.2.4 Position of the physical neutral axis

The asymmetry of the material properties in the FG beams in relation to the median surface leads to a membrane-bending effect in the beams. Therefore, to simplify the complexities arising due to this effect, the resultants of forces and moments are calculated with respect to the neutral axis, which is not aligned with the beams' median surface, as shown in figure 5.3. [136][192] In order to determine the position of the neutral physical axis, it is essential to calculate a value e where the axial force resulting from bending is zero. It is determined by the following equation:

$$z_{Ns} = z - e \tag{5.15}$$

$$e = \frac{\int_{\frac{-h}{2}}^{\frac{h}{2}} E(z) z dz}{\int_{\frac{-h}{2}}^{\frac{h}{2}} E(z) dz} \tag{5.16}$$

e represents the distance from the physical neutral axis to the centroid of the FG beam.

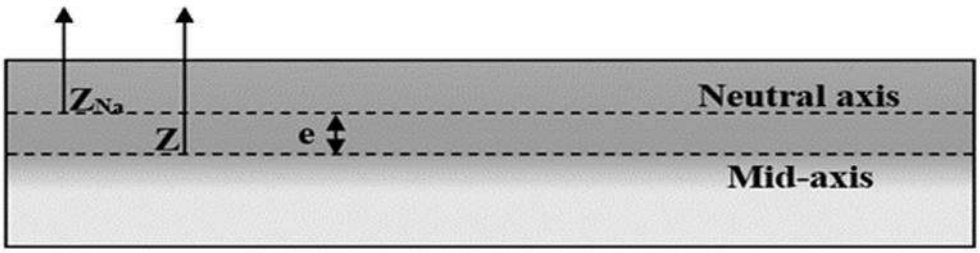

Figure 5.3 The position of the neutral axis of the FG beam [22].

5.3 the total potential energy

The total potential energy of the FG beam can be represented as follows:

$$\Pi = U - W_d + W_a \tag{5.17}$$

$U, W_d \text{ and } W_a$ represent the strain potential energy, the work performed by external loads and the work of distributed loads in relation to the physical neutral axis, respectively.

$$U = \frac{1}{2}\int_V (\{\varepsilon_x\}^T \sigma_x + \{\gamma_{xz}\}^T \tau_{xz})\, dV \tag{5.18}$$

$$U = \int_V (\{\varepsilon_0\}^T E(z)\{\varepsilon_0\} + (z-e)^2\{k_x\}^T E(z)\{k_x\} + f(z)^2\{\gamma_{xz}^0\}^T Q\{\gamma_{xz}^0\})\, dV \tag{5.19}$$

Where V denotes the volume of the beam.

By integrating Eq. (5.18) to the cross-sectional area S, we obtain the following expression:

$$U = \frac{1}{2}\int_0^L (\{\varepsilon_0\}^T A\{\varepsilon_0\} + \{k_x\}^T D\{k_x\} + \{\varepsilon^{nl}\}N + \{\gamma_{xz}^0\}^T H\{\gamma_{xz}^0\})\, dx - \int_0^L (\{\varepsilon_0\}^T N^T + \{k_x\}^T M^T) dx \quad (5.20)$$

A, H, and D are the elastic coefficients, defined as follows:

$$\{A \quad D \quad H\} = \int_s E(z) \times \{1 \ (z-e)^2 \qquad f(z)Q\}\, ds \quad (5.21)$$

$$N^T = b\int_{-\frac{h}{2}}^{\frac{h}{2}} E(z) - \alpha(z)\Delta T dz \quad (5.22)$$

$$M^T = b\int_{-\frac{h}{2}}^{\frac{h}{2}} E(z) - \alpha(z)\Delta T\ (z-e) dz \quad (5.23)$$

N^T and M^T represent the axial force and moment due to temperature rise.

The external work caused by the distributed load F(x) and the axial compressive force P is given by Eqs. (5.24) and (5.25), respectively:

$$W_a = \frac{1}{2}\int_0^L P\left(\frac{\partial w_0}{\partial x}\right)^2 dx \quad (5.24)$$

$$W_d = -\int_0^L F(x) w_0\, dx \quad (5.25)$$

5.4 Finite element formulation

A two-node component with three degrees of freedom (DOFs) per node, derived from enhanced Timoshenko beam theory, is used to investigate FG beams' static behavior and buckling.

The component displacement vectors of the element are interpolated as follows:

$$\nabla_d(x) = \sum_{i=1}^{2} N_i \nabla_d^i \qquad d = 1, 2, 3 \quad (5.26)$$

Where

$$\nabla_d^i = u_0^i, w_0^i, \varphi_0^i \qquad i = 1,2 \quad (5.27)$$

$\nabla_d(x)$ represents displacement and rotation of the element at a given point. ∇_d^i and N_i represent displacement components and Lagrange shape functions associated with the node *I,* respectively. Lagrange shape functions are defined as follows:

$$\begin{matrix} N_1 = 1 - \frac{x}{L} \\ N_2 = \frac{x}{L} \end{matrix} \quad (5.28)$$

By using shape functions, deformation-displacement relationships in Eqs. (5.5)–(5.7) can be expressed as:

$$\{\varepsilon_x^0\} = [B_a]\{q\} \tag{5.29}$$

$$\{k_x\} = [B_b]\{q\} \tag{5.30}$$

$$\{\gamma_{xz}^0\} = [B_s]\{q\} \tag{5.31}$$

$$\frac{\partial w}{\partial x} = [G]\{q\} \tag{5.32}$$

$[B_a], [B_b], [B_s]\ and\ [G]$ are (1×6) matrices, where the subscripts a,b, and s represent axial, bending, and shear strain, respectively. $\{q\}$ refers to the element's displacement vector.

Where

$$[B_a] = \left[\frac{\partial N_1}{\partial x} \quad 0 \quad 0 \quad \frac{\partial N_2}{\partial x} \quad 0 \quad 0 \quad \right] \tag{5.33}$$

$$[B_b] = \left[0 \quad 0 \quad \frac{\partial N_1}{\partial x} \quad 0 \quad 0 \quad \frac{\partial N_2}{\partial x}\right] \tag{5.34}$$

$$[B_s] = \left[0 \quad \frac{\partial N_1}{\partial x} N_1 \quad 0 \quad \frac{\partial N_2}{\partial x} N_2\right] \tag{5.35}$$

$$[G] = \left[0 \quad 0 \quad \frac{\partial N_1}{\partial x} \quad 0 \quad 0 \quad \frac{\partial N_2}{\partial x}\right] \tag{5.36}$$

$$\{q\}^T = \{u_1 w_1 \varphi_1 \ \ u_2 w_2 \varphi_2\} \tag{5.37}$$

The principle of total potential energy is applied to derive the elementary matrices of the element. By applying Eqs. (5.29)–(5.32). the total potential energy is expressed as follows:

$$U = \frac{1}{2}\int_0^L (\{q\}^T([B_a]^T A[B_a] + [B_b]^T D[B_b] + [G]^T N[G] + [B_s]^T H[B_s])\{q\})\, dx - \int_0^L \{q\}^T([B_a]^T N^T + [B_b]^T M^T) dx \tag{5.38}$$

5.4.1 Static analysis

$$W_d = -\int_0^L F(x) w_0\, dx \tag{5.39}$$

Substitution of Eqs. (5.38) and (5.39) into Eq. (5.17) leads to the following expression

$$\Pi = \frac{1}{2}\int_0^L (\{q\}^T([B_a]^T A[B_a] + [B_b]^T D[B_b] + [B_s]^T H[B_s])\{q\})\, dx - \int_0^L \{q\}^T([B_a]^T N^T + [B_b]^T M^T) dx - \int_0^L F(x) w_0\, dx \tag{5.40}$$

Eq (5.37) can be reformulated as follows:

$$\Pi = \frac{1}{2}\{q\}^T([K_a] + [K_b] + [K_s])\{q\} - \{q\}^T(\{F^e\} + \{F^T\}) \tag{5.41}$$

Eliminating the initial variation in total potential energy as a function of nodal values {q}, we obtain the equilibrium equation:

$$([K_e])\{q\} = \{F^e\} + \{F^T\} \tag{5.42}$$

With

$$[K_e] = \int_0^L ([B_a]^T A[B_a] + [B_b]^T D[B_b] + +[B_s]^T H[B_s])\, dx \tag{5.43}$$

$$[K_e] = [K_a] + [K_b] + [K_s] \tag{5.44}$$

$$\{F^e\} = \int_0^L [N] F(x)\, dx \tag{5.45}$$

$$\{F^T\} = \int_0^L ([B_a]^T N^T + [B_b]^T M^T) dx \tag{5.46}$$

$$[N] = [0 \quad 0 \quad N_1 N_2 \quad 0 \quad 0] \tag{5.47}$$

where$[K_e]$,$[K_g]$and $[N]$ are respectively the elementary stiffness matrix, the geometric matrix and the shape function matrix.

$\{F^e\}$ is the mechanical force vector, while$\{F^T\}$ represents the thermal force vector.

5.4.2 Mechanical buckling

The external work resulting from the compressive axial load can be expressed as follows:

$$W_a = \frac{1}{2} \int_0^L \{q\}^T [G]^T P[G]\{q\}\, dx \tag{5.48}$$

By substituting Eqs. (5.38) and (5.48) into Eq. (5.17), we obtain

$$\Pi = \frac{1}{2} \int_0^L (\{q\}^T([B_a]^T A[B_a] + [B_b]^T D[B_b] + [B_s]^T H[B_s])\{q\})\, dx + \int_0^L \{q\}^T [G]^T P[G]\{q\}\, dx \tag{5.49}$$

Eliminating the second variation from the total potential energy with regard to the nodal values$\{q\}$ leads to the next eigenvalue:

$$([K_e]+[K_g])\{q\}=0 \tag{5.50}$$

$$[K_g] = \int_0^L [G]^T P[G]\, dx \tag{5.51}$$

$[K_g]$ is the elementary geometrical matrix, using the loading factorλ, the load can be rewritten as:

$$P = \lambda P_0 \tag{5.52}$$

5.4.3 Thermal buckling

The stability of a beam subjected to thermo-mechanical loading is determined by the following eigenvalue problem.

$$\left([K_e] + [K_g]\right)\{q\} = 0 \tag{5.53}$$

$$[K_g] = \lambda[K_g^0] \tag{5.54}$$

The Eq. (5.53) can be rewritten as follows:

$$\left([K_e] + \lambda[K_g^0]\right)\{q\} = 0 \tag{5.55}$$

$$[K_g] = \int_0^L [G]^T N^T [G]\, dx \tag{5.56}$$

The critical buckling temperature ΔT_{cr}can be expressed as:

$$\Delta T_{cr} = \lambda_{cr} \Delta T \tag{5.57}$$

ΔT_0 represents the specified temperature rise.

5.5 conclusion

A two-node element, using simple high-order shear deformation theory(SHSDT), for three degrees of freedom (DOFs) per node, has been adapted to analyze the statics and buckling of FG beams. Material properties are assumed to vary across the thickness of the beam as a function of a power-law distribution fraction of the constituents and no correction factor is needed. Total potential energy, the principle of Hamilton, and Lagrange's equation were all used to formulate the geometric stiffness and mass matrices.

The results presented in the next chapter provide a clear assessment of the current finite element model's (SHSDT) contribution, by comparing it with the results in the literature.

Chapter 6: Application of finite element model (SHSDT) – Results and discussion:

6.1 introduction

This chapter presents and discusses several numerical examples to assess the performance of current finite elements. Precision, convergence and stability are assessed by examining the thermal and mechanical buckling behaviour of FG beams. For the purposes of validation, the results obtained are compared with results available in the literature. The impact of various parameters like length to thickness ratio, power law index and boundary conditions on the critical thermal buckling temperature and critical buckling load of FG beams are examined.

6.2 Numerical results and discussions

The results of the thermal and mechanical buckling analysis of FG beams are presented in the following to confirm the validity of the finite element model formulated.

6.2.1 Mechanical buckling analysis

Example 6.1

In this section, we examine FG beam buckling behavior subjected to axial compressive loads. The effects of the power law index, length/depth ratio, and boundary conditions on the critical buckling load are analyzed.

Tables 6.1 to 6.3 show the convergence of critical buckling load under three different boundary conditions for various values of the power law index and for L/h=5 and 10. the beam has been divided into 50, 100, 150,200, and 250 elements.

The properties of the materials are as follows:

Aluminium : E_{me} = 70 GPa, ν_{me}=0.3

Alumina: E_{cr} =380 GPa, ν_{cr} =0.3

Three boundary conditions are considered:

Clamped-clamped (C-C);

Simply supported (S-S) ;

Free of clamped (C-F).

The results obtained are presented in terms of dimensionless values:

$$\overline{P}_{cr} = 12\frac{L^2}{E_m h^3}P_{cr} \quad (6.1)$$

The results obtained are compared with those previously achieved by Benzidand Tati [22]

using enhanced Timoshenko beam theory. Li and Batra [187] using Tmoshenko beam theory (TB), and Nguyen et al[188] using HSDT. In all the cases studied, the comparison showed a significant concordance between the results obtained from the proposed element and those from the sources referenced. Tables 6.1–6.3 indicate indicate a decrease in the critical buckling load as the exponent p of the volume fraction increases. Additionally, the length-to-depth ratio has a substantial effect on the buckling behavior of the beam.It is evident that the critical buckling load increases as the length-to-thickness ratio increases.

Table 6.1 The critical buckling load P_{cr} of a C-C FG beam subjected to axial compressive loading with different power law indices and L/h.

		N ˚ element							
L/h	*P*	*50*	*100*	*150*	*200*	*250*	*SHSDT*[22]	*TB*[187]	*HSDT*[188]
5	0	152.05714	152.0890	152.0017	151.9711	151.9529	151.9500	154.35	154.5610
	1	79.7622	79.4770	79.4242	79.4058	79.3972	79.3929	80.498	80.5940
	2	60.0150	59.8232	59.7877	59.7753	59.7695	60.3060	62.614	61.7666
	5	44.7095	44.6058	44.5867	44.5801	44.5770	45.9138	50.384	47.7174
	10	39.2152	39.1315	39.1160	39.1106	39.1081	39.9214	44.267	41.7885
10	0	197.0875	195.0418	194.6633	194.5310	194.4696	194.4000	195.34	195.3623
	1	99.9435	98.7293	98.5048	98.4262	98.38972	98.3829	98.749	98.7885
	2	76.9699	76.1419	75.9889	75.9352	75.9103	76.1218	76.980	76.6538
	5	62.1723	61.7009	61.6136	61.5832	61.5690	62.1955	64.096	62.9580
	10	55.8474	55.4568	55.3851	55.3599	55.3482	55.7505	57.708	56.5926

Table 6.2 The critical buckling load P_{cr} of a S-S FG beam subjected to axial compressive loading with different power law indices and L/h.

		N ˚ element							
L/h	*P*	*50*	*100*	*150*	*200*	*250*	*SHSDT*[22]	*TB*[187]	*HSDT*[188]
5	0	48.7591	48.6314	48.6079	48.5995	48.5957	48.6000	48.835	48.8406
	1	24.6817	24.6059	24.5919	24.5870	24.5847	24.5786	24.687	24.6894
	2	19.0349	18.6833	18.9738	18.9704	18.9689	19.0286	19.245	19.1577
	5	15.4248	15.3954	15.3899	15.3880	15.3871	15.5437	16.024	15.7355
	10	13.8638	13.8396	13.8351	13.8336	13.8328	13.9335	14.227	14.1448
10	0	52.9232	52.4087	52.3134	52.2801	52.2646	52.2857	52.309	52.3083
	1	26.5476	26.2421	26.1858	26.1660	26.1568	26.1569	26.171	26.1707
	2	20.6145	20.4062	20.3676	20.3541	20.3478	20.3633	20.416	20.3909
	5	17.1640	17.0445	17.0222	17.0146	17.0110	17.0589	17.192	17.1091
	10	15.5639	15.4653	15.4470	15.4406	15.4377	15.4690	15.612	15.5278

Table 6.3 The critical buckling load P_{cr} of a C-F FG beam subjected to axial compressive loading with different power law indices and L/h.

		N ° element							
L/h	*P*	*50*	*100*	*150*	*200*	*250*	*SHSDT*[22]	*TB*[187]	*HSDT*[188]
5	0	13.1017	13.0697	13.0637	13.0616	13.0607	13.0714	13.213	13.0771
	1	6.5603	6.5413	6.5378	6.5365	6.5360	6.5357	6.6002	6.5427
	2	5.1014	5.0884	5.0860	5.0851	5.0847	5.0786	5.1495	5.0977
	5	4.2609	4.2535	4.2521	4.2516	4.2514	4.2634	4.3445	4.2772
	10	3.8662	3.8600	3.8589	3.8585	3.8583	3.8662	3.9502	3.8820
10	0	13.4807	13.3520	13.3280	13.3197	13.3158	13.3714	13.349	13.3741
	1	6.7420	6.6658	6.6517	6.6467	6.6445	6.6446	6.6571	6.6678
	2	5.2470	5.1949	5.1853	5.1808	5.1803	5.1816	5.1945	5.2025
	5	4.4058	4.3758	4.3703	4.3684	4.3674	4.3709	4.3902	4.3974
	10	4.0059	3.9812	3.9766	3.9750	3.9743	3.9765	3.9969	4.0045

6.2.2 Thermal buckling analysis

In this section, the current finite element formulation has been applied to examine the thermal buckling behavior of FG beams.

The properties of the materials used are as follows from[189]:

Si3N4: E(Pa)= 322.27e+9 α (1/K)= 7.4746e-6

SUS304: E(Pa)= 207.79e+9 α (1/K)= 15.32e-6

The Poisson's ratio ν of FG beam is considered constant and equal to 0.3.

Example 6.2

This example is performed for the critical thermal buckling temperature ΔT_{cr} of clamped-clamped supported Si3N4/SUS304 beams under temperature independent (TID) material

properties based on Timoshenko beam theory(L/h=25). The beam has been divided into 450 elements.

The results are presented in table 6.4 and compared with Timoshenko1[189],Timoshenko2[189], and Timoshenko[120]. In general, there is excellent agreement between the results.

Table 6.4 Critical thermal buckling temperature ΔT_{cr} comparisons of Si3N4/SUS304 beams with two clamped ends according to Timoshenko beam theory (L/h=25).

Theory	*P=1*	*P=2*	*P=5*	*P=10*
Present (N° element 450)	459.267	423.842	394.484	376.305
Timoshenko1[189]	458.780	423.624	394.488	376.223
Timoshenko2[189]	458.780	423.624	394.488	376.223
Timoshenko[120]	458.68	423.53	394.39	376.14

Example 6.3

In the second example. A clamped- clamped Si3N4/SUS304 beams based on temperature-independent material properties (TID) is examined. Table 6.5 show that the critical buckling temperature ΔT_{cr} calculated by Timoshenko beam theory for power-law index P= (1,2,5,10) and compared with Euler1 (Euler-Bernoulli model) ,Timoshenko1 (Timoshenko model), Reddy1 (from Reddy[190]) ,ASDBT (from Aydogdu[191]), HBTM1 (from Mantari et al.[192]), HBTM2(from Mantari et al[193], HBTAT1(from Akavci et al[194],HBTAT2(from Akavci et al.[194]),HBTV1 (from Viola et al.[195]) and HBTV2 (from Meiche et al.[196]).

It can be noted that the present results are in good agreement with the references mentioned.

Table 6.5 Critical thermal buckling temperature ΔT_{cr} of Si3N4/SUS304 beams with temperature independent (TID) material under various beam theory.

L/h	Theory		P=1	P=2	P=5	P=10
20	N ° element	100	719.998	663.927	616.927	588.628
		200	712.885	657.469	611.495	583.390
		300	711.568	656.322	610.489	582.420
		400	711.107	655.920	610.137	582.081
	Euler[1]		728.433	672.924	627.009	567.989
	Timoshenko[1]		710.485	655.876	610.569	582.294
	Reddy[1][190]		710.491	655.616	610.86	581.957
	ASDBT[191]		710.597	655.696	610.150	582.054
	HBTM1[192]		710.609	655.706	610.160	582.065
	HBTM2[193]		711.090	656.149	610.584	582.508
	HBTAT1[194]		710.504	655.620	610.084	581.968
	HBTAT[194]		710.645	655.797	610.282	582.097
	HBTV1[195]		716.672	661.877	616.470	587.905
	HBTV2[196]		725.715	670.387	624.603	595.673
30	N ° element	100	329.656	303.842	282.450	269.491
		200	322.538	297.640	277.015	264.250
		300	321.221	296.492	276.009	263.279
		400	320.760	296.091	275.657	262.940
	Euler1		323.748	299.076	278.671	265.722
	Timoshenko1		320.153	295.622	275.375	262.626
	Reddy1[190]		320.154	295.608	275.276	262.557
	ASDBT[191]		320.176	295.624	275.289	262.577
	HBTM1[192]		320.178	295.626	275.291	262.579
	HBTM2[193]		320.275	295.716	275.377	262.669
	HBTAT1[194]		320.157	295.609	275.276	262.560
	HBTAT2[194]		320.186	295.646	275.316	662.586
	HBTV1[195]		321.404	296.875	276.569	263.762
	HBTV2[196]		323.210	298.575	278.194	265.314

40	N° element	100	190.463	175.389	162.900	155.449
		200	183.345	169.197	157.465	150.208
		300	182.027	168.039	156.458	149.237
		400	181.567	167.637	156.106	148.900
	Euler[1]		182.108	168.23	156.752	149.497
	Timoshenko[1]		180.965	167.145	155.704	148.496
	Reddy[1][190]		180.966	167.128	155.672	148.474
	ASDBT[191]		180.972	167.133	155.676	148.480
	HBTM1[192]		180.973	167.133	155.677	148.481
	HBTM2[193]		181.004	167.162	155.704	148.510
	HBTAT1[194]		180.966	167.128	155.672	148.475
	HBTAT2[194]		180.976	167.140	155.685	148.483
	HBTV1[195]		181.364	167.532	156.085	148.859
	HBTV2[196]		181.938	168.072	156.601	149.352

Example 6.4

In this example, table 6.6 gives thethermal critical buckling temperature results. ΔT_{cr} of Si3N4/SUS304 beams under different boundary conditions (clamped-clamped and simply supported), respectively. For different L/h length to depth ratio and power law index P= (0, 1,2,5,10).

The aim of the example is to study the effect of boundary conditions on thermal buckling of Si3N4/SUS304 beams. For a better illustration, the data in Table 6.6 are plotted in figures 6.1 and 6.2 respectively .Figures 6.1 and 6.2 depict the impact of length to depth ratio L/h on critical thermal buckling temperature of Si3N4/SUS304 beams with different boundary conditions. The figures show that for a given power index P, the critical buckling temperature $\Delta T\, cr$ decreases as length-to-depth ratio L/h increases.

Table 6.6 Critical thermal buckling temperature $\Delta T cr$ of Si3N4/SUS304 beams with different boundary conditions.

	Clamped-clamped (C-C)					Simply supported (S-S)				
L/h	P=0	P=1	P=2	P=5	P=10	P=0	P=1	P=2	P=5	P=10
20	1073.7	711.107	655.92	610.137	582.081	273.555	181.121	167.25	155.766	157.57
30	484.412	320.76	296.091	275.657	262.94	122.135	80.862	74.681	69.565	66.349
40	284.216	181.567	167.637	156.106	148.9	68.883	45.606	42.119	39.234	37.42
50	176.218	116.678	107.731	100.325	95.691	44.19	29.258	27.019	25.167	24.003
60	122.796	81.307	75.068	69.905	66.677	30.765	20.369	18.809	17.517	16.708
70	90.519	59.937	55.332	51.522	49.143	22.666	15.008	13.856	12.903	12.307
80	69.544	46.05	42.506	39.574	37.748	17.407	11.526	10.64	9.907	9.449
90	55.152	36.522	33.705	31.375	29.928	13.801	9.139	8.435	7.82	7.49
100	44.851	29.702	27.406	25.506	24.331	11.22	7.431	6.857	6.382	6.088

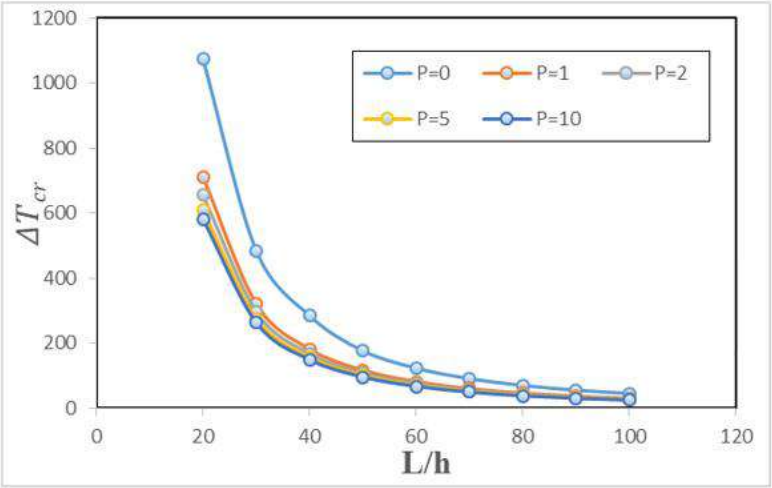

Figure 6. 1 The effect of length-to-depth ratio L/h on critical thermal buckling temperature of Si3N4/SUS304 beams with two clamped ends.

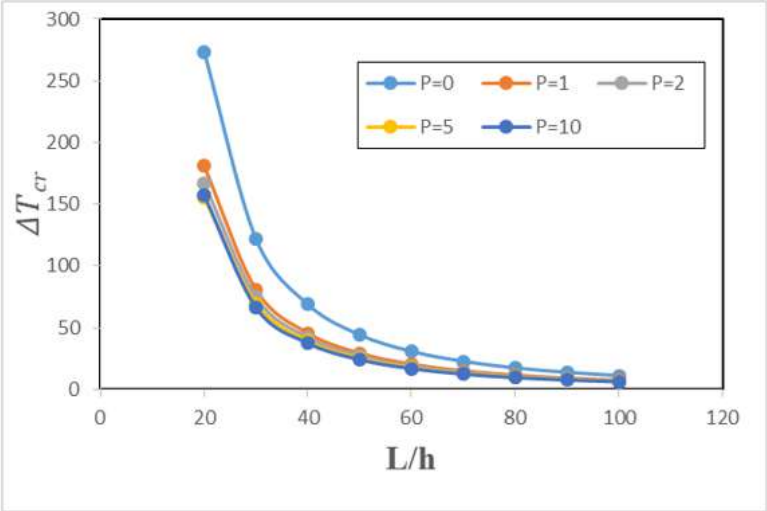

Figure 6. 2 The effect of length-to-depth ratio L/h critical thermal buckling temperature of Si3N4/SUS304 beams with simply supported ends.

6.3 Conclusion

This chapter examines the mechanical and thermal buckling behaviors of FG beams using the current finite element method (SHSDT), which is based on the enhanced Timoshenko beam theory. Critical buckling load numerical findings are shown and contrasted with those found in the body of available literature. The effectiveness and accuracy of the current finite element formulation are validated by the comparisons, which show that the results achieved with the current element closely match those from the references. The effects of some parameters like

length-to-thickness ratio, the power law index, and boundary conditions, on behavior of the FG beams has been also examined.

- The primary findings of this research can be summed up as follows:

The results show that the stability responses of functionally graded (FG) beams are accurately predicted by the developed finite element SHSDT.

- With an increase in the volume fraction exponent p, the critical buckling load reduces.
- The greater the length-to-thickness ratio, the higher the critical buckling load.
- The various boundary conditions have a major impact on the beam's buckling characteristics.
- As the length-to-thickness ratio increases, the dimensionless thermal critical buckling temperature drops.

General Conclusion

The impact of thermal conditions on the behavior of structural elements is particularly critical in Saharan environments. Structures in these regions experience thermal loads resulting from significant daily temperature fluctuations, ranging from intense daytime heat to cooler nighttime temperatures. The behavior of structures is influenced by the behavior of their individual elements. such as beams and columns. In this study, we chose Functionally Graded Materials FGM because a new class of advanced composites that are increasingly being used in various fields of engineering, particularly in high-temperature applications such as thermomechanical load-bearing structures.

Contributing to the modeling of the static, vibrational, and stability behavior of structures under heat conditions is the main objective of this work, by developing of finite elements model that can precisely represent these behaviors. First, a finite element model has been adapted to examine the static and vibration behavior of steel beams while accounting for temperature rise using the Euler-Bernoulli beam theory. Furthermore, an innovative analytical method for examining the static behavior of steel beams with elastic support under uniform temperature rise has been created. Secondly, the buckling analysis of functionally graded beams under thermo-mechanical loading is carried out using the proposed finite element model, based on the simply high-order shear deformation theory (SHSDT) with three degrees of freedom (DOFs) per node and the enhanced Timoshenko beam theory.

In the first part of the thesis, the generalities of temperature, fire, damages caused by fire, and some notable fire incidents of the last years have been presented. Furthermore, Other side, an overview on functionally graded materials and their application areas has been presented. An overview of previous research from the body of literature on the buckling, vibration, and static analysis of concrete, steel, and FGMs beams has been briefly outlined in chapter two.

In the second part, A novel finite element model using Bernoulli beam theory and nonlinear von Karman deformation has been adapted to analyze the static and vibration behavior of steel beams in temperature conditions. The total potential energy principle is used to derive elemental stiffness and geometric matrices. In addition, an analytical approach has been introduced to study the static behavior of elastically supported steel beams exposed to a uniform temperature rise. The supports are modeled by translational and rotational springs, representing the influence of the columns in finite element simulations. the validation of the performance of the finite element developed by comparing its results against those available in the literature. All comparisons show that results obtained with the proposed element agree perfectly with those of the references, confirming the performance and precision of the formulation. Additionally, a parametric study was conducted using both the analytical and finite element models to examine the impact of various support conditions on the thermoelastic behavior of the steel beams. The study revealed that temperature rise significantly influences the static behavior of structural elements, notably affecting their stiffness and strength, leading to a marked increase in deflections and bending moments.

The following points highlight some of the study's important observations:

- From dynamic *behavior* of steel beams under heating conditions:
  The natural frequency decreases with increasing temperature.

As the length of the steel beam is reduced, while the thickness remains constant, the natural frequency increases.

The critical temperature rise for a clamped beam is greater than for a simply supported beam

The natural frequency decreases as the slenderness ratio increases.

When the slenderness ratio decreases so the critical temperature increases.

- From static behavior of steel beams under temperature conditions:
  In all cases , it is observed that as the temperature increases and nears the critical buckling point, the deflection and bending moment at the beam's mid-span increase significantly, approaching infinity.

In the third part, A two-node element, using simple high-order shear deformation theory(SHSDT), for three degrees of freedom (DOFs) per node. The finite element model has been adapted to analyze the statics and buckling of FG beams. Material properties are assumed to vary across the thickness of the beam as a function of a power-law distribution fraction of the constituents and no correction factor is needed. Total potential energy, the principle of Hamilton, and Lagrange's equation were all used to formulate the geometric stiffness and mass matrices. The effectiveness and accuracy of the current finite element formulation are validated by the comparisons, which show that the results achieved with the current element closely match those from the references. The effects of some parameters like length-to-thickness ratio, the power law index, and boundary conditions, on behavior of the FG beams has been also examined.

The following points highlight several of important observations:

- The results show that the stability responses of functionally graded (FG) beams are accurately predicted by the developed finite element (SHSDT).

- With an increase in the volume fraction exponent p, the critical buckling load reduces.
- The greater the length-to-thickness ratio, the higher the critical buckling load.
- The various boundary conditions have a major impact on the beam's buckling characteristics.
- As the length-to-thickness ratio increases, the dimensionless thermal critical buckling temperature drops.

Perspectives:

From a perspective, the SHSDT element will be used to analyze the vibration response of FG beams in thermal setting. This model will also be used to analyze dynamic, buckling, and static behaviors on different types of FG structures.

Finally, this doctoral work contributes to the development of novel theories and finite elements for the analysis of FG structure behavior by the **LGEM** and **EVRANZA** laboratories.

Bibliography

[1] S. HAKKOUM, “Etude des caractéristiques thermiques et mécaniques des briques en terre cuite traditionnelles dans les régions de la wilaya de Ouargla.” 2015.

[2] H. Chaib, “Contribution à l’Etude des Propriétés Thermo-Mécaniques des Briques en Terre Confectionnée par des Fibres Végétale Locale.(Cas de la ville de Ouargla).” 2017.

[3] Y. Wu, S. Fan, B. He, M. Liu, and H. Zhou, “Research on the fire resistance design of high-strength steel hollow columns under axial compression,” *Eng. Struct.*, vol. 234, no. February, p. 111943, 2021, doi: 10.1016/j.engstruct.2021.111943.

[4] G. M. E. Cooke, “An introduction to the mechanical properties of structural steel at elevated temperatures,” *Fire Saf. J.*, vol. 13, no. 1, pp. 45–54, Apr. 1988, doi: 10.1016/0379-7112(88)90032-X.

[5] Z. Zhang, D. Zhou, X. Xu, and X. Li, “Analysis of thick beams with temperature-dependent material properties under thermomechanical loads,” 2020, doi: 10.1177/1369433220901810.

[6] J. Singer, J. Arbocz, and T. Weller, *Buckling experiments: experimental methods in buckling of thin-walled structures, volume 2: shells, built-up structures, composites and additional topics*, vol. 2. John Wiley & Sons, 2002.

[7] L. T. G. Archambault, “sécurité incendie Collection Mémentos acier,” *Nouv. édition*, 2005.

[8] J.-F. Denoël, *Sécurité incendie et constructions en béton*. FEBELCEM, 2007.

[9] R. Ouache, K. M. Nahiduzzaman, K. Hewage, and R. Sadiq, “Performance investigation of fire protection and intervention strategies: Artificial neural network-based assessment framework,” *J. Build. Eng.*, vol. 42, no. September 2020, p. 102439, 2021, doi: 10.1016/j.jobe.2021.102439.

[10] M. Fernández-Vigil, B. Gil Rodríguez, and J. B. Echeverría Trueba, “Fire safety strategies to reduce mortality in dwellings occupied by elderly people: the Spanish case,” *Fire Technol.*, vol. 56, no. 5, pp. 2257–2281, 2020.

[11] J. Smith, A. Dhinsa, F. Rajabali, A. Zheng, S. Bruin, and I. Pike, “The epidemiology of residential fires among children and youth in Canada,” 2018.

[12] J. Clare and H. Kelly, “Fire and at risk populations in Canada,” *Anal. Can. Natl. Fire Inf. Database Abbotsford, BC*, 2017.

[13] J. H. Troitzsch, “Fires, statistics, ignition sources, and passive fire protection measures,” *J. fire Sci.*, vol. 34, no. 3, pp. 171–198, 2016.

[14] Y. Hao, C. Liu, L. Li, J. Wang, Y. Chen, and J. Chen, “Fire Loss Assessment Model Based on Internet Search Engine Query Data,” *Fire Technol.*, 2023, doi:

10.1007/s10694-023-01509-1.

[15] M. Shokouhi *et al.*, “Preventive measures for fire-related injuries and their risk factors in residential buildings: a systematic review,” *J. Inj. violence Res.*, vol. 11, no. 1, p. 1, 2019.

[16] F. J. M. Sierra, J. C. Rubio-Romero, and M. C. R. Gámez, “Status of facilities for fire safety in hotels,” *Saf. Sci.*, vol. 50, no. 7, pp. 1490–1494, 2012.

[17] S. Li, G. Tao, and L. Zhang, “Fire risk assessment of high-rise buildings based on gray-FAHP mathematical model,” *Procedia Eng.*, vol. 211, pp. 395–402, 2018.

[18] S. Granda and T. M. Ferreira, “Assessing vulnerability and fire risk in old urban areas: application to the historical centre of Guimarães,” *Fire Technol.*, vol. 55, pp. 105–127, 2019.

[19] G. Hou, Q. Li, Z. Song, and H. Zhang, “Optimal fire station locations for historic wood building areas considering individual fire spread patterns and different fire risks,” *Case Stud. Therm. Eng.*, vol. 28, p. 101548, 2021.

[20] L. Chen and T. Goto, “Functionally Graded Materials,” *Handb. Adv. Ceram. Mater. Appl. Process. Prop.*, vol. 2–2, pp. 445–464, 2003, doi: 10.1016/B978-012654640-8/50043-2.

[21] M. Koizumi, “FGM activities in Japan,” *Compos. part b Eng.*, vol. 28, no. 1–2, pp. 1–4, 1997.

[22] A. Benzid and A. Tati, “Static and buckling behaviors analysis of FG beams using a three unknowns finite element based on enhanced Timoshenko theory,” *Mech. Adv. Mater. Struct.*, vol. 0, no. 0, pp. 1–12, 2023, doi: 10.1080/15376494.2023.2270969.

[23] S. Amira, “Modeling of Functionally Graded structures behavior Modélisation du comportement des structures en Matériaux Fonctionnellement Gradués (FGM).” Faculté des Sciences et de la technologie, 2022.

[24] S. ELMASCRI, “Contribution à l’étude de l’effet de température sur le comportement vibratoire des structures en matériaux composites avancés.” 2020.

[25] F. Ebrahimi, E. Salari, and S. A. H. Hosseini, “Thermomechanical Vibration Behavior of FG Nanobeams Subjected to Linear and Non-Linear Temperature Distributions,” *J. Therm. Stress.*, vol. 38, no. 12, pp. 1360–1386, 2015, doi: 10.1080/01495739.2015.1073980.

[26] Z. Zhong and G. Nie, *Analytical or Semi-analytical Solutions of Functionally Graded Material Structures*. 2021. doi: 10.1007/978-981-16-2004-1.

[27] M. Herrmann and W. Sobek, “Introduction 1.1,” pp. 1–23, 2016, doi: 10.1002/suco.201600011.Submitted.

[28] J. Caron and J. R. Markusen, *済無No Title No Title No Title*. 2016.

[29] A. Rubert and P. Schaumann, “Structural steel and plane frame assemblies under fire action,” *Fire Saf. J.*, vol. 10, no. 3, pp. 173–184, 1986, doi: 10.1016/0379-7112(86)90014-7.

[30] H. A. Saab and D. A. Nethercot, “Modelling steel frame behaviour under fire conditions,” *Eng. Struct.*, vol. 13, no. 4, pp. 371–382, 1991, doi: 10.1016/0141-

0296(91)90024-7.

[31] S. R. Najjar and I. W. Burgess, “A nonlinear analysis for three-dimensional steel frames in fire conditions,” *Eng. Struct.*, vol. 18, no. 1, pp. 77–89, 1996, doi: 10.1016/0141-0296(95)00101-5.

[32] A. Pchelintsev, Y. Hasemi, T. Wakarnatsu, and Y. Yokobayashi, “Experimental And Numerical Study On The Behaviour Of A Steel Beam Under Ceiling Exposed To A Localized Fire,” *Fire Saf. Sci.*, vol. 5, no. m, pp. 1153–1164, 1997, doi: 10.3801/iafss.fss.5-1153.

[33] C. G. Bailey, D. B. Moore, and T. Lennon, “The structural behaviour of steel columns during a compartment fire in a multi-storey braced steel-frame,” *J. Constr. Steel Res.*, vol. 52, no. 2, pp. 137–157, 1999, doi: 10.1016/S0143-974X(99)00036-X.

[34] C. G. Bailey, “The influence of the thermal expansion of beams on the structural behaviour of columns in steel-framed structures during a fire,” *Eng. Struct.*, vol. 22, no. 7, pp. 755–768, 2000, doi: 10.1016/S0141-0296(99)00028-0.

[35] J. P. C. Rodrigues, I. Cabrita Neves, and J. C. Valente, “Experimental research on the critical temperature of compressed steel elements with restrained thermal elongation,” *Fire Saf. J.*, vol. 35, no. 2, pp. 77–98, 2000, doi: 10.1016/S0379-7112(00)00018-7.

[36] B. A. Izzuddin, L. Song, A. S. Elnashai, and P. J. Dowling, “An integrated adaptive environment for fire and explosion analysis of steel frames — Part II : verification and application,” vol. 53, pp. 87–111, 2000.

[37] A. S. Usmani, J. M. Rotter, S. Lamont, A. M. Sanad, and M. Gillie, “Fundamental principles of structural behaviour under thermal effects,” *Fire Saf. J.*, vol. 36, no. 8, pp. 721–744, 2001, doi: 10.1016/S0379-7112(01)00037-6.

[38] T. C. H. Liu, M. K. Fahad, and J. M. Davies, “Experimental investigation of behaviour of axially restrained steel beams in fire,” *J. Constr. Steel Res.*, vol. 58, no. 9, pp. 1211–1230, 2002, doi: 10.1016/S0143-974X(01)00062-1.

[39] K. H. Tan, S. K. Ting, and Z. F. Huang, “Visco-Elasto-Plastic Analysis of Steel Frames in Fire,” *J. Struct. Eng.*, vol. 128, no. 1, pp. 105–114, 2002, doi: 10.1061/(asce)0733-9445(2002)128:1(105).

[40] Z. Huang, I. Burgess, and R. Plank, “3D Modelling of Beam-columns with General Cross-sections in Fire,” *Third Int. Work. Struct. Fire*, no. May, 2004.

[41] H. M. Ali, P. E. Senseny, and R. L. Alpert, “Lateral displacement and collapse of single-story steel frames in uncontrolled fires,” *Eng. Struct.*, vol. 26, no. 5, pp. 593–607, 2004, doi: 10.1016/j.engstruct.2003.12.007.

[42] P. J. Moss, A. H. Buchanan, J. Seputro, C. Wastney, and R. Welsh, “Effect of support conditions on the fire behaviour of steel and composite beams,” *Fire Mater.*, vol. 28, no. 2–4, pp. 159–175, 2004, doi: 10.1002/fam.855.

[43] Y. Z. Yin and Y. C. Wang, “A numerical study of large deflection behaviour of restrained steel beams at elevated temperatures,” *J. Constr. Steel Res.*, vol. 60, no. 7, pp. 1029–1047, 2004, doi: 10.1016/j.jcsr.2003.09.005.

[44] F. Wald *et al.*, “Experimental behaviour of a steel structure under natural fire,” *Fire Saf. J.*, vol. 41, no. 7, pp. 509–522, 2006, doi: 10.1016/j.firesaf.2006.05.006.

[45] G. Li, P. Wang, and J. Shouchao, "Non-linear finite element analysis of axially restrained steel beams at elevated temperatures in a fire," *J. Constr. Steel Res.*, vol. 63, no. 9, pp. 1175–1183, 2007, doi: 10.1016/j.jcsr.2006.11.009.

[46] K. T. Ng and L. Gardner, "Buckling of stainless steel columns and beams in fire," *Eng. Struct.*, vol. 29, no. 5, pp. 717–730, 2007, doi: 10.1016/j.engstruct.2006.06.014.

[47] G. Q. Li and S. X. Guo, "Experiment on restrained steel beams subjected to heating and cooling," *J. Constr. Steel Res.*, vol. 64, no. 3, pp. 268–274, 2008, doi: 10.1016/j.jcsr.2007.07.007.

[48] M. A. Bradford, T. K. Luu, and A. Heidarpour, "Generic nonlinear modelling of a steel beam in a frame sub-assembly at elevated temperatures," vol. 64, pp. 732–736, 2008, doi: 10.1016/j.jcsr.2007.12.015.

[49] Z. H. Qian, K. H. Tan, and I. W. Burgess, "Numerical and analytical investigations of steel beam-to-column joints at elevated temperatures," *J. Constr. Steel Res.*, vol. 65, no. 5, pp. 1043–1054, 2009, doi: 10.1016/j.jcsr.2008.11.010.

[50] A. Heidarpour and M. A. Bradford, "Generic nonlinear modelling of restrained steel beams at elevated temperatures," *Eng. Struct.*, vol. 31, no. 11, pp. 2787–2796, 2009, doi: 10.1016/j.engstruct.2009.07.006.

[51] A. Heidarpour, A. Azim Abdullah, and M. A. Bradford, "Non-linear thermoelastic analysis of steel arch members subjected to fire," *Fire Saf. J.*, vol. 45, no. 3, pp. 183–192, 2010, doi: 10.1016/j.firesaf.2010.02.004.

[52] M. M. S. Dwaikat, V. K. R. Kodur, S. E. Quiel, and M. E. M. Garlock, "Experimental behavior of steel beam-columns subjected to fire-induced thermal gradients," *J. Constr. Steel Res.*, vol. 67, no. 1, pp. 30–38, 2011, doi: 10.1016/j.jcsr.2010.07.007.

[53] K. H. Lien, Y. J. Chiou, R. Z. Wang, and P. A. Hsiao, "Vector Form Intrinsic Finite Element analysis of nonlinear behavior of steel structures exposed to fire," *Eng. Struct.*, vol. 32, no. 1, pp. 80–92, 2010, doi: 10.1016/j.engstruct.2009.08.018.

[54] M. M. S. Dwaikat and V. K. R. Kodur, "A performance based methodology for fire design of restrained steel beams," *J. Constr. Steel Res.*, vol. 67, no. 3, pp. 510–524, 2011, doi: 10.1016/j.jcsr.2010.09.004.

[55] N. Lopes, P. Vila Real, L. Simões Da Silva, and J. M. Franssen, "Numerical analysis of stainless steel beam-columns in case of fire," *Fire Saf. J.*, vol. 50, pp. 35–50, 2012, doi: 10.1016/j.firesaf.2012.02.003.

[56] Y. Xu and D. Zhou, "Two-dimensional thermoelastic analysis of beams with variable thickness subjected to thermo-mechanical loads," *Appl. Math. Model.*, vol. 36, no. 12, pp. 5818–5829, 2012, doi: 10.1016/j.apm.2012.01.048.

[57] A. E. Jeffers and E. D. Sotelino, "An efficient fiber element approach for the thermo-structural simulation of non-uniformly heated frames," *Fire Saf. J.*, vol. 51, pp. 18–26, 2012, doi: 10.1016/j.firesaf.2012.02.002.

[58] J. Jiang and A. Usmani, "Modeling of steel frame structures in fire using OpenSees," *Comput. Struct.*, vol. 118, pp. 90–99, 2013, doi: 10.1016/j.compstruc.2012.07.013.

[59] C. Zhang, J. L. Gross, and T. P. McAllister, "Lateral torsional buckling of steel W-beams subjected to localized fires," *J. Constr. Steel Res.*, vol. 88, pp. 330–338, 2013, doi:

10.1016/j.jcsr.2013.06.004.

[60] J. N. Sharma and R. Kaur, "Flexural response of thermoelastic thin beam resonators due to thermal and mechanical loads," *Int. J. Mech. Sci.*, vol. 101–102, pp. 170–179, 2015, doi: 10.1016/j.ijmecsci.2015.07.014.

[61] C. Couto, P. Vila Real, N. Lopes, and B. Zhao, "Resistance of steel cross-sections with local buckling at elevated temperatures," *J. Constr. Steel Res.*, vol. 109, pp. 101–114, 2015, doi: 10.1016/j.jcsr.2015.03.005.

[62] M. Prachar, J. Hricak, M. Jandera, F. Wald, and B. Zhao, "Experiments of Class 4 open section beams at elevated temperature," *Thin-Walled Struct.*, vol. 98, pp. 2–18, 2016, doi: 10.1016/j.tws.2015.04.025.

[63] P. Wang, C. Liu, and M. Liu, "Large deflection behavior of restrained corrugated web steel beams in a fire," *J. Constr. Steel Res.*, vol. 126, pp. 92–106, 2016, doi: 10.1016/j.jcsr.2016.07.017.

[64] W. F. Ragheb, "Local buckling capacity of steel I-section beams subjected to uniform or linear temperature gradient," *Thin-Walled Struct.*, vol. 119, no. January, pp. 304–314, 2017, doi: 10.1016/j.tws.2017.06.017.

[65] G. Q. Li and C. Zhang, "Integrated fire-structure simulation of a localzied fire test on a ceiling steel beam," *Adv. Steel Constr.*, vol. 13, no. 2, pp. 132–143, 2017, doi: 10.18057/IJASC.2017.13.2.3.

[66] H. Varol and K. A. Cashell, "Numerical modelling of high strength steel beams at elevated temperature," *Fire Saf. J.*, vol. 89, no. December, pp. 41–50, 2017, doi: 10.1016/j.firesaf.2017.02.005.

[67] L. Zhang, X. Zhang, S. Li, and J. Qian, "Study on thermal response of building steel structure components in fire," *Chem. Eng. Trans.*, vol. 66, pp. 379–384, 2018, doi: 10.3303/CET1866064.

[68] A. Pournaghshband, S. Afshan, and M. Theofanous, "Elevated temperature performance of restrained stainless steel beams," *Structures*, vol. 22, no. August, pp. 278–290, 2019, doi: 10.1016/j.istruc.2019.08.015.

[69] S. Ramesh, L. Choe, and C. Zhang, "Experimental investigation of structural steel beams subjected to localized fire," *Eng. Struct.*, vol. 218, no. October 2019, p. 110844, 2020, doi: 10.1016/j.engstruct.2020.110844.

[70] M. Zhou, R. P. R. Cardoso, H. Bahai, and A. Usmani, "A thermo-mechanical analysis of stainless steel structures in fire," *Eng. Struct.*, vol. 210, no. July 2019, p. 110091, 2020, doi: 10.1016/j.engstruct.2019.110091.

[71] M. Kucukler, "Lateral instability of steel beams in fire: Behaviour, numerical modelling and design," *J. Constr. Steel Res.*, vol. 170, p. 106095, 2020, doi: 10.1016/j.jcsr.2020.106095.

[72] J. Yang, W. Wang, Y. Shi, and L. Xu, "Experimental study on fire resistance of cold-formed steel built-up box columns," *Thin-Walled Struct.*, vol. 147, no. December 2019, p. 106564, 2020, doi: 10.1016/j.tws.2019.106564.

[73] L. Laím, H. D. Craveiro, R. Simões, A. Escudeiro, and A. Mota, "Experimental analysis of cold-formed steel columns with intermediate and edge stiffeners in fire," *Thin-Walled*

Struct., vol. 146, no. February 2019, 2020, doi: 10.1016/j.tws.2019.106481.

[74] G. Segura, A. Pournaghshband, S. Afshan, and E. Mirambell, "Numerical simulation and analysis of stainless steel frames at high temperature," *Eng. Struct.*, vol. 227, no. November 2020, p. 111446, 2021, doi: 10.1016/j.engstruct.2020.111446.

[75] X. T. Nguyen and J. S. Park, "Nonlinear Buckling Strength of Steel H-Beam under Localized Fire and Pure Bending," *KSCE J. Civ. Eng.*, vol. 25, no. 2, pp. 561–573, 2021, doi: 10.1007/s12205-020-0291-z.

[76] S. Suman and A. Samanta, "Behavior of laterally unsupported monosymmetric steel I-section beams at elevated temperature under non-uniform moments," *Structures*, vol. 33, no. April, pp. 3324–3356, 2021, doi: 10.1016/j.istruc.2021.06.070.

[77] S. Suman and A. Samanta, "A new proposal for design of laterally unsupported monosymmetric steel I-section beams at elevated temperature," *Structures*, vol. 38, no. February, pp. 1277–1294, 2022, doi: 10.1016/j.istruc.2022.02.057.

[78] S. Suman and A. Samanta, "Proposed design methodology for laterally unrestrained monosymmetric I-beams in fire," *Innov. Infrastruct. Solut.*, vol. 7, no. 6, pp. 1–18, 2022, doi: 10.1007/s41062-022-00972-z.

[79] M. Kucukler, "In-plane structural response and design of steel I-section beam-columns at elevated temperatures," *Structures*, vol. 39, no. February, pp. 1045–1062, 2022, doi: 10.1016/j.istruc.2022.03.026.

[80] S. Suman, R. Singh, S. Shukla, and A. Samanta, "Experimental and numerical investigation of hot-rolled steel beam in localized fire," *Mater. Today Proc.*, vol. 65, pp. 741–745, 2022, doi: 10.1016/j.matpr.2022.03.283.

[81] B. G. A. Gurupatham, K. Roy, G. M. Raftery, and J. B. P. Lim, "Influence of Intermediate Stiffeners on Axial Capacity of Thin-Walled Built-Up Open and Closed Channel Section Columns," *Buildings*, vol. 12, no. 8, 2022, doi: 10.3390/buildings12081071.

[82] Z. Fang *et al.*, "Structural behaviour of back-to-back cold-formed steel channel sections with web openings under axial compression at elevated temperatures," *J. Build. Eng.*, vol. 54, no. May, p. 104512, 2022, doi: 10.1016/j.jobe.2022.104512.

[83] S. Suman and A. Samanta, "Behavior of unrestrained hot-rolled steel I-beams exposed to localized fire: An experimental study," *Eng. Struct.*, vol. 296, no. June, p. 116953, 2023, doi: 10.1016/j.engstruct.2023.116953.

[84] Y. X. Guo, F. Xi, Y. H. Tan, F. Liu, and Y. C. Hu, "Effects of connection types and elevated temperature on the impact behaviour of restrained beam in portal steel frame," *Def. Technol.*, vol. 25, pp. 174–191, 2023, doi: 10.1016/j.dt.2022.04.017.

[85] S. Suman, A. Samanta, and P. K. Singh, "Behaviour, design, and reliability of monosymmetric I-beams at elevated temperature," *Structures*, vol. 63, no. March, p. 106342, 2024, doi: 10.1016/j.istruc.2024.106342.

[86] M. Habashneh, R. Cucuzza, M. Domaneschi, and M. Movahedi Rad, "Advanced elasto-plastic topology optimization of steel beams under elevated temperatures," *Adv. Eng. Softw.*, vol. 190, no. October 2023, p. 103596, 2024, doi: 10.1016/j.advengsoft.2024.103596.

[87] R. Aldarf, M. Al-Allaf, A. Salem, H. Meree, F. Mubark, and B. Akkari, "Fire

Performance of Reinforced Concrete Slabs: Direct Flame Effects," *Jordan J. Civ. Eng.*, vol. 18, no. 1, pp. 95–109, 2024, doi: 10.14525/JJCE.v18i1.08.

[88] U. Schneider, "Concrete at high temperatures - A general review," *Fire Saf. J.*, vol. 13, no. 1, pp. 55–68, 1988, doi: 10.1016/0379-7112(88)90033-1.

[89] M. J. Terro, "Numerical modeling of the behavior of concrete structures in fire," *ACI Struct. J.*, vol. 95, no. 2, pp. 183–193, 1998, doi: 10.14359/538.

[90] J. M. Franssen, "Failure temperature of a system comprising a restrained column submitted to fire," *Fire Saf. J.*, vol. 34, no. 2, pp. 191–207, 2000, doi: 10.1016/S0379-7112(99)00047-8.

[91] L. Lim and C. Wade, "Experimental Fire Tests of Two-Way Concrete Slabs - Fire Engineering Research Report 02/12," no. June 2015, pp. 1–96, 2002.

[92] L. Lim, A. Buchanan, P. Moss, and J. M. Franssen, "Numerical modelling of two-way reinforced concrete slabs in fire," *Eng. Struct.*, vol. 26, no. 8, pp. 1081–1091, 2004, doi: 10.1016/j.engstruct.2004.03.009.

[93] C. G. Bailey and W. S. Toh, "Behaviour of concrete floor slabs at ambient and elevated temperatures," *Fire Saf. J.*, vol. 42, no. 6–7, pp. 425–436, 2007, doi: 10.1016/j.firesaf.2006.11.009.

[94] I. A. Fletcher, S. Welch, J. L. Torero, R. O. Carvel, and A. Usmani, "Behaviour of concrete structures in fire," *Therm. Sci.*, vol. 11, no. 2, pp. 37–52, 2007, doi: 10.2298/TSCI0702037F.

[95] V. K. R. Kodur and M. Dwaikat, "A numerical model for predicting the fire resistance of reinforced concrete beams," *Cem. Concr. Compos.*, vol. 30, no. 5, pp. 431–443, 2008, doi: 10.1016/j.cemconcomp.2007.08.012.

[96] B. Young and E. Ellobody, "Performance of axially restrained concrete encased steel composite columns at elevated temperatures," *Eng. Struct.*, vol. 33, no. 1, pp. 245–254, 2011, doi: 10.1016/j.engstruct.2010.10.019.

[97] A. A. Hammadi, A. F. Izzat, and J. A. Farhan, "Effect of Fire Flame (High Temperature) on the Self Compacted Concrete (SCC) One Way Slabs," *J. Eng.*, vol. 18, no. 10, pp. 1083–1099, 2023, doi: 10.31026/j.eng.2012.10.01.

[98] Y. Wang, Y. L. Dong, and G. C. Zhou, "Nonlinear numerical modeling of two-way reinforced concrete slabs subjected to fire," *Comput. Struct.*, vol. 119, pp. 23–36, 2013, doi: 10.1016/j.compstruc.2012.12.029.

[99] M. Mohamed Bikhiet, N. F. El-Shafey, and H. M. El-Hashimy, "Behavior of reinforced concrete short columns exposed to fire," *Alexandria Eng. J.*, vol. 53, no. 3, pp. 643–653, 2014, doi: 10.1016/j.aej.2014.03.011.

[100] F. Liao and Z. Huang, "An extended finite element model for modelling localised fracture of reinforced concrete beams in fire," *Comput. Struct.*, vol. 152, pp. 11–26, 2015, doi: 10.1016/j.compstruc.2015.02.006.

[101] J. P. C. Rodrigues and L. Laim, "Fire response of restrained composite columns made with concrete filled hollow sections under different end-support conditions," *Eng. Struct.*, vol. 141, pp. 83–96, 2017, doi: 10.1016/j.engstruct.2017.02.073.

[102] J. Jiang and G. Q. Li, "Parameters affecting tensile membrane action of reinforced concrete floors subjected to elevated temperatures," *Fire Saf. J.*, vol. 96, no. January, pp. 59–73, 2018, doi: 10.1016/j.firesaf.2017.12.006.

[103] W. A. Waryosh and H. H. Hashim, "Behavior of Reinforced Concrete Bubbled Slabs Exposed to Fire Flame under Static Load," *Int. J. Latest Eng. Res. Appl.*, vol. 4, no. 12, pp. 25–37, 2019.

[104] D. Yang, F. Liu, S. S. Huang, and H. Yang, "Structural fire safety design of square and rectangular tubed-reinforced-concrete columns," *Structures*, vol. 29, no. June 2020, pp. 1286–1321, 2021, doi: 10.1016/j.istruc.2020.12.014.

[105] B. Kanagaraj *et al.*, "Mechanical Properties and Microstructure Characteristics of Self-compacting Concrete with Different Admixtures Exposed to Elevated Temperatures," *Jordan J. Civ. Eng.*, vol. 17, no. 1, 2023, doi: 10.14525/jjce.v17i1.01.

[106] B. Li, Z. Li, Z. Chen, Z. Yang, and Y. Zhang, "Experimental Study on the Structural Performance of Reinforced Truss Concrete Composite Slabs during and after Fire," *Buildings*, vol. 13, no. 7, 2023, doi: 10.3390/buildings13071615.

[107] F. Salihu, Z. Guri, M. Cvetkovska, and F. Pllana, "Fire Resistance Analysis of Two-Way Reinforced Concrete Slabs," *Civ. Eng. J.*, vol. 9, no. 5, pp. 1085–1104, 2023, doi: 10.28991/CEJ-2023-09-05-05.

[108] P. GN and R. JN, "Nonlinear transient thermoelastic analysis of functionally graded ramic–metal plates," *Int. J. Solids Struct.*, vol. 35, no. 1987, pp. 4457–76, 1998.

[109] A. A. Khdeir, "Thermal buckling of cross-ply laminated composite beams," *Acta Mech.*, vol. 149, no. 1–4, pp. 201–213, 2001, doi: 10.1007/BF01261672.

[110] A. Mossavarali and M. R. Eslami, "Thermoelastic buckling of plates with imperfections based on a higher order displacement field," *J. Therm. Stress.*, vol. 25, no. 8, pp. 745–771, 2002, doi: 10.1080/01495730290074513.

[111] A. Rastgo, H. Shafie, and A. Allahverdizadeh, "Instability of curved beams made of functionally graded material under thermal loading," *Int. J. Mech. Mater. Des.*, vol. 2, no. 1–2, pp. 117–128, 2005, doi: 10.1007/s10999-005-4446-3.

[112] S. R. Li, J. H. Zhang, and Y. G. Zhao, "Thermal post-buckling of functionally graded material Timoshenko beams," *Appl. Math. Mech. (English Ed.*, vol. 27, no. 6, pp. 803–810, 2006, doi: 10.1007/s10483-006-0611-y.

[113] X. Song and S. R. Li, "Thermal buckling and post-buckling of pinned-fixed Euler-Bernoulli beams on an elastic foundation," *Mech. Res. Commun.*, vol. 34, no. 2, pp. 164–171, 2007, doi: 10.1016/j.mechrescom.2006.06.006.

[114] S. R. Li and R. C. Batra, "Thermal buckling and postbuckling of Euler-Bernoulli beams supported on nonlinear elastic foundations," *AIAA J.*, vol. 45, no. 3, pp. 712–720, 2007, doi: 10.2514/1.24720.

[115] R. Kadoli, K. Akhtar, and N. Ganesan, "Static analysis of functionally graded beams using higher order shear deformation theory," *Appl. Math. Model.*, vol. 32, no. 12, pp. 2509–2525, 2008, doi: 10.1016/j.apm.2007.09.015.

[116] M. A. Vaz, M. S. Nascimento, and R. F. Solano, "Initial postbuckling of elastic rods subjected to thermal loads and resting on an elastic foundation," *J. Therm. Stress.*, vol.

30, no. 4, pp. 381–393, 2007, doi: 10.1080/01495730601146352.

[117] X. Zhao, Y. Y. Lee, and K. M. Liew, "Mechanical and thermal buckling analysis of functionally graded plates," *Compos. Struct.*, vol. 90, no. 2, pp. 161–171, 2009, doi: 10.1016/j.compstruct.2009.03.005.

[118] Y. Kiani and M. R. Eslami, "Thermal buckling analysis of functionally graded material beams," *Int. J. Mech. Mater. Des.*, vol. 6, no. 3, pp. 229–238, 2010, doi: 10.1007/s10999-010-9132-4.

[119] L. S. Ma and D. W. Lee, "A further discussion of nonlinear mechanical behavior for FGM beams under in-plane thermal loading," *Compos. Struct.*, vol. 93, no. 2, pp. 831–842, 2011, doi: 10.1016/j.compstruct.2010.07.011.

[120] S. E. Esfahani, Y. Kiani, and M. R. Eslami, "Non-linear thermal stability analysis of temperature dependent FGM beams supported on non-linear hardening elastic foundations," *Int. J. Mech. Sci.*, vol. 69, pp. 10–20, 2013, doi: 10.1016/j.ijmecsci.2013.01.007.

[121] H. S. Shen and Z. X. Wang, "Nonlinear analysis of shear deformable FGM beams resting on elastic foundations in thermal environments," *Int. J. Mech. Sci.*, vol. 81, pp. 195–206, 2014, doi: 10.1016/j.ijmecsci.2014.02.020.

[122] Y. Sun, S. R. Li, and R. C. Batra, "Thermal buckling and post-buckling of FGM Timoshenko beams on nonlinear elastic foundation," *J. Therm. Stress.*, vol. 39, no. 1, pp. 11–26, 2016, doi: 10.1080/01495739.2015.1120627.

[123] C. P. Wu and S. Ding, "Thermal buckling of FGEM plates integrated with surface-bonded piezoelectric layers and temperature-dependent material properties," *J. Therm. Stress.*, vol. 40, no. 4, pp. 420–447, 2017, doi: 10.1080/01495739.2016.1256009.

[124] A. M. Dehrouyeh-Semnani, "On the thermally induced non-linear response of functionally graded beams," *Int. J. Eng. Sci.*, vol. 125, pp. 53–74, 2018, doi: 10.1016/j.ijengsci.2017.12.001.

[125] A. Mojahedin, M. Jabbari, and T. Rabczuk, "Thermoelastic analysis of functionally graded porous beam," *J. Therm. Stress.*, vol. 41, no. 8, pp. 937–950, 2018, doi: 10.1080/01495739.2018.1446374.

[126] H. Babaei, Y. Kiani, and M. Reza Eslami, "Thermal buckling and post-buckling analysis of geometrically imperfect FGM clamped tubes on nonlinear elastic foundation," *Appl. Math. Model.*, vol. 71, pp. 12–30, 2019, doi: 10.1016/j.apm.2019.02.009.

[127] H. Babaei, Y. Kiani, and M. Reza Eslami, "Buckling and Post-Buckling Analysis of Geometrically Imperfect FGM Pin-Ended Tubes Surrounded by Nonlinear Elastic Medium Under Compressive and Thermal Loads," *Int. J. Struct. Stab. Dyn.*, vol. 19, no. 8, pp. 1–31, 2019, doi: 10.1142/S0219455419500895.

[128] C. Wen, L. Tang, and G. Yang, "Buckling and post-buckling of pinned Euler beams on weakened Winkler foundation under thermal loading," *J. Therm. Stress.*, vol. 43, no. 5, pp. 529–542, 2020, doi: 10.1080/01495739.2020.1734128.

[129] R. Penna, L. Feo, and G. Lovisi, "Hygro-thermal bending behavior of porous FG nano-beams via local/nonlocal strain and stress gradient theories of elasticity," *Compos. Struct.*, vol. 263, no. January, p. 113627, 2021, doi: 10.1016/j.compstruct.2021.113627.

[130] A. Tati, “Finite element analysis of thermal and mechanical buckling behavior of functionally graded plates,” *Arch. Appl. Mech.*, vol. 91, no. 11, pp. 4571–4587, 2021, doi: 10.1007/s00419-021-02025-w.

[131] M. Ali Rachedi, A. Bouhadra, B. Mamen, S. Benyoucef, A. Tounsi, and M. H. Ghazwani, “Assessment of the effect of the materials composition on the bending response of FG plates lying on two models of elastic foundations in thermo-hygro-mechanical environments,” *Acta Mech.*, vol. 234, no. 12, pp. 6315–6340, 2023, doi: 10.1007/s00707-023-03696-y.

[132] J. Avsec and M. Oblak, “Thermal vibrational analysis for simply supported beam and clamped beam,” *J. Sound Vib.*, vol. 308, no. 3–5, pp. 514–525, 2007, doi: 10.1016/j.jsv.2007.04.002.

[133] C. Alkalah, “**済無**No Title No Title No Title,” vol. 19, no. 5, pp. 1–23, 2016.

[134] R. D. Nayeri, S. F. Masri, R. G. Ghanem, and R. L. Nigbor, “A novel approach for the structural identification and monitoring of a full-scale 17-story building based on ambient vibration measurements,” *Smart Mater. Struct.*, vol. 17, no. 2, 2008, doi: 10.1088/0964-1726/17/2/025006.

[135] R. Sun, Z. Huang, and I. W. Burgess, “Progressive collapse analysis of steel structures under fire conditions,” *Eng. Struct.*, vol. 34, pp. 400–413, 2012, doi: 10.1016/j.engstruct.2011.10.009.

[136] W. Zhang, H. Chen, D. Zhu, and X. Kong, “The thermal effects on high-frequency vibration of beams using energy flow analysis,” *J. Sound Vib.*, vol. 333, no. 9, pp. 2588–2600, 2014, doi: 10.1016/j.jsv.2013.12.020.

[137] D. F. Cui and H. Y. Hu, “Thermal buckling and natural vibration of the beam with an axial stick-slip-stop boundary,” *J. Sound Vib.*, vol. 333, no. 8, pp. 2271–2282, 2014, doi: 10.1016/j.jsv.2013.11.042.

[138] S. K. Lai and L. H. Zhang, “Thermal effect on vibration and buckling analysis of thin isotropic/orthotropic rectangular plates with crack defects,” *Eng. Struct.*, vol. 177, no. March, pp. 444–458, 2018, doi: 10.1016/j.engstruct.2018.07.010.

[139] A. C. Santos Silva, C. M. Sebastian, J. Lambros, and E. A. Patterson, “High temperature modal analysis of a non-uniformly heated rectangular plate: Experiments and simulations,” *J. Sound Vib.*, vol. 443, pp. 397–410, 2019, doi: 10.1016/j.jsv.2018.11.041.

[140] M. Hossain and J. Lellep, “Effect of temperature on dynamic behavior of cracked metallic and composite beam,” *Vibroengineering Procedia*, vol. 32, pp. 172–178, 2020, doi: 10.21595/vp.2020.21337.

[141] K. Kamei, M. A. Khan, and K. A. Khan, “Characterising modal behaviour of a cantilever beam at different heating rates for isothermal conditions,” *Appl. Sci.*, vol. 11, no. 10, pp. 10–19, 2021, doi: 10.3390/app11104375.

[142] M. J. Wu, J. Zhu, I. Azim, and X. H. Huang, “Thermal buckling and vibration analysis of cold-formed steel sections,” *Case Stud. Therm. Eng.*, vol. 32, no. February, p. 101910, 2022, doi: 10.1016/j.csite.2022.101910.

[143] J. Zang, H. M. Ren, X. Y. Song, Z. Zhang, Y. W. Zhang, and L. Q. Chen, “Vibration control of interconnected composite beams: Dynamical analysis and experimental

validations," *Mech. Syst. Signal Process.*, vol. 208, no. October 2023, p. 111008, 2024, doi: 10.1016/j.ymssp.2023.111008.

[144] Y. Xia, H. Hao, G. Zanardo, and A. Deeks, "Long term vibration monitoring of an RC slab: Temperature and humidity effect," *Eng. Struct.*, vol. 28, no. 3, pp. 441–452, 2006, doi: 10.1016/j.engstruct.2005.09.001.

[145] J. F. Clinton, S. C. Bradford, T. H. Heaton, and J. Favela, "The observed wander of the natural frequencies in a structure," *Bull. Seismol. Soc. Am.*, vol. 96, no. 1, pp. 237–257, 2006, doi: 10.1785/0120050052.

[146] C. Liu and J. T. DeWolf, "Effect of temperature on modal variability for a curved concrete bridge," *Smart Struct. Mater. 2006 Sensors Smart Struct. Technol. Civil, Mech. Aerosp. Syst.*, vol. 6174, no. December, p. 61743B, 2006, doi: 10.1117/12.655811.

[147] B. Jia, J. L. Tao, Z. L. Li, and R. Wang, "Dynamic mechanical performance of concrete at elevated temperatures," in *The 4th international conference on protection of structures against hazards, Beijing*, 2009, pp. 189–193.

[148] K. V. Yuen and S. C. Kuok, "Ambient interference in long-term monitoring of buildings," *Eng. Struct.*, vol. 32, no. 8, pp. 2379–2386, 2010, doi: 10.1016/j.engstruct.2010.04.012.

[149] Y. He, J. Huo, and Y. Xiao, "Experimental study on dynamic behavior of concrete at elevated temperatures," *Adv. Sci. Lett.*, vol. 4, no. 3, pp. 1128–1131, 2011.

[150] Y. Xia, Y. L. Xu, Z. L. Wei, H. P. Zhu, and X. Q. Zhou, "Variation of structural vibration characteristics versus non-uniform temperature distribution," *Eng. Struct.*, vol. 33, no. 1, pp. 146–153, 2011, doi: 10.1016/j.engstruct.2010.09.027.

[151] Z. Li, J. Xu, and E. Bai, "Static and dynamic mechanical properties of concrete after high temperature exposure," *Mater. Sci. Eng. A*, vol. 544, pp. 27–32, 2012.

[152] J. S. Huo, Y. M. He, L. P. Xiao, and B. S. Chen, "Experimental study on dynamic behaviours of concrete after exposure to high temperatures up to 700 C," *Mater. Struct.*, vol. 46, pp. 255–265, 2013.

[153] Y. Wang, D. S. Liu, and S. Li, "Static and dynamic mechanical properties of concrete after high temperature treatment," *J. Vib. Shock*, vol. 33, no. 20, pp. 16–19, 2014.

[154] Y. Li, "Influence of the Temperature to the Evolvement of Dynamic Characteriscs of Concrete Girder Bridge," *Beijing Jiaotong Univ. Beijing, China*, 2016.

[155] C. Zhai, L. Chen, Q. Fang, W. Chen, and X. Jiang, "Experimental study of strain rate effects on normal weight concrete after exposure to elevated temperature," *Mater. Struct.*, vol. 50, pp. 1–11, 2017.

[156] L. Sun, Y. Zhou, and Z. Min, "Experimental Study on the Effect of Temperature on Modal Frequencies of Bridges," *Int. J. Struct. Stab. Dyn.*, vol. 18, no. 12, 2018, doi: 10.1142/S0219455418501559.

[157] Y. Liu, Z. Li, B. Jin, and J. Huo, "Experimental investigation on dynamic behavior of concrete after exposure to elevated temperatures," *Eur. J. Environ. Civ. Eng.*, vol. 24, no. 13, pp. 2151–2167, 2020, doi: 10.1080/19648189.2018.1500310.

[158] Y. Cai, K. Zhang, Z. Ye, C. Liu, K. Lu, and L. Wang, "Influence of temperature on the

natural vibration characteristics of simply supported reinforced concrete beam," *Sensors*, vol. 21, no. 12, 2021, doi: 10.3390/s21124242.

[159] B. Zima and M. Krajewski, "The vibration-based assessment of the influence of elevated temperature on the condition of concrete beams with pultruded GFRP reinforcement," *Compos. Struct.*, vol. 282, p. 115040, 2022, doi: 10.1016/j.compstruct.2021.115040.

[160] C. Liu, X. Huang, Y. Zhao, and J. Miao, "Vibration analysis of concrete T-beam at elevated temperatures based on modified finite element model," *J. Build. Eng.*, vol. 52, no. October 2021, p. 104381, 2022, doi: 10.1016/j.jobe.2022.104381.

[161] N. Sundararajan, T. Prakash, and M. Ganapathi, "Nonlinear free flexural vibrations of functionally graded rectangular and skew plates under thermal environments," *Finite Elem. Anal. Des.*, vol. 42, no. 2, pp. 152–168, 2005, doi: 10.1016/j.finel.2005.06.001.

[162] N. Wattanasakulpong, B. G. Prusty, and D. W. Kelly, "Thermal buckling and elastic vibration of third-order shear deformable functionally graded beams," *Int. J. Mech. Sci.*, vol. 53, no. 9, pp. 734–743, 2011.

[163] F. Alijani, F. Bakhtiari-Nejad, and M. Amabili, "Nonlinear vibrations of FGM rectangular plates in thermal environments," *Nonlinear Dyn.*, vol. 66, no. 3, pp. 251–270, 2011, doi: 10.1007/s11071-011-0049-8.

[164] D.-G. Zhang, "Thermal post-buckling and nonlinear vibration analysis of FGM beams based on physical neutral surface and high order shear deformation theory," *Meccanica*, vol. 49, pp. 283–293, 2014.

[165] N. Dinh Duc and P. Hong Cong, "Nonlinear vibration of thick FGM plates on elastic foundation subjected to thermal and mechanical loads using the first-order shear deformation plate theory," *Cogent Eng.*, vol. 2, no. 1, p. 1045222, 2015.

[166] M. Taczała, R. Buczkowski, and M. Kleiber, "Nonlinear free vibration of pre-and post-buckled FGM plates on two-parameter foundation in the thermal environment," *Compos. Struct.*, vol. 137, pp. 85–92, 2016.

[167] Ş. D. Akbaş, "Wave propagation of a functionally graded beam in thermal environments," *Steel Compos. Struct.*, vol. 19, no. 6, pp. 1421–1447, 2015.

[168] P. Zahedinejad, "Free vibration analysis of functionally graded beams resting on elastic foundation in thermal environment," *Int. J. Struct. Stab. Dyn.*, vol. 16, no. 07, p. 1550029, 2016.

[169] N. Wattanasakulpong and V. Ungbhakorn, "Linear and nonlinear vibration analysis of elastically restrained ends FGM beams with porosities," *Aerosp. Sci. Technol.*, vol. 32, no. 1, pp. 111–120, 2014.

[170] L. C. Trinh, T. P. Vo, H.-T. Thai, and T.-K. Nguyen, "An analytical method for the vibration and buckling of functionally graded beams under mechanical and thermal loads," *Compos. Part B Eng.*, vol. 100, pp. 152–163, 2016.

[171] N. Dinh Duc, P. Dinh Nguyen, and N. Dinh Khoa, "Nonlinear dynamic analysis and vibration of eccentrically stiffened S-FGM elliptical cylindrical shells surrounded on elastic foundations in thermal environments," *Thin-Walled Struct.*, vol. 117, no. April, pp. 178–189, 2017, doi: 10.1016/j.tws.2017.04.013.

[172] Y. Chen, G. Jin, C. Zhang, T. Ye, and Y. Xue, "Thermal vibration of FGM beams with

general boundary conditions using a higher-order shear deformation theory," *Compos. Part B Eng.*, vol. 153, pp. 376–386, 2018.

[173] M. Amir and M. Talha, "Thermoelastic vibration of shear deformable functionally graded curved beams with microstructural defects," *Int. J. Struct. Stab. Dyn.*, vol. 18, no. 11, p. 1850135, 2018.

[174] M. Amir and M. Talha, "Nonlinear vibration characteristics of shear deformable functionally graded curved panels with porosity including temperature effects," *Int. J. Press. Vessel. Pip.*, vol. 172, no. November 2018, pp. 28–41, 2019, doi: 10.1016/j.ijpvp.2019.03.008.

[175] S. J. Singh and S. P. Harsha, "Nonlinear dynamic analysis of sandwich S-FGM plate resting on pasternak foundation under thermal environment," *Eur. J. Mech. A/Solids*, vol. 76, no. February, pp. 155–179, 2019, doi: 10.1016/j.euromechsol.2019.04.005.

[176] Z. Li, R. Zhong, Q. Wang, B. Qin, and H. Yu, "The thermal vibration characteristics of the functionally graded porous stepped cylindrical shell by using characteristic orthogonal polynomials," *Int. J. Mech. Sci.*, vol. 182, p. 105779, 2020.

[177] N. Van Thanh, N. D. Khoa, and N. D. Duc, "Nonlinear dynamic analysis of piezoelectric functionally graded porous truncated conical panel in thermal environments," *Thin-Walled Struct.*, vol. 154, p. 106837, 2020.

[178] T. Liu, C. Li, C. Wang, W. Hu, and T. Q. Bui, "Geometrically nonlinear isogeometric analysis of smart piezoelectric FG plates considering thermal effects of piezoelectric stress and dielectric constants," *Compos. Struct.*, vol. 266, p. 113795, 2021.

[179] C. T. Binh, N. Van Long, T. M. Tu, and P. Q. Minh, "Nonlinear vibration of functionally graded porous variable thickness toroidal shell segments surrounded by elastic medium including the thermal effect," *Compos. Struct.*, vol. 255, p. 112891, 2021.

[180] P. M. Ramteke, V. Kumar, N. Sharma, and S. K. Panda, "Geometrical nonlinear numerical frequency prediction of porous functionally graded shell panel under thermal environment," *Int. J. Non. Linear. Mech.*, vol. 143, p. 104041, 2022.

[181] S. Eiadtrong, N. Wattanasakulpong, and T. P. Vo, "Thermal vibration of functionally graded porous beams with classical and non-classical boundary conditions using a modified Fourier method," *Acta Mech.*, vol. 234, no. 2, pp. 729–750, 2023.

[182] B. Mamen *et al.*, "Combined effect of thickness stretching and temperature-dependent material properties on dynamic behavior of imperfect FG beams using three variable quasi-3D model," *J. Vib. Eng. Technol.*, vol. 11, no. 5, pp. 2309–2331, 2023.

[183] P. Code, "Eurocode 3: Design of steel structures-part 1-2: General rules-structural fire design," *London Eur. Comm. Stand.*, 2007.

[184] M. A. Bradford, T. K. Luu, and A. Heidarpour, "Generic nonlinear modelling of a steel beam in a frame sub-assembly at elevated temperatures," *J. Constr. Steel Res.*, vol. 64, no. 7–8, pp. 732–736, 2008.

[185] M. A. Khan, S. Z. Khan, W. Sohail, H. Khan, M. Sohaib, and S. Nisar, "Mechanical fatigue in aluminium at elevated temperature and remaining life prediction based on natural frequency evolution," *Fatigue Fract. Eng. Mater. Struct.*, vol. 38, no. 8, pp. 897–903, 2015, doi: 10.1111/ffe.12287.

[186] A. Sadgui and A. Tati, "A novel trigonometric shear deformation theory for the buckling and free vibration analysis of functionally graded plates," *Mech. Adv. Mater. Struct.*, vol. 29, no. 27, pp. 6648–6663, 2022.

[187] S. R. Li and R. C. Batra, "Relations between buckling loads of functionally graded timoshenko and homogeneous euler-bernoulli beams," *Compos. Struct.*, vol. 95, pp. 5–9, 2013, doi: 10.1016/j.compstruct.2012.07.027.

[188] T. K. Nguyen, T. Truong-Phong Nguyen, T. P. Vo, and H. T. Thai, "Vibration and buckling analysis of functionally graded sandwich beams by a new higher-order shear deformation theory," *Compos. Part B Eng.*, vol. 76, pp. 273–285, 2015, doi: 10.1016/j.compositesb.2015.02.032.

[189] G. L. She, F. G. Yuan, and Y. R. Ren, "Thermal buckling and post-buckling analysis of functionally graded beams based on a general higher-order shear deformation theory," *Appl. Math. Model.*, vol. 47, pp. 340–357, 2017, doi: 10.1016/j.apm.2017.03.014.

[190] J. N. Reddy, "A simple higher-order theory for laminated composite plates," *J. Appl. Mech. Trans. ASME*, vol. 51, no. 4, pp. 745–752, 1984, doi: 10.1115/1.3167719.

[191] M. Aydogdu, "A new shear deformation theory for laminated composite plates," *Compos. Struct.*, vol. 89, no. 1, pp. 94–101, 2009, doi: 10.1016/j.compstruct.2008.07.008.

[192] J. L. Mantari, A. S. Oktem, and C. Guedes Soares, "Static and dynamic analysis of laminated composite and sandwich plates and shells by using a new higher-order shear deformation theory," *Compos. Struct.*, vol. 94, no. 1, pp. 37–49, 2011, doi: 10.1016/j.compstruct.2011.07.020.

[193] J. L. Mantari, A. S. Oktem, and C. Guedes Soares, "A new higher order shear deformation theory for sandwich and composite laminated plates," *Compos. Part B Eng.*, vol. 43, no. 3, pp. 1489–1499, 2012, doi: 10.1016/j.compositesb.2011.07.017.

[194] S. S. Akavci and A. H. Tanrikulu, "Buckling and free vibration analyses of laminated composite plates by using two new hyperbolic shear-deformation theories," *Mech. Compos. Mater.*, vol. 44, no. 2, pp. 145–154, 2008, doi: 10.1007/s11029-008-9004-2.

[195] E. Viola, F. Tornabene, and N. Fantuzzi, "General higher-order shear deformation theories for the free vibration analysis of completely doubly-curved laminated shells and panels," *Compos. Struct.*, vol. 95, pp. 639–666, 2013, doi: 10.1016/j.compstruct.2012.08.005.

[196] N. El Meiche, A. Tounsi, N. Ziane, I. Mechab, and E. A. El, "A new hyperbolic shear deformation theory for buckling and vibration of functionally graded sandwich plate," *Int. J. Mech. Sci.*, vol. 53, no. 4, pp. 237–247, 2011, doi: 10.1016/j.ijmecsci.2011.01.004.